sinta S2 Sinta Score

e-ISSN 2503-5010
p-ISSN 2087-0965

Accredited by Ristekdikti: Nomor 21/E/KPT/2018

JURNAL RISET TEKNOLOGI PENCEGAHAN PENCEMARAN INDUSTRI

Research Journal of Industrial Pollution Prevention Technology

Vol. 11, No. 2, November 2020

JURNAL RISET Teknologi Pencegahan Pencemaran Industri	Vol.11	No. 2	Page 1 - 50	Semarang, November 2020	ISSN No. 2087-0965

Kementerian Perindustrian REPUBLIK INDONESIA

Published by :
BADAN PENELITIAN DAN PENGEMBANGAN INDUSTRI
BALAI BESAR TEKNOLOGI PENCEGAHAN PENCEMARAN INDUSTRI

Jurnal Riset
Teknologi Pencegahan Pencemaran Industri
Volume 11 No. 2, November 2020

FOCUS AND SCOPE

Jurnal Riset Teknologi Pencegahan Pencemaran Industri (Research Journal of Industrial Pollution Prevention Technology) seeks to promote and disseminate original research as well as review, related to following area:

Environmental Technology : within the area of air pollution technology, wastewater treatment technology, and management of solid waste and harzardous toxic substance.

Process Technology and Simulation : technology and/or simulation in industrial production process aims to minimize waste and environmental degradation.

Design Engineering : device engineering to improve process efficiency, measurement accuracy and to detect pollutant.

Material Fabrication : environmental friendly material fabrication as subtitution material for industry.

Energy Conservation : process engineering/ technology/ conservation of resources for energy generation.

Jurnal Riset

Teknologi Pencegahan Pencemaran Industri

Volume 11 No. 2, November 2020

IMPRINT

Jurnal Riset Teknologi Pencegahan Pencemaran Industri (JRTPPI) published by the Center for Technology of Pollution Prevention Industry (BBTPPI) – Research and Development Industry, Ministry of Industry. JRTPPI is published online twice in every year.

ISSN print edition : 2087-0965

ISSN electronic edition : 2503-5010

Electronic edition available on :
ejournal.kemenperin.go.id/jrtppi

INDEXING

JRTPPI has been covered by these following indexing services :
Directory Of Open Access Journals (DOAJ), Crossref, Indonesian Scientific Journal Database (ISJD), Mendeley, Infobase Index, Indonesian Publication Index (IPI), Bielefeld Academic Search Engine (BASE), Google Scholar, Directory of Research Journals Indexing (DRJI).

MAILING ADDRESS

Center of Industrial Pollution Prevention Technology.
Jl. Ki Mangunsarkoro No. 6 Semarang, Jawa Tengah, 50136 Indonesia.
Telp. +62 24 8316315
Fax. +62 24 8414811
e-mail: jurnalrisettppi@kemenperin.go.id
Jam kerja : Senin – Jum'at
07.30 – 16.00 GMT+7

EDITORIAL BOARD

MANAGING EDITOR

COPY EDITOR

LAYOUT EDITOR

PROOFREADER

Jurnal Riset
Teknologi Pencegahan Pencemaran Industri
Volume 11 No. 2, November 2020

PREFACE

Thanks to Allahu Robbie 'Alamin, Journal of Industrial Pollution Prevention Technology (JRTPPI) again will publish scientific articles, especially in the field of environmental technology for volume 11 no 2. Our high appreciation is directed to the authors and editorial board who have actively participated so as to maintain consistency of quality and punctuality of our periodic publications. We would like to acknowledge our high appreciation to the head at center of industrial pollution prevention technology, The agency of Industial Research and Development of Indonesia, Ministry of Industry.

This edition of the issue is fifth series published that in full-text English. This continous policy is an attempt of the editorial board to improve the author's performance in delivering the results of their researches. Articles in full-text English are more likely to be read by broader audience so that it will increase the number of citations. This policy is also applied in order to actualize our hope of being a globally indexed international journal.

The articles contained in this edition consist of wastewater technology and renewable energy. The wastewater treatments are destined for batik and pharmacheutical industries, while membraneless microbial fuel cell and battery articles as renewable energy. The six manuscripts accepted and published in this edition are from researcher and lecturer in Lembaga Ilmu Pengetahuan indonesia, Universitas Lampung, Institut Teknologi Indonesia, Badan Tenaga Atom Nasional, Balai Besar Bahan dan Barang Teknik, Institut Teknologi Bandung, Balai Besar Teknologi Pencegahan Pencemaran Industri, and Institut Ilmu Kesehatan Bhakti Wiyata. The duration of submission, review, and editing of the manuscripts ranged from 2-5 months.

Hopefully, these scientific articles may be new source of knowledge and experience for readers from academic, researcher, industry, and society at large. We realize that nothing is perfect until the improvement of all parties involved is continuously done.

Semarang, November 2020

Chief Editor

Jurnal Riset
Teknologi Pencegahan Pencemaran Industri
Volume 11 No. 2, November 2020

TABLE OF CONTENT

Jurnal Riset
Teknologi Pencegahan Pencemaran Industri
Volume 11 No. 2, November 2020

ABSTRACT

Published on 19 November 2020

Fery Eko Pujiono[1*], Tri Ana Mulyati[1], Miftakhul Nor Fizakia[1] ([1]Departement of Chemistry, Institut Ilmu Kesehatan Bhakti Wiyata Kediri, Indonesia)

Activated Carbon of Coconut Shell Modified TiO_2 as a Batik Waste Treatment

Jurnal Riset Teknologi Pencegahan Pencemaran Industri, November 2020, Vol. 11, No. 2, p. 1-10, 4 ill, 4 tab, 27 ref

Research about the modification of activated carbon of coconut shell with TiO_2 as a waste treatment Batik has been done. The purpose of this study was to determine the effect of modified TiO_2 on activated carbon characteristics and the effect of TiO_2 concentration on the adsorption power of activated carbon in batik waste. The method utilized was activated carbon soaked in TiO_2 with 5% and 10% concentrations in a ratio of 1: 5, then stirred with a magnetic stirrer for 2 hours. Next, the mixture was placed in an autoclave bottle and an oven (200°C for 30 minutes). The results were then washed with distilled water and dried (100°C for 5 hours), then the material was characterized by FTIR, XRD, SEM-EDX, and application to batik waste. FTIR results indicated the presence of Ti-O-Ti groups after modification at wave number 682 cm^{-1}, XRD indicated the presence of a combination of amorphous KA and crystalline TiO_2 at 25,2°; 37,7°; 48,1°; 53,8°; and 55°, and SEM results of TiO_2 agglomeration on the surface of the railroad. Adsorption of batik waste showed $KATiO_2$-10 (0,052) lower than KA (0,059) and $KATiO_2$-5 (0,057), as well as the presence of COD KA results = 705,6 mg / L (pH = 8), $KATiO_2$-5 = 504,0 mg / L (pH pH = 7) and $KATiO_2$-10= 403,2 mg / L (pH = 7). Based on this research, the activated carbon modified TiO_2 can be used as a material for processing batik waste with the most significant concentration of TiO_2 represent 10%.

(Author)

Keywords: Activated carbon, Coconut shell, TiO_2, Batik waste

Tri Hadi Jatmiko[1] ([1]Balai Penelitian Teknologi Bahan Alam, Lembaga Ilmu Pengetahuan Indonesia)

Optimization of Production Activated Carbon for Removal of Pharmaceuticals Wastewater Using Taguchi Method and Grey Relational Analysis

Jurnal Riset Teknologi Pencegahan Pencemaran Industri, November 2020, Vol. 11, No. 2, p. 11-18, 1 ill, 4 tab, 27 ref

The development of the pharmaceutical industry has led to increased environmental pollution by pharmaceutical wastewater. This encourages efforts to develop effective and inexpensive pharmaceutical wastewater management. One effort to handle pharmaceutical wastewater is to use activated carbon. In the manufacture of activated carbon there are several factors that affect the quality and performance of activated carbon produced. This research seeks to determine the optimum factors in making activated carbon and study its application in adsorbing pharmaceutical wastewater contain carbamazepine, sulfamethoxazole, and paroxetine. Multi-response analysis based on the Taguchi Grey relational analysis method was used to determine the optimum conditions. The most influential factors in the production of activated carbon, respectively, were pyrolysis temperature (800°C), ratio of precursors and activating agents (1:1), residence time (150 minutes) and finally the type of activator (KOH).

(Author)

Keywords: Activated carbon, Taguchi, Grey Relational Analysis

Aris Mukimin[1], Nur Zen[1], Hanny Vistanty[1], Agus Purwanto[1] ([1]Centre of Indutrial Pollution Prevention Technology, Jl. Ki Mangunsarkoro No. 6, Semarang 50241, Indonesia)

High Electric Production by Membraneless Microbial Fuel Cell with Up Flow Operation using Acetate Wastewater

Jurnal Riset Teknologi Pencegahan Pencemaran Industri, November 2020, Vol. 11, No. 2, p. 19-27, 8 ill, 27 ref

Microbial fuel cell (MFC) is a new proposed technology reported to generate renewable energy while simultaneously treating wastewater. Membraneless microbial fuel cell (ML-MFC) system was developed to eliminate the requirement of membrane which is expensive and prone to clogging while enhancing electricity generation and wastewater treatment efficiency. For this purpose, a reactor was designed in two chambers and connected via three pipes (1 cm in diameter) to enhance fluid diffusion. Influent flowrate was maintained by adjusting peristaltic

pump at the base of anaerobic chamber. Carbon cloth (235 cm2) was used as anode and paired with gas diffusion layer (GDL) carbon-Pt as cathode. Anaerobic sludge was filtered and used as starter feed for the anaerobic chamber. The experiment was carried out by feeding synthetic wastewater to anaerobic chamber; while current response and potential were recorded. Performance of reactor was evaluated in terms of chemical oxygen demand (COD). Electroactive microbe was inoculated from anaerobic sludge and showed current response (0.55-0.65 mA) at 0,35 V, range of diameter 1.5-2 μm. The result of microscopics can showed three different species. The microbial performance was increased by adding ferric oxide 1 mM addition as acceptor electron. The reactor was able to generate current, voltage, and electricity power of 0.36 mA, 110 mV, and 40 mWatt (1.5 Watt/m2), respectively, while reaching COD removal and maximum coulomb efficiency (EC) of 16% and 10.18%, respectively.

(Author)

Keywords: ML-MFC, Carbon cloth, GDL carbon-Pt, Acetate, Renewable energy

Susanto Sigit Rahardi[1], Muhamad Ilham Bayquni[1], Bambang Sunendar Purwasasmita[2] ([1]Balai Besar Bahan dan Barang Teknik (B4T), Ministry of Industry, Sangkuriang Street No.14 Bandung City 40135, Indonesia, [2]Program Studi Teknik Fisika, Institut Tekologi Bandung, Ganesha Street No.10 Bandung City, Indonesia)

Preliminary Study of Synthesis of Sodium Manganese Oxide using Sol-Gel Method as Sodium Ion Battery Material

Jurnal Riset Teknologi Pencegahan Pencemaran Industri, November 2020, Vol. 11, No. 2, p. 28-34, 4 ill, 3 tab, 25 ref

Sodium ion battery is one of the promising alternatives to lithium ion battery. Sodium manganese oxide as the sodium ion battery catode material has been synthesized by modifying the sol-gel method used to obtain lithium manganese oxide. The precursors used were table salt and manganese chloride. The sol-gel process used was water solvent, citric acid as a chelating agent and chitosan as the template. Thermal decomposition and formation zone obtained from simple thermal analysis using furnace and digital scales. Calcination was carried out at 600°C and 850°C for 2 hours. Crystal properties and morphology were analyzed using XRD and SEM. Based on the analysis of XRD pattern, sodium manganese oxide crystals ($Na_{0.7}MnO_{2.05}$ JCPDS 27-0751) have been formed at both of the calcination temperature. Observed morphology of the sample showed the domination Mn_3O_4 JCPDS 18-0803 in accordance with crystalline phase identification. These results demonstrate that the modified sol-gel method could be used to obtain sodium manganese oxide as sodium ion battery cathode material.

(Author)

Keywords: Sodium manganese oxide, Sol-gel method, Salt

Ratnawati[1], Marcelinus Christwardana[1], Sudirman[2], Enjarlis[1] ([1]Chemical Engineering Department, Institut Teknologi Indonesia, [2]Badan Tenaga Atom Nasional, Kawasan Puspiptek, Serpong)

Zinc Removal from ZnO Industrial Wastewater by Hydroxide Precipitation and Coagulation Methods: The Role of pH and Coagulant Dose

Jurnal Riset Teknologi Pencegahan Pencemaran Industri, November 2020, Vol. 11, No. 2, p. 35-42, 4 ill, 2 tab, 22 ref

Liquid waste from the ZnO industry must be treated to meet the quality standards of wastewater into water bodies, according to the Minister of Environment Regulations No.5, 2014. It still contains 79 mg/L of Zn metal, cloudy with turbidity above 500 NTU, and COD value around 222 mg/L. This study aims to determine the effect of pH on reducing Zn metal and the coagulant dose to minimize turbidity and COD in liquid waste produced by the ZnO factory in Depok, West Java. The waste treatment has been carried out by adding alkaline to neutralize the acid conditions in the equalization basin. However, the results have not met the requirements. It is necessary to vary the pH (8.5; 9.0; 9.5; 10.0 and 10.5) to precipitate of Zn optimally, modify the dose of coagulants (50; 100 and 150 mg/L) and reaction times (10; 15 and 20 minutes) to reduce its turbidity and COD concentration. The best results were obtained at a pH of 9.5 with a coagulant dose of 50 mg/L and a reaction time of 10 minutes. This condition can reduce Zn concentration (79 to 3.71 mg/L), turbidity (557 to 1.42 NTU), COD (222 to 68 mg/L) with a removal efficiency of 95.3%; 99.7%; and 69.4% respectively. These values have met the standard requirements according to government regulations.

(Author)

Keywords: Zn, pH, Coagulant, Turbidity, COD

Muhammad Amin[1], Slamet Sumardi[1], Roniyus Marjunus[2], Frista Clarasati[2], David Candra B[1], Muhammad Al Muttaqi[1],
Kusno Isnugroho[1], Yusup Hendronursito[1] ([1]Research Unit for Mineral Technology, Indonesian Institute of Sciences (BPTM-LIPI), [2]Department of Physics, Faculty of Mathematics and Natural Sciences, University of Lampung)

Processing of Granite Quarry Solid Waste into Industrial High Silica Materials using Leaching Process with HCl Concentration Variation

Jurnal Riset Teknologi Pencegahan Pencemaran Industri, November 2020, Vol. 11, No. 2, p. 43-50, 9 ill, 7 tab, 21 ref

This study was aimed to increase granite's silica content using the leaching process with HCl concentration variation. The granite used in this study came from Lematang, South Lampung. This study aims to determine the effect of variations in HCl concentration, particle size, and rotational speed on the crystalline phase and chemical elements formed in the silica product produced from granite. The HCl concentration variations were 6.0 M, 7.2 M, 8.4 M, and 9.6 M, the variation in particle size used was 270 and 400 mesh. Variations in rotational speed during leaching were 500 and 750 rpm. Granite powder was calcined at 1000 °C for 2 hours. Characterization was performed using X-Ray Fluorescence (XRF), X-Ray Diffraction (XRD), and Inductively Coupled Plasma-Optical Emission Spectroscopy (ICP-

OES). The results showed that the silica content increased with increasing HCl concentration, the finer the particle size, and the higher the rotational speed. XRF analysis showed that the silica with the highest purity was leached with 9.6 HCl with a particle size of 400 mesh and a rotational speed of of 750 rpm, which was 73.49%. Based on the results above, by leaching using HCl, the Si content can increase from before. The XRD diffractogram showed that the granite powder formed the Quartz phase.

(Author)

Keywords: Granite, Silica, Leaching, HCl

Vol. 11 No. 2 (2020) 1-10

Jurnal Riset
Teknologi Pencegahan Pencemaran Industri

Journal homepage : http://www.jrtppi.id

Kementerian Perindustrian
REPUBLIK INDONESIA

Activated Carbon of Coconut Shell Modified TiO_2 as a Batik Waste Treatment

Fery Eko Pujiono[1*], Tri Ana Mulyati[1], Miftakhul Nor Fizakia[1]

[1] Departement of Chemistry, Institut Ilmu Kesehatan Bhakti Wiyata Kediri, Indonesia

ARTICLE INFO

Article history:
Received 06 June 2020
Received in revised form 28 July 2020
Accepted 28 July 2020
Available online 19 November 2020

Keywords :
Activated carbon
Coconut shell
TiO_2
Batik waste

ABSTRACT

Research about the modification of activated carbon of coconut shell with TiO_2 as a waste treatment Batik has been done. The purpose of this study was to determine the effect of modified TiO_2 on activated carbon characteristics and the effect of TiO_2 concentration on the adsorption power of activated carbon in batik waste. The method utilized was activated carbon soaked in TiO_2 with 5% and 10% concentrations in a ratio of 1: 5, then stirred with a magnetic stirrer for 2 hours. Next, the mixture was placed in an autoclave bottle and an oven (200°C for 30 minutes). The results were then washed with distilled water and dried (100°C for 5 hours), then the material was characterized by FTIR, XRD, SEM-EDX, and application to batik waste. FTIR results indicated the presence of Ti-O-Ti groups after modification at wave number 682 cm^{-1}, XRD indicated the presence of a combination of amorphous KA and crystalline TiO_2 at 25,2°; 37,7°; 48,1°; 53,8°; and 55°, and SEM results of TiO_2 agglomeration on the surface of the railroad. Adsorption of batik waste showed $KATiO_2$-10 (0,052) lower than KA (0,059) and $KATiO_2$-5 (0,057), as well as the presence of COD KA results = 705,6 mg / L (pH = 8), $KATiO_2$-5 = 504,0 mg / L (pH pH = 7) and $KATiO_2$-10= 403,2 mg / L (pH = 7). Based on this research, the activated carbon modified TiO_2 can be used as a material for processing batik waste with the most significant concentration of TiO_2 represent 10%.

1. INTRODUCTION

The development of the batik industry in recent years has been extraordinarily rapid. This is appropriate to an increase in the number of batik enthusiasts both in terms of producers and consumers. However, the problem that arises from this development is the waste generated from batik production process . Batik liquid waste contains dyes, color enhancers, and collections that can cause damage to the aquatic environment (Mukimin et al. 2018). One way to overcome pollution due to batik liquid waste is to use activated carbon as an adsorbent.

Currently, commercial activated carbon has a relatively high selling price According to Global and China Activated Carbon Industry Report 2017-2021 coconut shell-based activated carbon commands the highest price, above USD 1427,98/t. This causes, it is necessary to synthesize activated carbon from materials containing high carbon sources but at a low price like an agricultural waste (Pujiono, et al. 2017; and Mulyati, 2018). One of the agricultural waste that is used as raw material for making activated carbon is coconut shell. The results of Hidayu, et. al. (2016) research shows that with the same activator, the surface area of activated carbon of coconut shell is greater (1.011 m^2 / g) than that of oil palm shells (584 m^2 / g).

The potential of activated carbon from a coconut shell as water treatment has been reported in several studies. Omo-Okoro, et al. (2018) shows that activated carbon from coconut shells can be used as a potent adsorbent for organic wastes and polyfluoroalkyl in aqueous waste. Aljabore, et al. (2017) also reported that activated carbon from coconut shells was effectively used as an adsorbent for toxic textile

*Correspondence author.
E-mail : ferypujiono@gmail.com (F.E. Pujiono)

doi : https://10.21771/jrtppi.2020.v11.no.2.p1-10

Accreditation number : (LIPI) 756/Akred/P2MI-LIPI/08/2016

dyes. A similar thing was reported by Cazetta et al. (2011) which shows that activated carbon has an adsorption power of 916 mg/g for dyes. On the other hand, activated carbon can still be increased its adsorption power through modification of the carbon structure. One compound that is usually used as a modifier for activated carbon is TiO_2.

Modification of activated carbon using TiO_2 has several advantages, namely relatively inexpensive, excellent potential economic value to remove pollutants, good availability, inert, excellent photocatalytic activity, relatively excellent chemical stability, effective form of remediation and can prevent the formation of undesirable by-products (Schneider et al. 2014 and Skocaj et al. 2011). Research by Simonetti et al. (2018) showed that activated carbon from coconut shells modified with TiO_2 can be used to increase the adsorbent power of activated carbon to 60.53 m^2/g dye waste using the sol-gel method. MiarAlipour, et al. (2018) determined a combination of TiO_2 photocatalysts which were immobilized in activated carbon to increase the adsorption and photocatalytic efficiency using the in situ method. Research by Pujiono, et al. (2019) showed that activated carbon modified with TiO_2 was able to reduce COD levels up to 93,28%.

Based on the background, a study was conducted on the modification of activated carbon from coconut shells with TiO_2 to adsorb batik liquid waste. Activated carbon synthesized from coconut shell agricultural waste was further modified with TiO_2 at various concentrations and applied to batik waste adsorption.

2. METHODS

2.1. Materials

Materials needed in this study are coconut shell from Bandar Traditional Market, Kediri, East Java; Batik Waste Derived from the batik home industry in Sampang, Madura; Sodium Hydroxide (NaOH) MERCK 99,9%; Titanium Dioxide (TiO_2)Sigma Aldrich 99%; Ferro Ammonium Sulfate ($(NH_4)_2Fe(SO_4)_2{\cdot}6H_2O$) Sigma Aldrich 99%; Ferroin indicator solution 0,1 wt.% in H_2O Sigma Aldrich; Potassium dichromate ($K_2Cr_2O_7$) 99% Sigma Aldrich and distilled water.

2.2. Instrumentation

The instrumentation in this study are glassware, oven for dry sample, furnace, for carbonized sample, magnetic stirrer, pH meter, UV-Vis spectrophotometer (Shimadzu), X-Ray Diffraction (JOEL diffractometer), Brucker FT-IR Spectrometer, Scanning Electron Microscopy (Zeiss EVO MA 10). Digestion vessel, Reflux, and Micro Burette

2.3. Procedure

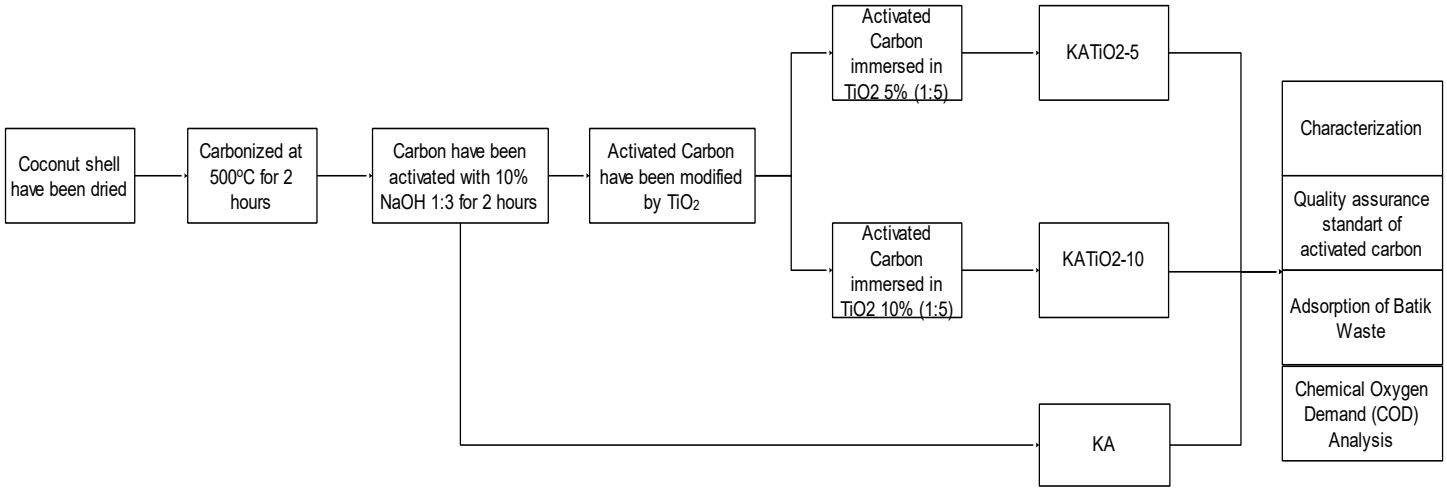

Figure 1. Procedure Synthesis and Characterization of Activated Carbon of Coconut Shell Modified TiO_2 as a Batik Waste Treatment

2.3.1 Sample Preparation

The coconut shell was washed to remove the dirt then dried. The dry coconut shell was then carbonated.

2.3.2 Synthesis of Activated Carbon

The coconut shell was carbonized in the furnace at 500°C for 2 hours. The carbon that has been produced was then ground to fine and sieved to homogenize at 100 mesh. The carbon from the coconut shell that has been produced was then soaked in 10% NaOH in a ratio of 1: 3 for 2 hours. After the stirring process, it was filtered and neutralized with hot distilled water to pH 6.5-7. The precipitate was dried in an oven at 130°C for 4 hours. The result is namely activated carbon (KA).

2.3.3 Modification of Activated Carbon with TiO_2

The activated carbon (KA) was then immersed in TiO_2 (1: 5) with 5% and 10% concentrations, respectively. Then it was added with 45 ml of distilled water and stirred with a magnetic stirrer for 2 hours. Next, the mixture was put in an autoclave bottle and heated at 200°C for 30 minutes. it was then washed with distilled water and dried at 100°C for 5 hours. Activated carbon modified with 5% TiO_2 is called $KATiO_2$-5 while those modified with 10% TiO_2 are called $KATiO_2$-10.

2.3.4 Characterization of Materials

The crystallinity of the material (activated carbon and activated carbon modified with TiO_2) was determined by XRD (X-Ray Diffraction) with CuKα radiation (λ = 1.54056 Å) at 40 kV and 30 mA. The diffractogram pattern is measured at 2θ between 5–50 °. Material functional groups are determined by FTIR (Fourier Transform Infrared) at wavelengths between 400–4000 cm^{-1}. The surface structure of the material is determined by SEM (Scanning Electron Microscope). In addition, the quality assurance standard of activated carbon material before and after the modification of TiO_2 was carried out, such as moisture content, ash content, iodine numbers, and methylene blue numbers.

2.3.5 Application in Batik Waste

Modified activated carbon TiO_2 ($KATiO_2$) is applied as batik wastewater material. it is mixed with batik wastewater (1:5) and stirred with a magnetic stirrer for 2 hours. Then the filtrate was measured using a UV-Vis spectrophotometer (at a wavelength of 400 - 800 nm).

2.3.6 Chemical Oxygen Demand (COD) Analysis

The sample is inserted digestion vessel with a digestion solution ($K_2Cr_2O_7$ 0,1 N) and sulfuric acid reactant. Next, the mixture is shaken until homogeneous. After that, the mixture is refluxed for 2 hours and cooled at room temperature. Then the test solution is titrated with Ferro Ammonium Sulfate (FAS) standard solution and Ferroin indicator until the color changes from bluish-green to reddish-brown. COD results are calculated by the equation :

$$\text{COD (mg/l)} = \frac{((Vb-Vc)\times NFAS\times 8000}{Vs}$$

With :

Vb = volume of FAS solution needed for blank (ml)

Vc = volume of FAS solution needed for the test sample (ml)

NFAS = normality of FAS solution (N)

Vs = sample volume (ml)

3. RESULT AND DISCUSSION

3.1 Activated Carbon Synthesis

In this research, activated carbon is synthesized from the coconut shell with NaOH activator. At first, the carbon is synthesized by heating it in a furnace at 500 °C. This process aims to release volatile molecules like CO_2 and H_2O (Asrijal, et al. 2014) and describe the components contained in coconut shells, namely cellulose, hemicellulose, and lignin (Hartanto and Ratnawati, 2010). The carbon produced is then activated with a 10% NaOH solution. NaOH activator acts as a dehydrating agent that can break C-O-C and C-O bonds from raw materials, causing a decrease in mass after activation (Bachrun, et al. 2016). The yield of activated carbon produced in this study reached 87.38% (Table 1).

Table 1. Yield of Activated Carbon

Carbon mass (g)	Activated carbon mass (g)	Yield (%)
10,006	8,743	87,38

3.2 Activated Carbon Modified with TiO_2

Activated carbon (KA) was modified with 5% and 10% TiO_2. The variation of TiO_2 concentration was chosen based on the research of Orha, et al (2017) and Pujiono, et al (2019). It aims to determine the effect of TiO_2 concentration on activated carbon characteristics. Modification of activated carbon is produced by stirring activated carbon with a TiO_2 solution for 2 hours to distribute TiO_2 evenly on the entire surface of activated carbon (Yuliusman, 2014). The precipitate was dried at 100 ºC to remove water vapor. Modified activated carbon at 5% TiO_2 hereinafter referred to as $KATiO_2$-5 while modification of 10% TiO_2 as $KATiO_2$-10.

3.3 Characterization

In this study, the quality assurance standard of activated carbon before and after TiO_2 modification was carried out by comparing data on moisture content, ash content, iodine numbers, and methylene blue numbers with SNI 06-37-30-1995 requirements. Table 2 shows that activated carbon and TiO_2 modified activated carbon have met the permitted activated carbon quality standard (SNI 06-37-30-1995).

Table 2. The quality assurance standard of activated carbon before and after TiO2 modification

Type of Test	Materials			SNI 06-37-30-1995
	KA	$KATiO_2$-5	$KATiO_2$-10	
Moisture content (%)	15,5	15,3	15,2	Max 25%
Ash content (%)	5,2	13,2	13,9	Max 15%
Iodine numbers (mg/g)	856,78	951,97	983,71	Min 750 mg/g
Methylene blue numbers (mg/g)	120,82	123,14	124,03	Min 120 mg/g

Table 2 shows that the modification of TiO_2 on activated carbon did not significantly change the moisture content. This is following the research of Anisuzzaman, et al (2015) which shows that there wasn't a significant correlation between moisture content and the ratio of impregnation to activated carbon modification. On the other hand, ash content increases after modification of TiO_2. This is due to TiO_2 is a metal oxide that has a bond between titanium tetravalent ions and oxygen ions so that it is stable at high temperatures (Nasution and Fitri, 2018). Table 2 also shows that activated carbon modified with TiO_2 has greater absorption of iodine and methylene blue when compared to activated carbon without modification of TiO_2. These results indicate the existence of modification of activated carbon with TiO_2 able to increase the ability of adsorption ability of activated carbon in adsorbing adsorbate. This is consistent with the research of Dey, et al., (2011) who reported that modification of carbon fiber with TiO_2 was able to increase the ability of adsorption of methylene blue.

Sample characterization was carried out to show that the activated carbon modified TiO_2 was successfully synthesized. Modification of activated carbon with TiO_2 based on Orha et al. (2017) showed that activated carbon modified with TiO_2 has two adsorption properties, that is physically by activated carbon and chemically by TiO_2 through photocatalytic reactions. It is expected that the activated carbon modification process can increase its adsorption capability. Characterization of the samples conducted in this study was FTIR, XRD, and SEM-EDX. The results of the characterization by FTIR are shown in Figure 2. The peak at wave number 3390 cm^{-1} indicates the hydroxyl group (-OH). The peak is increased in intensity on activated carbon. Because of the reaction of water vapor with free compounds on the activated carbon surface (Wibowo, et al. 2011; Pujiono, et al. 2017). However, the peak decrease occurs in carbon which has been modified with TiO_2. This is appropriate to the role of TiO_2 modifiers that can reduce hydrogen bonds between the surface of activated carbon and water vapor (Orha, et al. 2016).

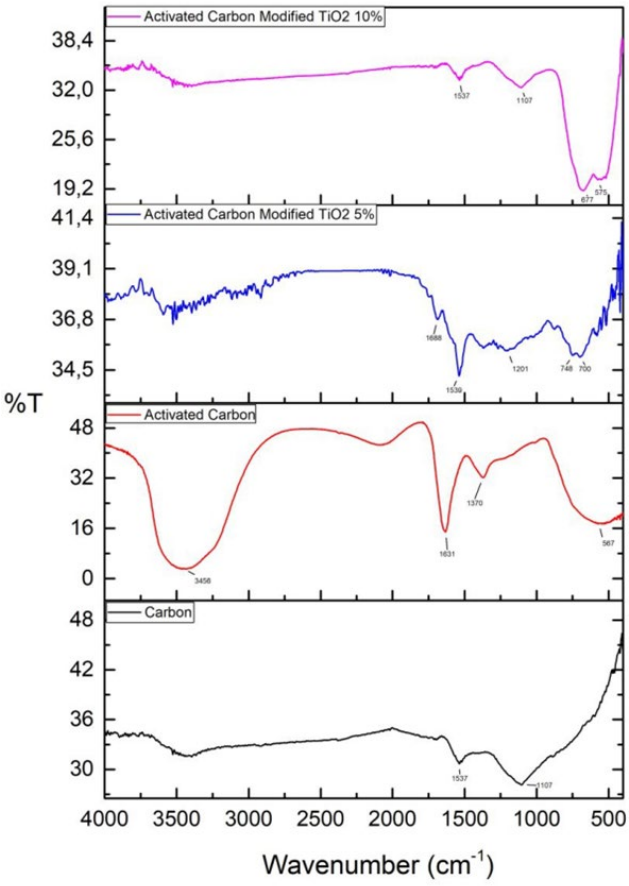

Figure 2. Spectra FTIR of the Materials

The difference between activated carbon before and after activation represents a peak in the wavenumber 1695 cm^{-1}. This peak indicates the stretching of titanium carboxylate (Ti-O-C). Besides that, it shows a peak at wavenumber 1572 cm^{-1} which indicates the presence of Ti-O-C groups. The wavenumbers 1695 cm^{-1} and 1572 cm^{-1} on modified carbon with the between activated carbon and TiO_2 (Irwan et al. 2016). $KATiO_2$-10 peaks at these wavelengths express a more extraordinary intensity than $KATiO_2$-5 which assumed there are more TiO_2 particles attached to activated carbon (Pujiono et. al., 2019). The peak at wave number 682 cm^{-1} indicates the presence of Ti-O-Ti stretching bonds indicating that TiO_2 has covered the activated carbon site.

The difference in a chemical structure on the surface of activated carbon modified TiO_2 equally affects its crystallinity as shown in Figure 3. The diffractogram pattern of activated carbon indicates the presence of widening peaks at 5-10° and 20-30°. This is the characteristic peak of activated carbon which indicates an amorphous form (Le, et al. 2012; Pujiono, et al., 2017; Mulyati, et al. 2017). Besides, the XRD patterns between $KATiO_2$-5 and $KATiO_2$-10 indicate a combination of widening peaks in the 5-10° and 20-30° indicate the presence of activated carbon characteristics and a sharp peak at 25,2°; 37,7°; 48,1°; 53,8°; and 55° which represent the characteristic peak of TiO_2 anatase (Theivasanthi and Alagar, 2013, Pujiono, et al. 2019). The decrease in the intensity of activated carbon modified TiO_2 compared to Anatase because there is an interaction between carbon which is amorphous, thereby reducing the crystallinity of TiO_2. The predominant ananthase in this material provides the advantage of being able to increase its photocatalytic ability when compared to rutile (He et al. 2013). This indicates that there is a combination of amorphous activated carbon forms and TiO_2 crystals which the modification of activated carbon with TiO_2 has been successfully synthesized.

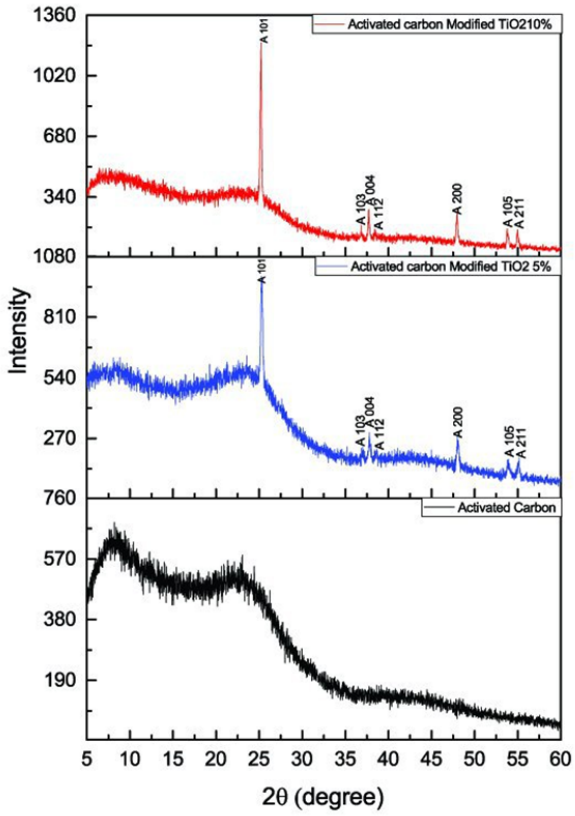

Figure 3. Diffractogram Patterns of The Materials

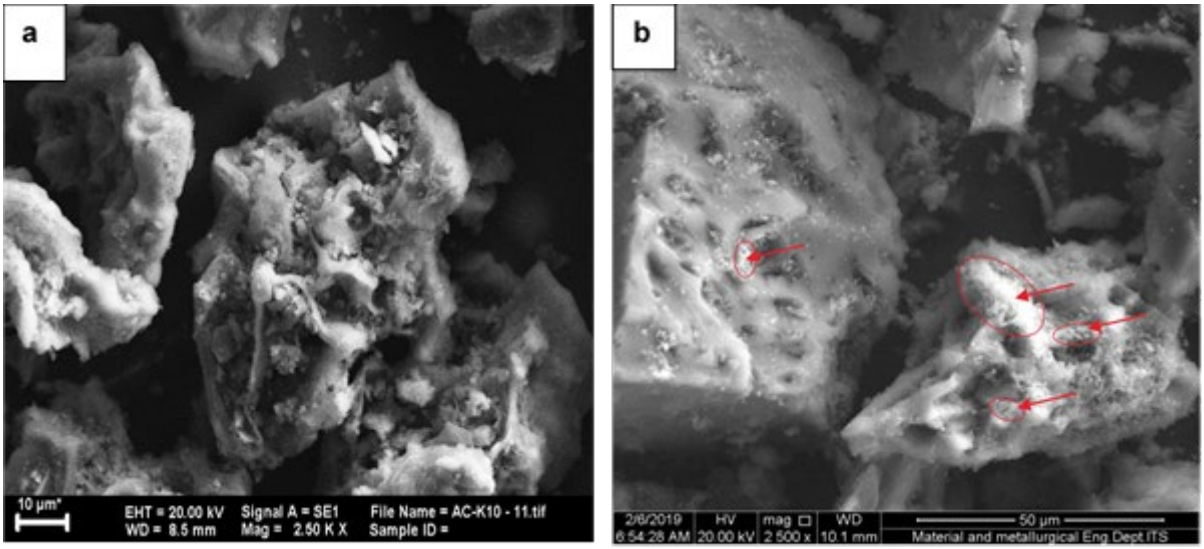

Figure 4. SEM Images of The Materials : (a) Activited Carbon (KA) (b) Activated Carbon Modified by TiO_2 10% ($KATiO_2$-10)

The morphology of activated carbon and activated carbon modified with TiO_2observed using SEM are shown in Figure 4. Figure 4 (a) shows the surface morphology of the activated carbon, while Figure 4 (b) shows the surface morphology of $KATiO_2$-10. Based on Figure 4 (a) it can be seen that pores have formed on the surface of activated carbon, this shows that activated carbon has been successfully synthesized. Figure 4 (b) shows that the modified carbon obtains a structure like activated carbon. However, the agglomeration of TiO_2 on the surface of activated carbon indicates the presence of TiO_2 on the surface of activated carbon (Pujiono, et al., 2019). This further proves it has been successfully synthesized.

3.4 Adsorption Batik Waste use Modified Activated Carbon

This modified TiO_2 activated carbon was applied to adsorb batik waste. Batik waste used in this study is Madura batik waste which is yellow and turbid. The waste has a pH = 8 and COD = 1500 mg / L. The results of batik waste adsorption are shown in Table 3. The measurement of batik liquid waste showed a peak at a wavelength of 400 nm with adsorption of 0,536. This is due to the color of the compounds in the batik liquid waste (Rahmawati, et al. 2009). The maximum wavelength of the batik waste solution obtained will be used to measure the absorbance of the waste solution using KA, $KATiO_2$-5, and $KATiO_2$-10 materials.

Table 3. Batik Waste Adsorption on Activated Carbon and Activated Carbon Modified with TiO_2

Materials	Absorbance
Batik Waste	0,536
KA	0,059
$KATiO_2$-5	0,057
$KATiO_2$-10	0,052

Table 3 shows that there are differences between KA, $KATiO_2$-5, and $KATiO_2$-10. $KATiO_2$-10 obtained lower adsorption that is equal to 0,052 when compared with KA and $KATiO_2$-5 respectively of 0,059 and 0,057. These results indicate that the adsorption ability obtained. This is because the amount of absorbance indicates the concentration of a dye, if the dye has been adsorbed then the concentration will decrease. This means that the smaller the absorbance, the smaller the concentration of the dye due to adsorbent which shows high adsorption ability (Nsami, et al., 2013). The absorbances obtained prove that TiO_2 not only causes photocatalytic reactions but also increases the adsorption power of activated carbon (Lubis et al. 2016).
This modified TiO_2 activated carbon is then applied to adsorb batik Increasing the number of dyes molecules adsorbed will increase the number of dyes undergoing an oxidation reaction with the formation of OH radicals on the catalyst surface of $KATiO_2$, then • OH will react with the

dye waste by attacking aromatic rings and the formation of open rings which contribute to the formation of intermediate compounds, which subsequently oxidized to CO_2 and H_2O (Lubis, et al. 2016). The reaction mechanism can be written as follows (Subramani, et al. 2007):

$TiO_2/KA + hv \rightarrow {}^{*}TiO_2 - KA$

$H_2O + h^{+} \xrightarrow{TiO_2^{\bullet} - KA} {}^{*}OH + H$

${}^{*}OH + \text{dyes} \rightarrow \text{intermediates} \rightarrow CO_2 + H_2O + \text{mineral salt}$

Table 3 also shows that the adsorption of batik waste with activated carbon before and after the modification of TiO2 did not show a significant difference. These results lead to the need for batik COD tests before and after adsorption to determine the ability of the most optimum activated carbon adsorption. COD test aims to determine the number of pollutants that still exist in batik waste. The result of the COD test on batik waste before and after adsorption was shown in Table 4.

Table 4. Batik Waste pH and COD after adsorbed with activated carbon and Activated Carbon Modified with TiO_2

Materials	pH	COD (mg/L)
Batik Waste		1500
KA	8	705,6
$KATiO_2$-5	7	504,0
$KATiO_2$-10	7	403,2

These results are supported by COD (chemical oxygen demand) analysis of batik waste after treatment with activated carbon. Table 4 shows that batik waste treated by KA was 705,6 mg / L (pH = 8). After being processed with $KATiO_2$-5 COD levels were obtained 28,57% and $KATiO_2$-10 increased COD levels by 42,86%. This shows that the presence of TiO_2 is effective in removing dyes from water and TiO_2 is efficient for degrading organic pollutants in liquid waste (Pujiono, et al. 2019). The results of the process of adsorption on batik waste showed that activated carbon modified with TiO_2 can be used as a material for processing batik waste.

4. CONCLUSION

Based on the results of the study showed that the influence of TiO_2concentration on the adsorption power of activated carbon in batik waste, where $KATiO_2$-10 had the lowest adsorption i.e 0,052 compared to KA (0,059) and $KATiO_2$-5 (0,057). The activated carbon modified TiO_2 can be used as a material for processing batik waste with the most significant concentration of TiO_2 represent 10%.

ACKNOWLEDGMENT

Researchers would like thanking the Bhakti Wiyata Foundation and the Institut Ilmu Kesehatan Bhakti Wiyata kediri for the assistance that has been given as well as to students who have assisted in the research process.

REFERENCE

Aljeboree, A. M., Alshirifi, A. N., & Alkaim, A. F. (2017). Kinetics and equilibrium study for the adsorption of textile dyes on coconut shell activated carbon. *Arabian Journal of Chemistry*, *10*, S3381–S3393.

Anisuzzaman, S. M., Joseph, C. G., Taufiq-Yap, Y. H., Krishnaiah, D., & Tay, V. V. (2015). Modification of commercial activated carbon for the removal of 2, 4-dichlorophenol from simulated wastewater. Journal of King Saud University-Science, 27(4), 318–330.

Cazetta, A. L., Vargas, A. M. M., Nogami, E. M., Kunita, M. H., Guilherme, M. R., Martins, A. C., … Almeida, V. C. (2011). NaOH-activated carbon of high surface area produced from coconut shell: Kinetics and equilibrium studies from the methylene blue adsorption. *Chemical Engineering Journal*, *174*(1), 117–125.

Dey, N. K., Kim, M. J., Kim, K.-D., Seo, H. O., Kim, D., Kim, Y. D., … Lee, K. H. (2011). Adsorption and photocatalytic degradation of methylene blue over TiO2 films on carbon fiber prepared by atomic layer deposition. Journal of Molecular Catalysis A: Chemical, 337(1–2), 33–38.

He, Z., Cai, Q., Fang, H., Situ, G., Qiu, J., Song, S., &

Chen, J. (2013). Photocatalytic activity of TiO2 containing anatase nanoparticles and rutile nanoflower structure consisting of nanorods. Journal of Environmental Sciences, 25(12), 2460–2468.

Hidayu, A. R., & Muda, N. (2016). Preparation and characterization of impregnated activated carbon from palm kernel shell and coconut shell for CO2 capture. *Procedia Engineering*, *148*, 106–113.

Ikawati, I., & Melati, M. (2010). Pembuatan Karbon Aktif dari Limbah Kulit Singkong UKM Tapioka Kabupaten Pati.

Irwan, I., Lubis, S., Ramli, M., & Sheilatina, S. (2016). Photocatalytic degradation of indigo carmine by TiO2/activated carbon derived from waste coffee grounds. *Jurnal Natural*, *16*(1).

Le, H. A., Chin, S., & Jurng, J. (2012). Photocatalytic degradation of methylene blue by a combination of TiO2-anatase and coconut shell activated carbon. *Powder Technology*, *225*, 167–175.

MiarAlipour, S., Friedmann, D., Scott, J., & Amal, R. (2018). TiO2/porous adsorbents: Recent advances and novel applications. *Journal of Hazardous Materials*, *341*, 404–423.

Mukimin, A., Vistanty, H., Zen, N., Purwanto, A., & Wicaksono, K. A. (2018). Performance of bioequalization-electrocatalytic integrated method for pollutants removal of hand-drawn batik wastewater. *Journal of Water Process Engineering*, *21*, 77–83.

Mulyati, T. A. (2018). PREPARASI DAN KARAKTERISASI KARBON AKTIF DARI LIMBAH AMPAS TEBU MENGGUNAKAN AKTIVATOR KOH. *Indonesian Chemistry and Application Journal*, *1*(2), 61–67.

Nasution, N., & Fitri, A. (n.d.). SINTESIS NANOPARTIKEL TiO2 FASA RUTILE DENGAN METODE KOPRESIPITASI.

Ndi Nsami, J., & Ketcha Mbadcam, J. (2013). The adsorption efficiency of chemically prepared activated carbon from cola nut shells by on methylene blue. Journal of Chemistry, 2013.

Omo-Okoro, P. N., Daso, A. P., & Okonkwo, J. O. (2018). A review of the application of agricultural wastes as precursor materials for the adsorption of per-and polyfluoroalkyl substances: a focus on current approaches and methodologies. *Environmental Technology & Innovation*, *9*, 100–114.

Orha, C., Pode, R., Manea, F., Lazau, C., & Bandas, C. (2017). Titanium dioxide-modified activated carbon for advanced drinking water treatment. *Process Safety and Environmental Protection*, *108*, 26–33.

Pujiono, F. E., Mulyati, T. A., & Fizakia, M. N. (2019). Modification of activated carbon with titanium dioxide as a water treatment material. *Journal of Public Health in Africa*, *10*.

Pujiono, F., & Mulyati, T. A. (2017). Potensi Karbon Aktif dari Limbah Pertanian Sebagai Material Pengolahan Air Limbah. *Jurnal Wiyata: Penelitian Sains Dan Kesehatan*, *4*(1), 37–44.

Rahmawati, N. I., Suhartana, S., & Gunawan, G. (2009). Pengolahan Limbah Cair Industri Batik dengan Metoda Elektrokoagulasi Menggunakan Seng Bekas Sebagai Elektroda. *Jurnal Kimia Sains Dan Aplikasi*, *12*(2), 40–46.

Schneider, J., Matsuoka, M., Takeuchi, M., Zhang, J., Horiuchi, Y., Anpo, M., & Bahnemann, D. W. (2014). Understanding TiO2 photocatalysis: mechanisms and materials. *Chemical Reviews*, *114*(19), 9919–9986.

Simonetti, E. A. N., de Simone Cividanes, L., da Silva Fonseca, B. C., de Freitas, A. P. B. R., dos Reis Coutinho, A., & Thim, G. P. (2018). TiO2Carbon composite using coconut waste as carbon source: Sonocatalysis and adsorption evaluation. *Surfaces and Interfaces*, *12*, 124–134.

Skocaj, M., Filipic, M., Petkovic, J., & Novak, S. (2011). Titanium dioxide in our everyday life; is it safe? *Radiology and Oncology*, *45*(4), 227–247.

Subramani, A. K., Byrappa, K., Ananda, S., Rai, K. M. L., Ranganathaiah, C., & Yoshimura, M. (2007).

Photocatalytic degradation of indigo carmine dye using TiO 2 impregnated activated carbon. *Bulletin of Materials Science*, *30*(1), 37–41.

Theivasanthi, T., & Alagar, M. (2013). Titanium dioxide (TiO2) nanoparticles XRD analyses: an insight. *ArXiv Preprint ArXiv:1307.1091*.

Wibowo, S., Syafi, W., & Pari, G. P. (2011). Karakterisasi permukaan arang aktif tempurung biji nyamplung. *Makara Journal of Technology*, *15*(1).

Yukselen, Y., & Kaya, A. (2008). Suitability of the methylene blue test for surface area, cation exchange capacity and swell potential determination of clayey soils. Engineering Geology, 102(1–2), 38–45.

Yukselen, Y., Kaya, A., He, Z., Cai, Q., Fang, H., Situ, G., … Gunawan, G. (2018). Performance of bioequalization-electrocatalytic integrated method for pollutants removal of hand-drawn batik wastewater. Powder Technology, 12(1), 167–175.

Vol. 11 No. 2 (2020) 11-18

Jurnal Riset
Teknologi Pencegahan Pencemaran Industri

Journal homepage : http://www.jrtppi.id

Kementerian Perindustrian
REPUBLIK INDONESIA

Optimization of Production Activated Carbon for Removal of Pharmaceuticals Wastewater Using Taguchi Method and Grey Relational Analysis

Tri Hadi Jatmiko[1]
[1]Balai Penelitian Teknologi Bahan Alam, Lembaga Ilmu Pengetahuan Indonesia

ARTICLE INFO

Article history:
Received 03 July 2020
Received in revised form 16 October 2020
Accepted 02 November 2020
Available online 19 November 2020

Keywords :
Activated carbon
Taguchi
Grey Relational Analysis

ABSTRACT

The development of the pharmaceutical industry has led to increased environmental pollution by pharmaceutical wastewater. This encourages efforts to develop effective and inexpensive pharmaceutical wastewater management. One effort to handle pharmaceutical wastewater is to use activated carbon. In the manufacture of activated carbon there are several factors that affect the quality and performance of activated carbon produced. This research seeks to determine the optimum factors in making activated carbon and study its application in adsorbing pharmaceutical wastewater contain carbamazepine, sulfamethoxazole, and paroxetine. Multi-response analysis based on the Taguchi Grey relational analysis method was used to determine the optimum conditions. The most influential factors in the production of activated carbon, respectively, were pyrolysis temperature (800°C), ratio of precursors and activating agents (1:1), residence time (150 minutes) and finally the type of activator (KOH).

1. INTRODUCTION

Population growth and the development of science, especially in the fields of health and pharmaceutical, had encouraged the increasing consumption of drugs so that the production of drugs had also increased rapidly. The growth of the pharmaceutical industry raises problems in the treatment of drug industry waste. Some pharmaceutical industry wastes, although in small amounts, are hazardous for the environment, so some pharmaceutical ingredients have become hazardous waste according to regulations in Europe. Pharmaceutical wastewater contains active compounds as drug residue with toxic substances, volatile organic compound that dangerous for the environment. Pharmaceutical wastewater also high in chemical oxygen demand and biological oxygen demand (Gadipelly et al., 2014; Guo, Qi, & Liu, 2017; Jaria, Silva, et al., 2019; Li & Li, 2015; Pal, 2018; Pereira, Calisto, & Santos, 2019; Rana et al., 2017)

Various efforts have made to prevent pharmaceutical pollution in the environment. Adsorption is one of the most promising techniques for processing pharmaceutical wastewater. One of the promising efforts to process pharmaceutical wastewater is adsorption with activated carbon (Jaria, Calisto, et al., 2019; Jaria, Silva, et al., 2019; Pereira et al., 2019; Vona et al., 2015). The adsorption process using activated carbon is often applied to eliminate organic compounds in water treatment (Bhatnagar, Hogland, Marques, & Sillanpää, 2013; Menya, Olupot, Storz, Lubwama, & Kiros, 2018; Rivera-Utrilla et al., 2011; Yu et al., 2019).

Activated carbon is a term commonly used to denote carbon-based materials that have a fine internal pore structure. Activated carbon is produced from various

*Correspondence author.
E-mail : trih011@lipi.go.id (T.H. Jatmiko)

doi : https://10.21771/jrtppi.2020.v11.no.2.p11-18

Accreditation number : (LIPI) 756/Akred/P2MI-LIPI/08/2016

carbon-rich materials such as biomass, coal, and lignite. Activated carbon has unique characteristics such as high surface area, large porosity with an internal pore structure consisting of micro, meso, and macropore and a broad spectrum of functional groups on the surface of activated carbon makes it applicable in many areas (Ahmed et al., 2019; Bhatnagar et al., 2013; González-García, 2018; Jaria, Silva, et al., 2019; Rivera-Utrilla et al., 2011; Yu et al., 2019).

An interesting raw material for activated carbon to be explored was an industrial waste. The utilization of waste into more useful materials will be a strategy towards an environmentally friendly and sustainable industry. One of the wastes that could be used as raw material for activated carbon was paper mill sludge (PMS) because of its high carbon content (Faubert, Barnabé, Bouchard, Côté, & Villeneuve, 2016). PMS is a solid waste generated from the processing of liquid waste from the paper industry, which is usually only stockpiled, causing environmental problems (Faubert et al., 2016; Jaria, Calisto, et al., 2019; Jaria, Silva, et al., 2019). The use of PMS as activated carbon will increase added value economically and also solve environmental problems.

The purpose of this study was to determine the optimum conditions for activated carbon production to remove pharmaceutical wastewater using the Taguchi Grey relational analysis (GRA) method. The Taguchi method is a systematic experimental design and analysis. This method has proven to be a practical approach to produce high quality products at a relatively low cost as it can reduce the number of experiments carried out (Kasemsiri, Dulsang, Pongsa, Hiziroglu, & Chindaprasirt, 2017; Lin, 2004; Roy, 2010). However, the Taguchi method is only designed to optimize one performance characteristic. For the multi-response optimization problem, the Taguchi method is equipped with GRA (Datta, Bandyopadhyay, & Pal, 2008; Kasemsiri et al., 2017; Lin, 2004).

2. METHODS

Data on activated carbon production, characteristics of activated carbon, and treatment of pharmaceutical wastewater with activated carbon were taken from Jaria et al. (2019). Activated carbon was made from primary paper mill sludge (PMS) from pulp and paper mill waste. Activated carbon was activated using KOH (Eka Pellet) or K_2CO_3 (AnalaR NORMAPUR) and pyrolyzed at 650 °C or 800 °C using muffle (Nüve, series MF 106) with a residence time of 60 minutes and 150 minutes. After that, activated carbon's characterization was carried out, including yield, surface area, and total organic carbon. The surface area of activated carbon was measured based on nitrogen isothermic adsorption using Micromeritics Instrument, Gemini VII 2380. Total organic carbon from activated carbon was determined using the TOC-VCPH Shimadzu equipped with a solid sample module SSM-5000A.

Adsorption test of artificial pharmaceutical wastewater was done in batches. Pharmaceutical solutions of Carbamazepine (CBZ) from Sigma-Aldrich which were anti-epilepsy, antibiotic sulfamethoxazole (SMX) from TCI, and antidepressant paroxetine (PAR) from TCI were prepared separately with an initial concentration of 5 mgL^{-1}. Each solution was contacted with 0.015 gL^{-1} activated carbon overnight at 25 °C and stirred at 80 rpm in overhead shaker (Heidolph, Reax 2). After the solution filtered, the amount of absorbed waste was analyzed using a spectrophotometer (T90 + UV / visible Spectrometer) at a wavelength of 200 nm (SMX and PAR) and 214 nm for CBZ.

Taguchi

The Taguchi method was used to design experiments using orthogonal arrays. Experimental design using the Taguchi method will reduce the overall number of experiments (Roy, 2010). In this study, four factors (pyrolysis temperature, residence time, precursor:activating agent ratio, activating agent) with two levels were used to optimize the characteristic of activated carbon and its performance for pharmaceutical wastewater removal. The orthogonal array in the Taguchi method for the number of parameters 4 with two levels is L8.

Grey relation analysis

The first stage in the grey relational analysis is grey relational formation. During this step, all experimental responses are normalized in the range between zero and one. Equation 1 is used to calculate the normalized value of the response with the expected value "the higher the better" (Datta et al., 2008; Kasemsiri et al., 2017; Lin, 2004).

$$x_i^*(k) = \frac{x_i(k) - \min x_i(k)}{\max x_i(k) - \min x_i(k)} \quad (1)$$

Where. i = 1. .... m; k = 1. .... n;

m is the number of experimental data,

n is the number of responses,

$x_i(k)$ the original sequence,

$x_i^*(k)$ the sequence after the data pre-processing.

max $x_i(k)$ the biggest value of $x_i(k)$,

min $x_i(k)$ the smallest value of $x_i(k)$.

The coefficient of grey relational is decided from normalized data to describe the connection between the preferred and actual response.

$$\xi_i(k) = \frac{\Delta_{min} + \zeta\Delta_{max}}{\Delta_{oi}(k) + \zeta\Delta_{max}} \quad (2)$$

Where $\Delta_{oi} = |x_0(k) - xi(k)|$ is the deviation sequence, ζ is coefficient, usually taken as 0.5.

Then, the grey relational level is calculated by the average of grey relational coefficient and overall evaluation of multiple performance characteristics is based on the degree of grey relationship.

3. RESULT AND DISCUSSION

The experimental design according to the orthogonal array from the Taguchi method for four factors with two levels, is shown in Table 1. Table 1 also shows the results of the experiment of activated carbon production along with its characteristics and performance in the adsorption of pharmaceutical wastewater. In general, SMX, CBZ, and PAR wastes could be adsorbed by activated carbon well. SMX could be absorbed by activated carbon with an absorption capacity of between 13±2% - 80±2%. CBZ that could be absorbed by activated carbon ranges from 6±1% - 81±3%, and PAR could be removed with activated carbon by 6±2% - 81±1%. The removal of pharmaceuticals by activated carbon depends on the activated carbon used to adsorb it. The higher the surface area of the activated carbon used, the higher the pharmaceuticals waste removal.

In the GRA evaluation, the first step was that the experimental data were normalized to a value between zero and one, commonly called gray relational generation.

Tabel 1. Orthogonal array of Taguchi L8 and multi response result (Jaria, Silva, et al., 2019)

No.	Factors				Responses					
	X1	X2	X3	X4	Yield (%)	S_{BET} ($m^2 g^{-1}$)	TOC (%)	% Adsorption		
								SMX	CBZ	PAR
1	1	1	1	1	27.5	244	58±0.4	13±2	6±1	8±2
2	1	1	2	2	7	523	54.9±0.5	16±1	6±1	6±2
3	1	2	1	2	21.6	372	59±1	14±3	6±2	9±2
4	1	2	2	1	5.2	766	54±1	23±6	13.8±0.3	20±5
5	2	1	1	2	30	637	40±1	19±5	34±2	54±2
6	2	1	2	1	3.7	1389	62.8±0.2	80±2	59±2	70±4
7	2	2	1	1	26.4	1017	42.5±0.2	23±3	31±3	55±3
8	2	2	2	2	2.7	1627	67±1	71±1	81±3	81±1

X1—Pyrolysis temperature (650 °C (–) and 800 °C (+)).

X2—Residence time (60 min (–) or 150 min (+)).

X3—Precursor:activating agent ratio (10:1 (–) and 1:1 (+)).

X4—Activating agent (K_2CO_3 (–) and KOH (+))

Table 2. Normalize

Run No.	Yield (%)	S_{BET} ($m^2 g^{-1}$)	TOC (%)	Ads (%) SMX	Ads (%) CBZ	Ads (%) PAR
1	0.91	0.00	0.67	0.00	0.00	0.03
2	0.16	0.20	0.55	0.04	0.00	0.00
3	0.69	0.09	0.70	0.01	0.00	0.04
4	0.09	0.38	0.52	0.15	0.10	0.19
5	1.00	0.28	0.00	0.09	0.37	0.64
6	0.04	0.83	0.84	1.00	0.71	0.85
7	0.87	0.56	0.09	0.15	0.33	0.65
8	0.00	1.00	1.00	0.87	1.00	1.00

Table 3. Grey relational coefficient & Grey relational grade

Run No.	Yield (%)	S_{BET} ($m^2 g^{-1}$)	TOC (%)	Ads (%) SMX	Ads (%) CBZ	Ads (%) PAR	GRG	Rank
1	0.85	0.33	0.60	0.33	0.33	0.34	0.46	5
2	0.37	0.39	0.53	0.34	0.33	0.33	0.38	8
3	0.62	0.36	0.63	0.34	0.33	0.34	0.44	6
4	0.36	0.45	0.51	0.37	0.36	0.38	0.40	7
5	1.00	0.41	0.33	0.35	0.44	0.58	0.52	3
6	0.34	0.74	0.76	1.00	0.63	0.77	0.71	2
7	0.79	0.53	0.36	0.37	0.43	0.59	0.51	4
8	0.33	1.00	1.00	0.79	1.00	1.00	0.85	1

Table 4. Factor

	Level			Rank
	1	2	Delta	
X1	0.42	0.65	0.23	1
X2	0.52	0.55	0.03	3
X3	0.48	0.59	0.11	2
X4	0.52	0.55	0.03	4

Table 2 shows the normalized data for the characteristic of activated carbon and the adsorption of pharmaceutical wastewater. Then, based on normalized experimental data, gray relation coefficient calculations are performed to state the relationship between experimental data and desired results as shown in Table 3. So that optimization of complex multifarious respond characteristics can be transformed into the optimization of a single gray relational level. The optimal process parameters are shown by the highest gray relational level.

An overall evaluation of some process responses is based on a grey relational Grade (GRG). GRG is the average of the grey relational coefficient that corresponds to each response. The results of calculations and analysis of GRG values as shown in Table 3, that the best performance was

obtained on activated carbon in the 8th experiment where all factors were at the highest level.

Table 4 shows the results of further calculations of the GRG difference for each parameter. It can be seen that the most influential factors in the production of activated carbon from waste with the best performance are X1, X3, X2 and finally X4. The highest temperature (X1) and the highest impregnation ratio (X3) are the most influential conditions in activated carbon production, whereas residence time (X2) and activating agent (X4) are less influential factors in activated carbon production. The results of this experiment show that temperature positively influences the development of porosity because activated carbon produced with a maximum pyrolysis temperature (800 °C) has a high S_{BET} and the highest adsorption percentage for CBZ, SMX and PAR. The carbonization process is strongly influenced by temperature, presence of inert gas, heating rate and residence time. A high carbonization temperature will produce a low yield because it produces more ash but good char quality (González-García, 2018).

Temperature of pyrolysis has the biggest effect on adsorption capacity of activated carbon. This phenomena correspondence with another study that the higher the pyrolysis temperature would increase the performance of activated carbon as seen in Figure 1a. The increase in pyrolysis temperature will cause more volatile content in the precursor to be released (Heidarinejad et al., 2020; Sun et al., 2014) so that it will increase the surface area of activated carbon due to the opening of the pores (Ahmad et al., 2012; Heidarinejad et al., 2020; Jaria, Silva, et al., 2019; Zhang, Liu, & Liu, 2015). With the increase of surface area, the adsorption capacity of the activated carbon also increases, as seen in Figure 1a.

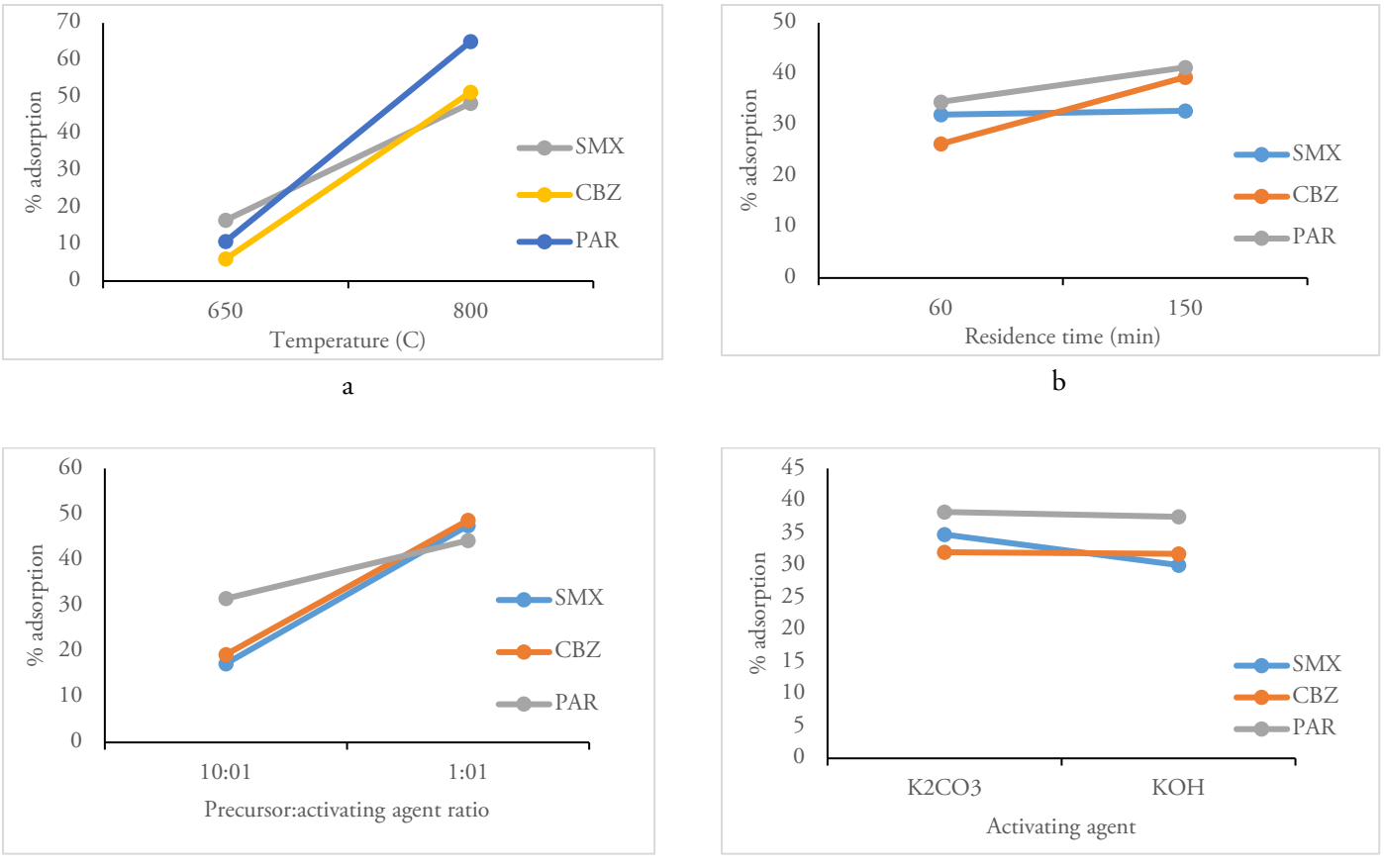

Figure 1. Effect operating condition on activated carbon adsorption performance a) temperature; b) Residence Time; c) Precursor:activating agent; d) Activating agent

Table 5. Effect opertaing condition on activated carbon

Operating condition		Yield (%)	S_{BET} ($m^2 g^{-1}$)	TOC (%)
Temperature (C)	650	7	476,25	57
	800	30	1167,5	53,5
Time (min)	60	18,5	698,25	49
	150	13,975	945,5	60
Precursor:activating agent	10:1	30	567,5	52,33
	1:1	7	1076,25	60,5
Activating agent	K_2CO_3	27,5	854	56
	KOH	18,5	789,75	55,33

Ratio precursor:activating agent also has affected to the activated carbon performance. Increasing the activating agent would activate precursor more optimum. In general, the activation process using chemicals will occur diffusion of chemicals into the precursors' internal structure so that it will open new pores and widen existing pores. When the activating agent (K_2CO_3 or KOH) was increased, the activation process becomes more optimal. The activated carbon formed has a high surface area and increases its ability to absorb adsorbate (Foo & Hameed, 2012; Heidarinejad et al., 2020).

Increasing residence time will increase the quality of activated carbon, as shown in Figure 1b and Table 5. The longest the residence time will increase the activated carbon processed more optimum, resulting in high surface area and TOC.

From the study results, as shown in Figure 1d and Table 5, activation using K_2CO_3 is slightly better than KOH; this is in accordance with several previous studies (Abbas & Ahmed, 2016; Heidarinejad et al., 2020). This is likely due to the ability of K_2CO_3 to inhibit the formation of tar and other liquid products during the pyrolysis process (Adinata, Wandaud, & Aroua, 2007), so that activated carbon that is activated using K_2CO_3 has a slightly larger surface area and TOC than with activated carbon activated with KOH.

4. CONCLUSION

Activated carbon produced from PMS waste shows satisfactory characteristics and adsorption performance of pharmaceutical wastewater. Multi-response analysis based on the Taguchi GRA method can illustrate well the factors that influence the production of active carbon from PMS waste. The most influential factors in the production of activated carbon are pyrolysis temperature (800°C), ratio of precursors and activating agents (1:1), residence time (150 minutes) and finally the type of activator (KOH).

REFERENCE

Abbas, A. F., & Ahmed, M. J. (2016). Mesoporous activated carbon from date stones (Phoenix dactylifera L.) by one-step microwave assisted K2CO3 pyrolysis. *Journal of Water Process Engineering*, *9*, 201–207. https://doi.org/10.1016/j.jwpe.2016.01.004

Adinata, D., Wandaud, W., & Aroua, M. (2007). Preparation and characterization of activated carbon from palm shell by chemical activation with K2CO3. *Bioresource Technology*, *98*(1), 145–149. https://doi.org/10.1016/j.biortech.2005.11.006

Ahmad, M., Lee, S. S., Dou, X., Mohan, D., Sung, J.-K., Yang, J. E., & Ok, Y. S. (2012). Effects of pyrolysis temperature on soybean stover- and peanut shell-derived biochar properties and TCE adsorption in water. *Bioresource Technology*, *118*, 536–544. https://doi.org/10.1016/j.biortech.2012.05.042

Ahmed, M. B., Hasan Johir, M. A., Zhou, J. L., Ngo, H. H., Nghiem, L. D., Richardson, C., … Bryant, M. R. (2019). Activated carbon preparation from

biomass feedstock: Clean production and carbon dioxide adsorption. *Journal of Cleaner Production*, *225*, 405–413. https://doi.org/10.1016/j.jclepro.2019.03.342

Bhatnagar, A., Hogland, W., Marques, M., & Sillanpää, M. (2013). An overview of the modification methods of activated carbon for its water treatment applications. *Chemical Engineering Journal*, *219*, 499–511. https://doi.org/10.1016/j.cej.2012.12.038

Datta, S., Bandyopadhyay, A., & Pal, P. K. (2008). Grey-based taguchi method for optimization of bead geometry in submerged arc bead-on-plate welding. *The International Journal of Advanced Manufacturing Technology*, *39*(11–12), 1136–1143. https://doi.org/10.1007/s00170-007-1283-6

Faubert, P., Barnabé, S., Bouchard, S., Côté, R., & Villeneuve, C. (2016). Pulp and paper mill sludge management practices: What are the challenges to assess the impacts on greenhouse gas emissions? *Resources, Conservation and Recycling*, *108*, 107–133. https://doi.org/10.1016/j.resconrec.2016.01.007

Foo, K. Y., & Hameed, B. H. (2012). Preparation, characterization and evaluation of adsorptive properties of orange peel based activated carbon via microwave induced K2CO3 activation. *Bioresource Technology*, *104*, 679–686. https://doi.org/10.1016/j.biortech.2011.10.005

Gadipelly, C., Pérez-González, A., Yadav, G. D., Ortiz, I., Ibáñez, R., Rathod, V. K., & Marathe, K. V. (2014). Pharmaceutical Industry Wastewater: Review of the Technologies for Water Treatment and Reuse. *Industrial & Engineering Chemistry Research*, *53*(29), 11571–11592. https://doi.org/10.1021/ie501210j

González-García, P. (2018). Activated carbon from lignocellulosics precursors: A review of the synthesis methods, characterization techniques and applications. *Renewable and Sustainable Energy Reviews*, *82*, 1393–1414. https://doi.org/10.1016/j.rser.2017.04.117

Guo, Y., Qi, P. S., & Liu, Y. Z. (2017). A Review on Advanced Treatment of Pharmaceutical Wastewater. *IOP Conference Series: Earth and Environmental Science*, *63*, 012025. https://doi.org/10.1088/1755-1315/63/1/012025

Heidarinejad, Z., Dehghani, M. H., Heidari, M., Javedan, G., Ali, I., & Sillanpää, M. (2020). Methods for preparation and activation of activated carbon: a review. *Environmental Chemistry Letters*, *18*(2), 393–415. https://doi.org/10.1007/s10311-019-00955-0

Jaria, G., Calisto, V., Silva, C. P., Gil, M. V., Otero, M., & Esteves, V. I. (2019). Obtaining granular activated carbon from paper mill sludge – A challenge for application in the removal of pharmaceuticals from wastewater. *Science of The Total Environment*, *653*, 393–400. https://doi.org/10.1016/j.scitotenv.2018.10.346

Jaria, G., Silva, C. P., Oliveira, J. A. B. P., Santos, S. M., Gil, M. V., Otero, M., … Esteves, V. I. (2019). Production of highly efficient activated carbons from industrial wastes for the removal of pharmaceuticals from water—A full factorial design. *Journal of Hazardous Materials*, *370*, 212–218. https://doi.org/10.1016/j.jhazmat.2018.02.053

Kasemsiri, P., Dulsang, N., Pongsa, U., Hiziroglu, S., & Chindaprasirt, P. (2017). Optimization of Biodegradable Foam Composites from Cassava Starch, Oil Palm Fiber, Chitosan and Palm Oil Using Taguchi Method and Grey Relational Analysis. *Journal of Polymers and the Environment*, *25*(2), 378–390. https://doi.org/10.1007/s10924-016-0818-z

Li, X., & Li, G. (2015). A Review: Pharmaceutical Wastewater Treatment Technology and Research in China. In *Proceedings of the 2015 Asia-Pacific Energy Equipment Engineering Research Conference*. Zhuai City, China: Atlantis Press.

https://doi.org/10.2991/ap3er-15.2015.81

Lin, C. L. (2004). Use of the Taguchi Method and Grey Relational Analysis to Optimize Turning Operations with Multiple Performance Characteristics. *Materials and Manufacturing Processes*, *19*(2), 209–220. https://doi.org/10.1081/AMP-120029852

Menya, E., Olupot, P. W., Storz, H., Lubwama, M., & Kiros, Y. (2018). Production and performance of activated carbon from rice husks for removal of natural organic matter from water: A review. *Chemical Engineering Research and Design*, *129*, 271–296. https://doi.org/10.1016/j.cherd.2017.11.008

Pal, P. (2018). Treatment and Disposal of Pharmaceutical Wastewater: Toward the Sustainable Strategy. *Separation & Purification Reviews*, *47*(3), 179–198. https://doi.org/10.1080/15422119.2017.1354888

Pereira, J. M., Calisto, V., & Santos, S. M. (2019). Computational optimization of bioadsorbents for the removal of pharmaceuticals from water. *Journal of Molecular Liquids*, *279*, 669–676. https://doi.org/10.1016/j.molliq.2019.01.167

Rana, R. S., Singh, P., Kandari, V., Singh, R., Dobhal, R., & Gupta, S. (2017). A review on characterization and bioremediation of pharmaceutical industries' wastewater: an Indian perspective. *Applied Water Science*, *7*(1), 1–12. https://doi.org/10.1007/s13201-014-0225-3

Rivera-Utrilla, J., Sánchez-Polo, M., Gómez-Serrano, V., Álvarez, P. M., Alvim-Ferraz, M. C. M., & Dias, J. M. (2011). Activated carbon modifications to enhance its water treatment applications. An overview. *Journal of Hazardous Materials*, *187*(1), 1–23. https://doi.org/10.1016/j.jhazmat.2011.01.033

Roy, R. K. (2010). *A primer on the Taguchi method* (2nd ed). Dearborn, MI: Society of Manufacturing Engineers.

Sun, Y., Gao, B., Yao, Y., Fang, J., Zhang, M., Zhou, Y., … Yang, L. (2014). Effects of feedstock type, production method, and pyrolysis temperature on biochar and hydrochar properties. *Chemical Engineering Journal*, *240*, 574–578. https://doi.org/10.1016/j.cej.2013.10.081

Vona, A., di Martino, F., Garcia-Ivars, J., Picó, Y., Mendoza-Roca, J.-A., & Iborra-Clar, M.-I. (2015). Comparison of different removal techniques for selected pharmaceuticals. *Journal of Water Process Engineering*, *5*, 48–57. https://doi.org/10.1016/j.jwpe.2014.12.011

Yu, L.-J., Rengasamy, K., Lim, K.-Y., Tan, L.-S., Tarawneh, M., Zulkoffli, Z. B., & Se Yong, E. N. (2019). Comparison of activated carbon and zeolites' filtering efficiency in freshwater. *Journal of Environmental Chemical Engineering*, *7*(4), 103223. https://doi.org/10.1016/j.jece.2019.103223

Zhang, J., Liu, J., & Liu, R. (2015). Effects of pyrolysis temperature and heating time on biochar obtained from the pyrolysis of straw and lignosulfonate. *Bioresource Technology*, *176*, 288–291. https://doi.org/10.1016/j.biortech.2014.11.011.

Vol. 11 No. 2 (2020) 19-27

Jurnal Riset
Teknologi Pencegahan Pencemaran Industri

Journal homepage : http://www.jrtppi.id

Kementerian Perindustrian
REPUBLIK INDONESIA

High Electric Production by Membraneless Microbial Fuel Cell with Up Flow Operation using Acetate Wastewater

Aris Mukimin[1], Nur Zen[1], Hanny Vistanty[1], Agus Purwanto[1]

[1] Center of Industrial Pollution Prevention Technology, Jl. Ki Mangunsarkoro No. 6, Semarang 50241, Indonesia

ARTICLE INFO

Article history:
Received 12 August 2020
Received in revised form 30 October 2020
Accepted 31 October 2020
Available online 19 November 2020

Keywords :
ML-MFC
Carbon cloth
GDL carbon-Pt
Acetate
Renewable energy

ABSTRACT

Microbial fuel cell (MFC) is a new proposed technology reported to generate renewable energy while simultaneously treating wastewater. Membraneless microbial fuel cell (ML-MFC) system was developed to eliminate the requirement of membrane which is expensive and prone to clogging while enhancing electricity generation and wastewater treatment efficiency. For this purpose, a reactor was designed in two chambers and connected via three pipes (1 cm in diameter) to enhance fluid diffusion. Influent flowrate was maintained by adjusting peristaltic pump at the base of anaerobic chamber. Carbon cloth (235 cm2) was used as anode and paired with gas diffusion layer (GDL) carbon-Pt as cathode. Anaerobic sludge was filtered and used as starter feed for the anaerobic chamber. The experiment was carried out by feeding synthetic wastewater to anaerobic chamber; while current response and potential were recorded. Performance of reactor was evaluated in terms of chemical oxygen demand (COD). Electroactive microbe was inoculated from anaerobic sludge and showed current response (0.55-0.65 mA) at 0,35 V, range of diameter 1.5-2 μm. The result of microscopics can showed three different species. The microbial performance was increased by adding ferric oxide 1 mM addition as acceptor electron. The reactor was able to generate current, voltage, and electricity power of 0.36 mA, 110 mV, and 40 mWatt (1.5 Watt/m2), respectively, while reaching COD removal and maximum coulomb efficiency (EC) of 16% and 10.18%, respectively.

1. INTRODUCTION

Microbial Fuel Cells (MFC) is a combination of biological redox activities and electrochemical reaction in one cell system. MFC has received increasing attention and becomes an interesting issue over the past decade (Santoro, Arbizzani, Erable, & Ieropoulos, 2017). The most important factor in an MFC system is the simultaneous process of degradation of organic wastewater and electricity generation (Fornero, Rosenbaum, & Angenent, 2010; Wang, 2014). These two main benefits will boost the research towards application on full scale as a solution to the limitation of non-renewable energy as well as prevention of environmental pollution. Several studies have applied MFC on the treatment of various wastewater such as dyes (Thung et al., 2015), palm oil (Baranitharan et al., 2015), starch (Pant, Bogaert, Diels, & Vanbroekhoven, 2010), brewery (Feng, Wang, Logan, & Lee, 2008), and sewage (Ahn & Logan, 2010).

Researchers are usually focused on the material of electrode, microorganisms used and reactor designs. Noble metal catalysts, such as Pt and Au, are commonly used because of their inertness. However, other materials are also considered more feasible and widely used as anode-cathode, i.e., steel-graphite (Jadhav & Ghangrekar, 2009), paper-paper (Roma, 2008), graphite-graphite (Liu & Li, 2007; Reimers et al., 2007; Tartakovsky & Guiot, 2006), graphite granula-graphite granula (Zhuwei, Qinghai, Meng, &

*Correspondence author.
E-mail : arismukimin@gmail.com (A. Mukimin)

doi : https://10.21771/jrtppi.2020.v11.no.2.p19-27

Accreditation number : (LIPI) 756/Akred/P2MI-LIPI/08/2016

Shaohua, 2008), carbon-carboncloth (Feng et al., 2008) and carboncloth-platinized titanium mesh (Larrosa-guerrero et al., 2010). Carbon-based materials now proposed as the attachment media of microbial cells to facilitate electron transfer directly via cytochrome protein and conductive pili (Santoro et al., 2017). Power production is significantly determined by the electrode material as well as the distance between electrodes, shape and dimension of electrodes.

Double-chamber MFC is the most investigated model of MFC reactor, in which the electrode chambers are separated by proton exchange membranes (Ali, Gomaa, Fathey, Abd, & Kareem, 2015; Baranitharan et al., 2015; Greenman, Gálvez, Giusti, & Ieropoulos, 2009; Larrosa-guerrero et al., 2010; Li, Zhang, Lin, Han, & Lei, 2010; Sun, Li, Li, Hu, & Zhang, 2013). However, this model has its limitation to a full-scale plant application, due to the high cost of membranes used and high possibility of clogging thus inhibiting the hydrogen transfer. In order to overcome this obstacle, single chamber air cathode MFC is then designed and resulting in a reduced total volume, simplified design and improved power output (Feng et al., 2008; Larrosa-guerrero et al., 2010; Thung et al., 2015; Wardana & Effendi, 2019; Wei, Han, & Shen, 2012; Zhu, Wang, Zhang, & Tao, 2011). MFC-MBR models as single chamber has been review to potential applied in the wastewater treatment (Bhargavi, Venu, & Renganathan, 2018). Single chamber system utilizes atmospheric air directly in their reaction at the electrode surface. The cathodes are encased by proton exchange membranes, thus proton migration is still obstructed and competition of substrate utilization will occur (Barbara & Pawel, 2020; Kim, Kim, An, Lee, & Chang, 2016).

Finally, membrane less microbial fuel cell (ML-MFC) has been developed as a response to all previous challenges. The absence of membrane will simplify the system configuration and reduce both the cost of maintenance and reactor (Kim et al., 2016; Thung et al., 2015). However, the absence of barrier between anaerobic (anode) and aerobic (cathode) chambers will lead to uncontrolled mixing of electrolyte in both chambers via migration, convection, and diffusion. This study has applied an up-flow system to indirectly separate anode and cathode chambers while facilitating hydrogen transfer to the cathode. This design reactor and operation system can reduce a potential influx of oxygen from cathodic to anodic chamber and lower the cost investment. Carbon cloth and Pt-coated carbon GDL (gas diffusion layer) were used as anode and cathode, respectively, to observe their ability to remove synthetic wastewater as organic pollutant. Acetate was chosen as synthetic waste based on a simplicity of structure that have convenience to oxidation. This condition will facilitate evaluation of a ML-MFC that have designed in this research. The performance of ML-MFC was investigated on varied up flow rate and electricity generation were chosen as an indicator based on potential and current response.

2. EXPERIMENTAL SECTION

2.1. Inoculum and substrates

The ML-MFC was inoculated with mixed cultures anaerobic sludge. 1 L of phosphate buffer that consisted of 0,1 g KCl; 0,2 g NH_4Cl; 0,6 g NaH_2PO_4; 10 mL of trace element; 2 g $NaHCO_3$; 2,722 CH_3COONa and 15 g ferric oxide, was added to 400 mL of anaerobic sludge. It was then mixed and filtered using a vacuum pump. Filtrate obtained was then pumped into ML-MFC reactor at a fixed flow rate of 8 mL/min using a peristaltic pump. 4 L of nutrient that consisted of 0,4 g KCl; 0,8 g NH_4Cl; 2,4 g NaH_2PO_4; 40 mL of trace element; 8 g $NaHCO_3$, 60 g ferric oxide, and 10,8 g CH_3COONa was further fed to the reactor at a fixed flow rate of 11mL/min under anaerobic condition (The nitrogen gas given during the filling process). DC potential was set (DY 2030 POTENTIOSTAT DIGI-IVY) at anode and cathode at 0.3 V. The anode chamber was operated in a circulated system. All the chemicals used, except for ferric oxide, were of analytical grade. Biofilm formed at anode surface was observed using *Scanning Electron Microscopy* (SEM) and identified using a digital microscope and Gram staining.

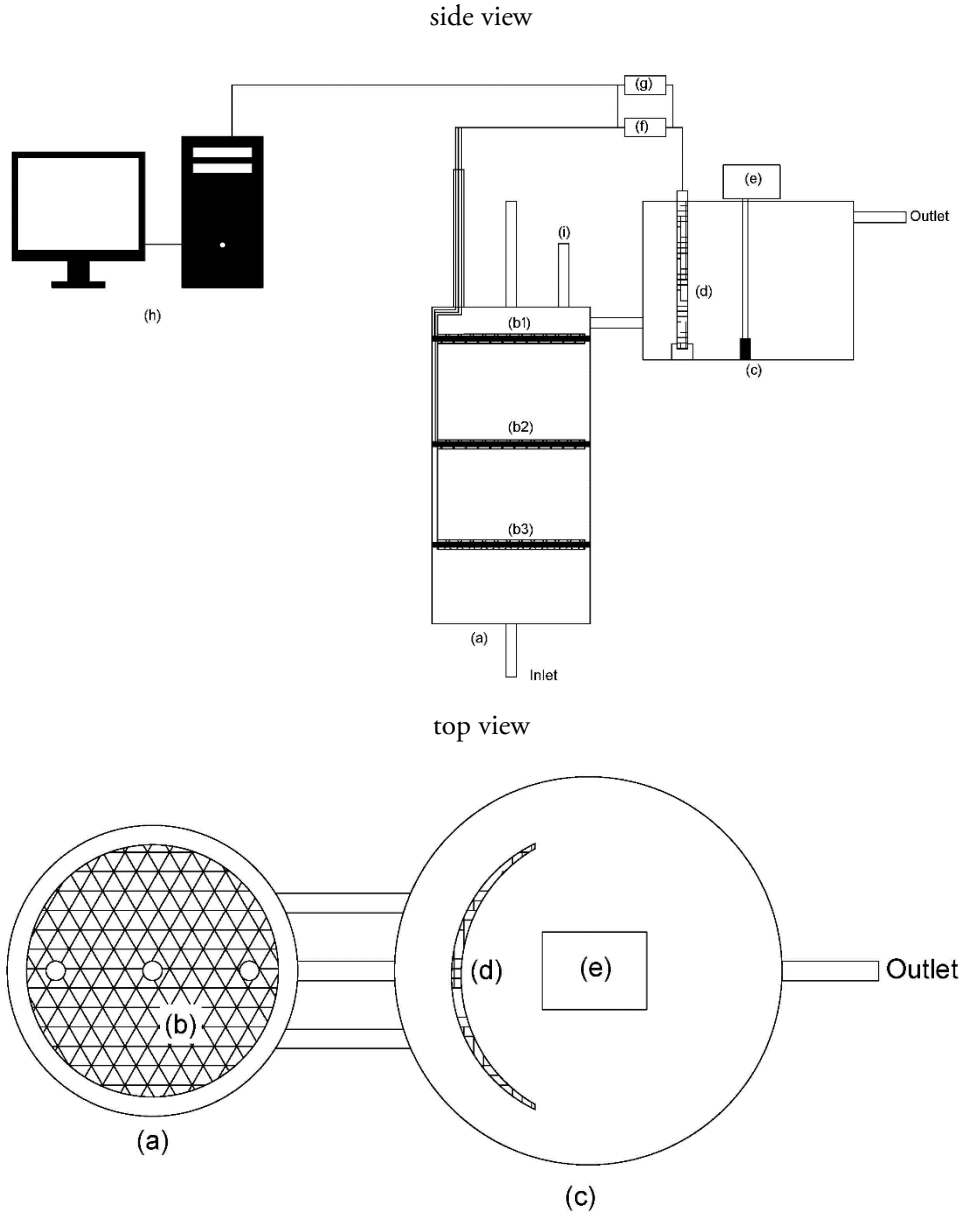

Figure 1. Configuration of up flow membrane less microbial fuel cell with (a) anode chamber, (b) MPL-carbon cloth anode, (c) cathode chamber, (d) GDL Pt/C cathode, (e) aerator, (f) resistor, (g) data logger, and (h) PC.

2.2. Configuration and operation of ML-MFC reactor

The configuration of ML-MFC reactor depicted in Fig. 1. Carbon cloth with MPL (Microporous Layer) and Gas Diffusion Electrode (GDE) cloth with 20% Platinum were used as anode and cathode, respectively, and obtained from Fuel Cell Store, U.S.

Soon after biofilm formed on anode surface, synthetic wastewater was then fed to the reactor. The constituent in the synthetic wastewater was 1000 mg/L CH_3COONa. It was fed to the reactor using a peristaltic pump at fixed flow rate of 12 mL/min. Current response and potential obtained during experiment were monitored (the frequency record is 30 s) using GWINSTEK GDM-396 with interface program Ver1.00 and HANTEK 365D. Water was sampled in the inlet and outlet points of reactor and analysed for COD. The performance of reactor in optimum power output generation was evaluated at varied flowrate of 12, 14, and 16 mL/min. This scale flow rate is

chosen based on HRT and specification of peristaltic pump. To obtain coulombic efficiency, a closed flow system was used with an initial COD concentration of 1000 mg/L, the flow has been setting at 12 mL/min. The value of COD in the next cycle is based on the measurement results of the sample taken (intake point and output cathodic chamber).

2.3. Analysis and evaluation

Three anodes (Carbon Cloth with MPL) and one cathode (GDL Pt/C 20%) were connected. A 300 Ω resistor was used in the external circuit. Potential and current response were both recorded using a data logger (DC Voltage 60 mV, DC Current 6-600 mA, Capacitor 4-400 μF, Diode 0-2 V). Water samples taken from inlet (container before anodic chamber) and outlet points (overflow at cathodic chamber) were all preserved using sulfuric acid (Merck: pro analysis 98%) to obtain a condition pH<2. The chemical oxygen demand (COD) was tested by APHA AWWA method (SM 5220 C). Coulombic efficiency (CE) was calculated based on specific formula of $CE=MI/(F\ b\ q\ \Delta COD)$, where M is the atomic weight of acetate, I is current, F is the Faraday number (96485 C/mol), b is the number of electrons generated per 1 mol of acetate, q is the flowrate and ΔCOD is the difference of influent and effluent COD.

3. RESULT AND DISCUSSION

3.1. Microbial growth, attachment, and enrichment on anode surface

Electroactive microorganisms commonly grow on the surface of anode. Phosphate buffer was used to provide a suitable and optimum condition for microbial growth of anaerobic sludge (Zhao et.al., 2016 and DSMZ, 2007). Disodium hydrogen phosphate and sodium dihydrogen phosphate were used as buffer in this experiment. pH value was adjusted to 6,8 to reduce the growth rate of methanogenic bacteria as competitor. It should be prevented due to their role in faster degradation of simple organic compounds to methane. The Gibbs free energy of methanation is higher thus making it more favourable than simple oxidation which would hinder the production of electron in MFC.

Electron donor on anode and supplement addition of 0,1 M ferric oxide was carried out to support microbial growth and enrichment. Ferric oxide plays an important role as electron acceptor via reduction of three-valent to two-valent iron (Wei et al., 2012). The role of electron acceptor was significant on the transfer of electron liberated by the activity of electroactive microorganisms in organic oxidation, especially acetate. The presence of electroactive microorganisms and the effect of ferric oxide on reactor performance were indicated by current response, as depicted in Fig. 2.

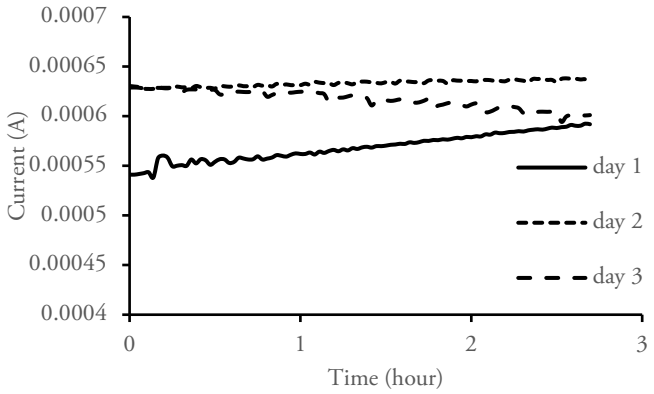

Figure 2. Current response observed for 1, 2, and 3 days at 0.35 V vs Ag/AgCl reference electrode

The presence of electroactive microorganisms was indicated by a gradual increase of current response. The increase was detected at 30 min interval for a few days. Current response was decreased after day 3 at 0.0006 A from 0.000625A for 3 hours. However, it was still higher than the response detected without ferric oxide (0.000029 A). Microbial growth at anode surface was also confirmed by SEM images of anode surface. As depicted in Fig. 3, biofilm has been shown to grow in virtual layer on anode surface.

Thin long layer was clearly observed on carbon anode surface (Fig. 3b); 1.5 – 2 μm in diameter and 6 μm in length. In addition, there were also clumps of biofilm in the shape of irregular mass on anode surface. Further confirmation of microorganism on anode surface, or so-called biofilm, was also conducted using a microscope via Gram staining of bacterial colonies (Fig. 4)

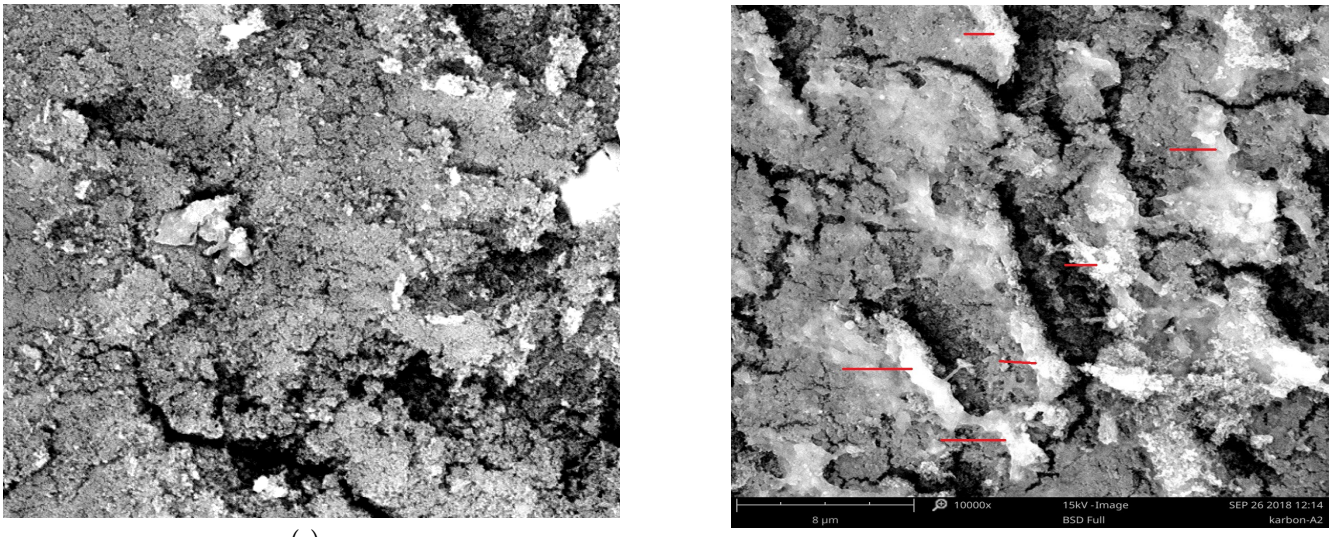

(a) (b)

Figure 3. Surface image of anode before (a) and after microbial growing (b)

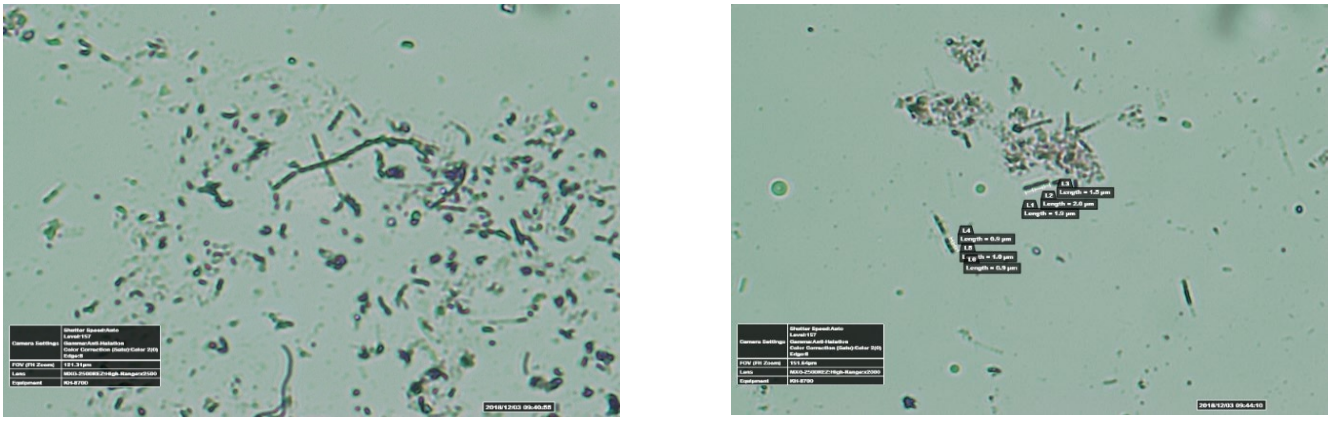

Figure 4. Microbial identification by microscope method

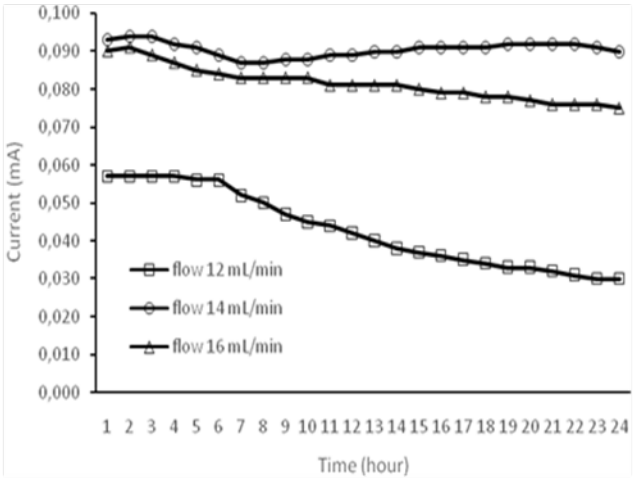

Figure 5. Current production of 1000 mg/L synthetic acetate wastewater at varied flowrate and operational time

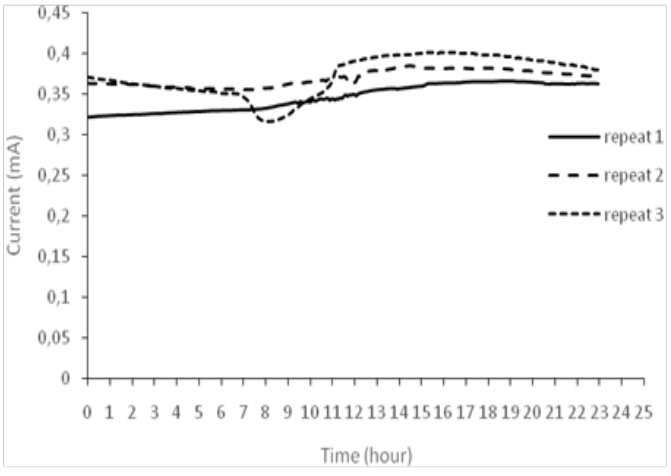

Figure 6. Current production to time process using ferric oxide as media with constant flowrate 12 mL/min

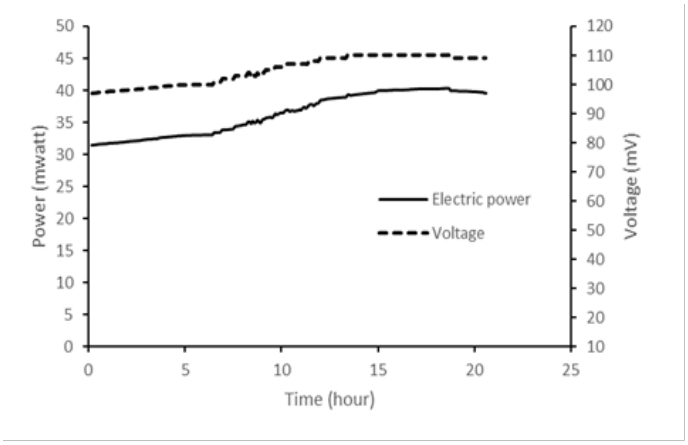

Figure 7. Potential and power production at various operational time

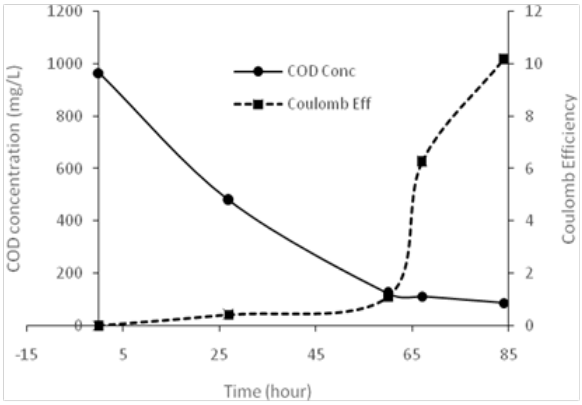

Figure 8. COD removal and coulombic efficiency at operational time

The Gram staining shows three distinct types of bacteria, i.e. *bacillus*, *coccus*, and *streptococcus*. *Bacillus* bacterium was identified as long, rod-shaped cell while *coccus* as spherical and round-shaped. *Streptococcus* bacterium also detected as strings of beads grouping in chains.

3.2. The production of current, voltage and power in reactor application

Up flow ML-MFC was able to convert energy contained in organic matter into electricity. Bioelectricity obtained was represented as current response (A), potential (V), and power (P). Current output obtained during experiment was monitored (Fig. 5 and 6). Current was generated when electricigens oxidized organic compounds in wastewater and produced electron, carbon dioxide, and hydrogen. The electron will be transferred to anode and further transmitted to external circuit. While hydrogen will be transported to anode in liquid phase and serve as electron acceptor and further converted into H_2O. This closed cycle is the main mechanism of electricity generation.

Fig. 5 shows current trends at varied operational time and flowrate. It tended to decrease at flowrate 12 and 16. Interestingly, the opposite increasing trend was observed at flowrate 14, though a decrease was observed after 20 h. Compared to operational time, flowrate is more influential towards current. Current production at flowrate 12 mL/min was lower than higher flowrate (14 and 16 mL/min). It was possibly attributed to low electron and hydrogen transport to anode in anaerobic chamber (Zhu et al., 2011) and hydrogen to cathode in aerobic chamber, respectively, as those transfer were mostly affected by diffusion. It was further confirmed by current response data at flowrate 14 mL/min. Generally, higher flowrate means shorter retention time of wastewater inside the reactor and leads to lower electron production. However, current response observed at flowrate 14 mL/min was 64% higher (0.094 mA) than 12 mL/min (0.058 mA). This trend indicated that the impact of electron and ion (hydrogen) transport was more dominant than electron production from the oxidation by microorganisms. Lorenzo et al 2009 (Di, Curtis, Head, & Scott, 2009) mentioned that electrochemical activity of microorganisms will be enhanced at higher mass transfer due to increasing flowrate. Higher flowrate will also decrease internal resistance of fluid (Wang, 2014) and leads to an increasing electricity production. However, this trend was not observed at flowrate 16 mL/min, in which the current response was lower than flowrate 14 mL/min. It was possibly due to electron production as a limiting factor and resulted in negative correlation between electron/ion transfer and electrical production.

Low current response observed was possibly due to slow electron transfer. However, it can be controlled by using electron acceptor, as clearly revealed in Fig. 6. Ferric oxide addition to anodic chamber as electron acceptor will

facilitate biofilm growth at anode surface. This trend was in accordance with the finding of Bond dan Lovley, 2003 (Bond, Lovley, Bond, & Lovley, 2003). Ferric oxide addition was able to increase current response from 0.058 mA to 0.35 mA or six times higher, at flow rate 12 mL/min.

The positive effect of electron acceptor (ferric oxide) on energy production of ML-MFC reactor was also supported by potential and power density as shown in Fig. 7. The specific design and operational of reactor used in this experiment resulted into high potential of 88-110 mV and power production of 32-40 mW at flowrate 12 mL/min. Power density obtained was about 1.5 W/m^2, in which anode surface area was 235 cm^2. It was higher than the findings of other studies by Ahn and Logan 0.422 W/m^2 (Ahn & Logan, 2010), Ali et al 0.209 W/m^2 (Ali et al., 2015),Du et al 0.536 W/m^2 (Zhuwei et al., 2008) and Kim et al 0.46 W/m^2 (Kim et al., 2016)).

The maximum production of energy was likely because of the high effectivity of electron and hydrogen transfer in anaerobic and aerobic chamber, respectively. Electron transport was facilitated by high contribution of fluid diffusion and electron acceptor (ferric oxide). While cation transport relied on diffusion and migration processes that went unhindered by materials (membrane).

3.3. COD removal and Coulombic efficiency

Another essential feature of up flow ML-MFC is the organic compound's degradation. Fig. 8 shows that reactor was able to achieve high efficiency of organic compounds degradation. Synthetic wastewater was treated and reached 13% efficiency at retention time of 6.9 h. This tendency was linear at initial COD of 500 – 1000 mg/L and increased to 16% at initial COD of 500 – 125 mg/L. COD removal was lower at initial COD less than 125 mg/L (9% lower). Low COD removal (13 – 16%) indicated that anaerobic microorganism growth at anode was still unsatisfactory. It was in accordance with relatively low efficiency at high COD (>521 mg/L) and increased rate of efficiency at COD 521-125 mg/L. Significantly poor performance at low initial COD (<125 mg/L) was likely because of the declining probability of contact between pollutant and microorganisms.

Power was generated from degradation of substrate via biological redox activities and measured as coulombic efficiency (CE). It was calculated based on COD removal and output voltage. Initial COD significantly affected coulombic efficiency, ranging from 0.42%, 1.1%, 6.27%, and 10.18% at initial COD 500-1000, 125-500, 112-125 and less than 112 mg/L respectively. Higher coulombic efficiency observed at low initial COD implied positive correlation between substrate concentration and microorganisms at anode surface.

4. CONCLUSION

Up flow ML-MFC was able to avoid uncontrolled mixing of electrolytes in anaerobic and aerobic chamber and ensure unhindered hydrogen transfer. Carbon cloth was a potential material to be used as anode as it effectively supported microbial growth. Addition of electron acceptor (ferric oxide) gave a significant effect on reactor performance. Reactor was able to generate current, potential and electrical power of 0.36 mA, 110 mV, and 40 mWatt (1.5 Watt/m^2), respectively, from synthetic wastewater treatment (1000 mg/L acetate) at 6.9 h of hydraulic retention time (HRT). Coulombic efficiency (EC) and COD removal was significantly determined by substrate load, 10.18% (<112 mg/L) dan 0.42% (>500 mg/L).

ACKNOWLEDGMENT

This work was financed by Center of Industrial Pollution Prevention Technology (Project 21/BPPI/BBTPPISK/I/2018). This work was also supported by physical laboratory of UNNES and biotech laboratory of CIPPT.

REFERENCE

Ahn, Y., & Logan, B. E. (2010). Bioresource Technology Effectiveness of domestic wastewater treatment using microbial fuel cells at ambient and mesophilic temperatures. *Bioresource Technology*, *101*(2), 469–

475. https://doi.org/10.1016/j.biortech.2009.07.039

Ali, A. E., Gomaa, O. M., Fathey, R., Abd, H., & Kareem, E. (2015). Optimization of double chamber microbial fuel cell for domestic wastewater treatment and electricity production. *Journal of Fuel Chemistry and Technology*, *43*(9), 1092–1099. https://doi.org/10.1016/S1872-5813(15)30032-3

Baranitharan, E., Khan, M. R., Yousuf, A., Fei, W., Teo, A., Yuan, G., & Tan, A. (2015). Enhanced power generation using controlled inoculum from palm oil mill effluent fed microbial fuel cell. *FUEL*, *143*, 72–79. https://doi.org/10.1016/j.fuel.2014.11.030

Barbara, W., & Pawel, W. (2020). The Membrane-Less Microbial Fuel Cell (ML-MFC) with Ni-Co and Cu-B Cathode Powered by the Process Wastewater from Yeast Production. *Energies*, *13153976*(1), 1–13.

Bhargavi, G., Venu, V., & Renganathan, S. (2018). Microbial fuel cells : recent developments in design and materials Microbial fuel cells : recent developments in design and materials. In *Materials Science and Engineering 330* (p. 012034). https://doi.org/10.1088/1757-899X/330/1/012034

Bond, D. R., Lovley, D. R., Bond, D. R., & Lovley, D. R. (2003). Electricity Production by Geobacter sulfurreducens Attached to Electrodes Electricity Production by Geobacter sulfurreducens Attached to Electrodes, *69*(3). https://doi.org/10.1128/AEM.69.3.1548

Di, M., Curtis, T. P., Head, I. M., & Scott, K. (2009). A single-chamber microbial fuel cell as a biosensor for wastewaters. *Water Research*, *43*(13), 3145–3154. https://doi.org/10.1016/j.watres.2009.01.005

Feng, Y., Wang, X., Logan, B. E., & Lee, H. (2008). Brewery wastewater treatment using air-cathode microbial fuel cells, 873–880. https://doi.org/10.1007/s00253-008-1360-2

Fornero, J. J., Rosenbaum, M., & Angenent, T. (2010). Electric Power Generation from Municipal , Food , and Animal Wastewaters Using Microbial Fuel Cells. https://doi.org/10.1002/elan.200980011

Greenman, J., Gálvez, A., Giusti, L., & Ieropoulos, I. (2009). Enzyme and Microbial Technology Electricity from landfill leachate using microbial fuel cells : Comparison with a biological aerated filter, *44*, 112–119. https://doi.org/10.1016/j.enzmictec.2008.09.012

Jadhav, G. S., & Ghangrekar, M. M. (2009). Bioresource Technology Performance of microbial fuel cell subjected to variation in pH , temperature , external load and substrate concentration. *Bioresource Technology*, *100*(2), 717–723. https://doi.org/10.1016/j.biortech.2008.07.041

Kim, J., Kim, B., An, J., Lee, Y. S., & Chang, I. S. (2016). Bioresource Technology Development of anode zone using dual-anode system to reduce organic matter crossover in membraneless microbial fuel cells. *BIORESOURCE TECHNOLOGY*, *213*, 140–145. https://doi.org/10.1016/j.biortech.2016.03.012

Larrosa-guerrero, A., Scott, K., Head, I. M., Mateo, F., Ginesta, A., & Godinez, C. (2010). Effect of temperature on the performance of microbial fuel cells. *Fuel*, *89*(12), 3985–3994. https://doi.org/10.1016/j.fuel.2010.06.025

Li, Z., Zhang, X., Lin, J., Han, S., & Lei, L. (2010). Bioresource Technology Azo dye treatment with simultaneous electricity production in an anaerobic – aerobic sequential reactor and microbial fuel cell coupled system. *Bioresource Technology*, *101*(12), 4440–4445. https://doi.org/10.1016/j.biortech.2010.01.114

Liu, Z., & Li, H. (2007). Effects of bio- and abio-factors on electricity production in a mediatorless microbial fuel cell, *36*, 209–214. https://doi.org/10.1016/j.bej.2007.02.021

Pant, D., Bogaert, G. Van, Diels, L., & Vanbroekhoven, K. (2010). Bioresource Technology A review of the substrates used in microbial fuel cells (MFCs) for

sustainable energy production. *Bioresource Technology*, *101*(6), 1533–1543. https://doi.org/10.1016/j.biortech.2009.10.017

Reimers, C. E., Iii, H. A. S., Westall, J. C., Alleau, Y., Howell, K. A., Soule, L., … Girguis, P. R. (2007). Substrate Degradation Kinetics , Microbial Diversity , and Current Efficiency of Microbial Fuel Cells Supplied with Marine Plankton Substrate Degradation Kinetics , Microbial Diversity , and Current Efficiency of Microbial Fuel Cells Supplied with Marine Plankton . https://doi.org/10.1128/AEM.01209-07

Roma, B. (2008). Importance of temperature and anodic medium composition on microbial fuel cell (MFC) performance, 1213–1218. https://doi.org/10.1007/s10529-008-9687-4

Santoro, C., Arbizzani, C., Erable, B., & Ieropoulos, I. (2017). Microbial fuel cells : From fundamentals to applications . A review. *Journal of Power Sources*, *356*, 225–244. https://doi.org/10.1016/j.jpowsour.2017.03.109

Sun, J., Li, W., Li, Y., Hu, Y., & Zhang, Y. (2013). Bioresource Technology Redox mediator enhanced simultaneous decolorization of azo dye and bioelectricity generation in air-cathode microbial fuel cell. *Bioresource Technology*, *142*, 407–414. https://doi.org/10.1016/j.biortech.2013.05.039

Tartakovsky, B., & Guiot, S. R. (2006). A Comparison of Air and Hydrogen Peroxide Oxygenated Microbial Fuel Cell Reactors, (Figure 1), 241–246.

Thung, W., Ong, S., Ho, L., Wong, Y., Ridwan, F., & Oon, Y. (2015). Bioresource Technology A highly efficient single chambered up-flow membrane-less microbial fuel cell for treatment of azo dye Acid Orange 7-containing wastewater. *BIORESOURCE TECHNOLOGY*, *197*, 284–288. https://doi.org/10.1016/j.biortech.2015.08.078

Wang, X. (2014). Production of Electricity during Wastewater Treatment Using Fluidized-Bed Microbial Fuel Cells, (4), 703–708. https://doi.org/10.1002/ceat.201300241

Wardana, K., & Effendi, A. (2019). The Concentration Variation of Wastewater from Pulp Washing Process in Membraneless Air Cathode Microbial Fuel Cell. *Jurnal Selulosa*, *9*(2), 75–86.

Wei, L., Han, H., & Shen, J. (2012). Effects of cathodic electron acceptors and potassium ferricyanide concentrations on the performance of microbial fuel cell. *International Journal of Hydrogen Energy*, *37*(17), 12980–12986. https://doi.org/10.1016/j.ijhydene.2012.05.068

Zhu, F., Wang, W., Zhang, X., & Tao, G. (2011). Bioresource Technology Electricity generation in a membrane-less microbial fuel cell with down-flow feeding onto the cathode. *Bioresource Technology*, *102*(15), 7324–7328. https://doi.org/10.1016/j.biortech.2011.04.062

Zhuwei, D. U., Qinghai, L. I., Meng, T., & Shaohua, L. I. (2008). Electricity Generation Using Membrane-less Microbial Fuel Cell during Wastewater Treatment *. *Chinese Journal of Chemical Engineering*, *16*(5), 772–777. https://doi.org/10.1016/S1004-9541(08)60154-8

Vol. 11 No. 2 (2020) 28-34

Jurnal Riset
Teknologi Pencegahan Pencemaran Industri

Journal homepage : http://www.jrtppi.id

Kementerian Perindustrian
REPUBLIK INDONESIA

Preliminary Study of Synthesis of Sodium Manganese Oxide using Sol-Gel Method as Sodium Ion Battery Material

Susanto Sigit Rahardi[1], Muhamad Ilham Bayquni[1], Bambang Sunendar Purwasasmita[2]

[1]Balai Besar Bahan dan Barang Teknik (B4T), Ministry of Industry, Sangkuriang Street No.14 Bandung City 40135, Indonesia

[2]Program Studi Teknik Fisika, Institut Tekologi Bandung, Ganesha Street No.10 Bandung City, Indonesia

ARTICLE INFO

Article history:
Received 22 August 2020
Received in revised form 29 September 2020
Accepted 29 September 2020
Available online 19 November 2020

Keywords :
Sodium manganese oxide
Sol-gel method
Salt

ABSTRACT

Sodium ion battery is one of the promising alternatives to lithium ion battery. Sodium manganese oxide as the sodium ion battery catode material has been synthesized by modifying the sol-gel method used to obtain lithium manganese oxide. The precursors used were table salt and manganese chloride. The sol-gel process used was water solvent, citric acid as a chelating agent and chitosan as the template. Thermal decomposition and formation zone obtained from simple thermal analysis using furnace and digital scales. Calcination was carried out at 600°C and 850°C for 2 hours. Crystal properties and morphology were analyzed using XRD and SEM. Based on the analysis of XRD pattern, sodium manganese oxide crystals ($Na_{0.7}MnO_{2.05}$ JCPDS 27-0751) have been formed at both of the calcination temperature. Observed morphology of the sample showed the domination Mn_3O_4 JCPDS 18-0803 in accordance with crystalline phase identification. These results demonstrate that the modified sol-gel method could be used to obtain sodium manganese oxide as sodium ion battery cathode material.

1. INTRODUCTION

As the base material for this sol-gel method, lithium manganese oxide or commonly known as LMO is one of the active lithium ion battery cathode materials that is widely used in the industrial world (Lee et al., 2014; Nishi, 2001; Nitta et al., 2015). Research on LMOs has been carried out for more than 20 years (Armstrong & Bruce, 1996; Sun, 1997; Thackeray & Rossouw, 1994), it is known that local structure and composition of $LiMn_2O_4$ cathode materials which affect the electrochemical properties of materials could be controlled using sol-gel method (Danks, Hall, & Schnepp, 2016; Liu, Neale, & Cao, 2016; W. Liu et al., 1996; Pegeng et al., 2006). The abundance of manganese resources give LMO some advantages : availability of materials, cost and environmentally friendly processing (Nitta et al., 2015). Indonesia itself has abundant high-quality manganese reserves in East Nusa Tenggara which are potential for LMO research (Supriadi et al., 2017).

As a consideration, it was reported on several previous study that $LiMn_2O_4$ (JCPDS 35-0782) was successfully synthesized through the sol-gel method using chitosan as a template (Rahardi, 2016). In addition, research on LMO production using the sol gel method on an augmented lab scale has also been successfully carried out along with the stages of LMO crystal formation which are observed in more detail so that they can be used as a reference procedure for mass production (Balai Besar Bahan dan Barang Teknik, 2020). However, the Geological Agency through the Center for Mineral, Coal and Geothermal Resources (PSDMBP) stated that lithium has not been found in the country even though we have nickel and cobalt reserves which are spread across

*Correspondence author.
E-mail : susantosr@kemenperin.go.id (Susanto Sigit Rahardi)

doi : https://10.21771/jrtppi.2020.v11.no.2.p28-34

Accreditation number : (LIPI) 756/Akred/P2MI-LIPI/08/2016

several islands (Ernowo, Sunuhadi, & Awaludin, 2020). Various studies have been carried out to find alternatives to lithium ion batteries (Hwang, Myung, & Sun, 2017; Parker et al., 2017; Xiao, Mcculloch, & Wu, 2017), one of which is sodium manganese oxide (NMO) which is analogous to the LMO, cathode of lithium ion battery (Adamczyk & Pralong, 2017; Gu et al., 2020; Guo et al., 2014; Hou et al., 2015; Lu et al., 2020; Song et al., 2019; Zheng et al., 2020). $Na_{0.7}MnO_{2.05}$ (JCPDS 27-0751) which was successfully synthesized through the sol-gel method is known to have a high capacity retention of 90% after 1200 cycles (Gu et al., 2020). Furthermore, the raw material used to synthesize NMO similar to LMO, even sodium resources as the substitute of lithium provided abundantly in Indonesia (Salim & Munadi, 2016).

In this study, we conducted an investigation on the active material of the sodium ion battery cathode to determine whether sodium manganese oxide (NMO) could be synthesized by the sol-gel method referring to the LMO synthesis process carried out in previous studies (Rahardi, 2016). We expect that NMO can be synthesized by the sol-gel method as was done to obtain LMO by slightly modifying the synthesis process based on initial identification, including visual inspection and simple thermal gravimetry to determine the calcination temperature. Through this journal, we would like to report the results of the initial study regarding the synthesis of sodium manganese oxide through sol-gel method and post-thermal treatment.

2. MATERIAL AND METHOD

2.1. Materials

Technical grade of sodium chloride (NaCl), manganese (II) chloride dihydrate ($MnCl_2.2H_2O$) and citric acid ($C_6H_8O_7$) were used as raw material, purchased from the local market in Bandung, Indonesia. Ammonia solution 25% was purchased from MERCK. Chitosan with deacetylation degree of 85-95% $(C_6H_{11}NO_4)_n$ was purchased from Biotech Surindo Cirebon, Indonesia. Distilled water was purchased from PT Alkin Global Bandung, Indonesia.

2.2. Methods

The procedure used in this study referred to thesis research about LMO synthesis (Rahardi, 2016). Synthesis of sodium manganese oxide (NMO) was carried out in a series of steps, started from dissolving of precursors and other compounds using distilled water and then mixed to obtain sol. Afterwards, sol was stirred to obtain gel, the gel was dried overnight to remove solvent to obtain xerogel, then xerogel was heated and calcined to obtain NMO crystalline powder. The NMO samples obtained from various calcination temperature of 600°C and 800°C were abbreviated as N1 and N2 respectively. NMO samples were synthesized using precursors and chelating agent with concentration of 1 M and stoichiometric molar ratio of the precursors and also pH adjustment to assist the gelling process. The solution was prepared using magnetic stirrer hotplate NESCO LAB MS-H280-Pro, gel drying and calcination process was carried out in KBO-90M oven and KOEHLER K24110 furnace box respectively.

Visual inspections of NMO samples were initially carried out over a certain temperature range, including 200°C, 400°C, 600°C, and 675°C, to compare the physical appearance of NMO with LMO samples from previous study (Balai Besar Bahan dan Barang Teknik, 2020). Thermogravimetric and differential thermal analysis (TG/DTA) were used to investigate the thermal behavior of samples, carried out with simplified measurement using the KOEHLER K24110 box furnace and analytical balance HAND-20152348 Fuzhou minheng electronic instrument, at the Center for Materials and Technical Products (B4T), Ministry of Industry, Republic of Indonesia. The samples were heated in crucibles from 200°C to 800°C, with a heating rate of 10°C/min in air atmosphere. The structure and phase composition of the crystalline sodium manganese oxide (NMO) was determined by x-ray diffractometry (XRD) using BRUKER-D8 Advance at the Laboratory of Electron Microscopy, Center for Nanoscience and Nanotechnology Research (PPNN) Bandung Institute of Technology, with Cu x-ray tube. Kα at 1,54060 Å, 40 kV and 40mA, with a scan rate of 0.06° (2θ)/min over a 2θ range of 10°–90°. The obtained diffraction patterns were compared with the Joint Committee on Powder Diffraction Standards (JCPDS) and processed using the Xpowder program. The surface morphology of the samples was observed by scanning electron microscopy (SEM) using HITACHI SU-3500, at the Electron Microscope Laboratory, Center for Nanoscience and Nanotechnology Research (PPNN) Bandung Institute of Technology.

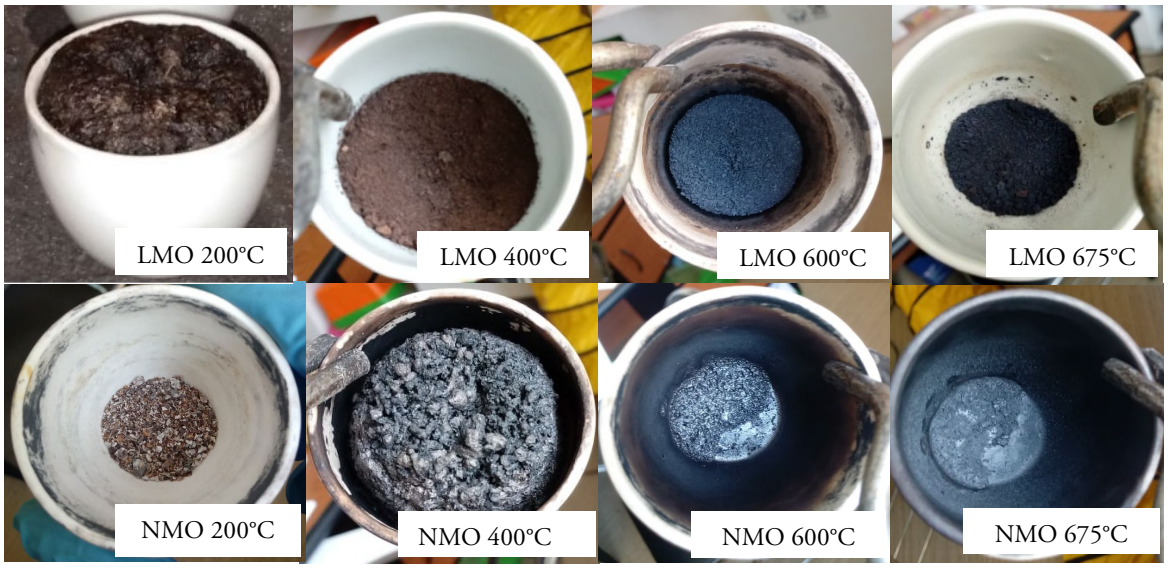

Figure 1. Visual inspection of NMO samples compared to LMO samples

3. RESULT AND DISCUSSION

Initially, the NMO sample was synthesized using NaCl and $MnCl_2$ precursors as well as chelating agents citric acid and chitosan as a template. The behavior of NMO samples during the synthesis process was observed and compared with LMOs through gradual visual inspection as in Figure 1. It was previously known that LMO samples experienced swelling at 200°C, while the NMO samples experienced swelling at 400°C. Based on a visual inspection of the LMO sample at 600°C, a bluish-black powder was found to indicate the formation of LMO crystals (Balai Besar Bahan dan Barang Teknik, 2020). Unlike the NMO sample, a bluish-black powder was not observed even after calcination both at temperature of 600°C and 850°C. We inferred that the color of the NMO powder was not the same with LMO powder as the structure and phase compositios of the crystals were different.

The NMO samples showed different behavior from LMO as long as they were subjected to thermal treatment, which will be discussed further with thermogravimetry analysis. We supposed that the different precursors used in the sol gel method could lead to different thermal behaviour of the samples while calcined. Based on the heat treatment of the NMO sample up to 675°C, it was found that the mass of the NMO sample decreased along with the increasing temperature given as in Table 1, including the LMO samples weight loss from previous study (Balai Besar Bahan dan Barang Teknik, 2020) as comparison. It was known that the NMO samples experienced autocombustion at about 520°C.

Table 1. Weight loss of NMO sample along with the heat treatment

	Initial	250°C	400°C	600°C
NMO Sample				
Mass (gr)	58.9	18.4	14.37	(finding: auto-combustion)
Weight Loss (%)	-	68.76	75.60	(finding: auto-combustion)
LMO Sample (Balai Besar Bahan dan Barang Teknik, 2020)				
Mass (gr)	72.556	28.84	26.35	22.65
Weight Loss (%)	-	60.25	63.68	68.78

3.1. Thermal analysis

Thermogravimetric (TG) measurements were carried out on NMO xerogel samples ranging from 200°C to 800°C, while the DTA curve obtained from the derivative of the TG curve as in Figure 2. As comparison, thermogravimetric of LMO samples from previous study (Balai Besar Bahan dan Barang Teknik, 2020) was also featured. All volatile compounds completely decomposed at 400°C, indicated by a large mass loss up to 35% of the initial total mass. Based on the TG/DTA curve of the NMO sample, it is known that there is exothermic reaction of around 450°C to 700°C, with an estimated formation zone between 580°C and 600°C, also between 660°C and 720°C, and also started from 760°C to more than 800°C. Therefore, the calcination temperature of the NMO samples were chosen at 600°C and 850°C.

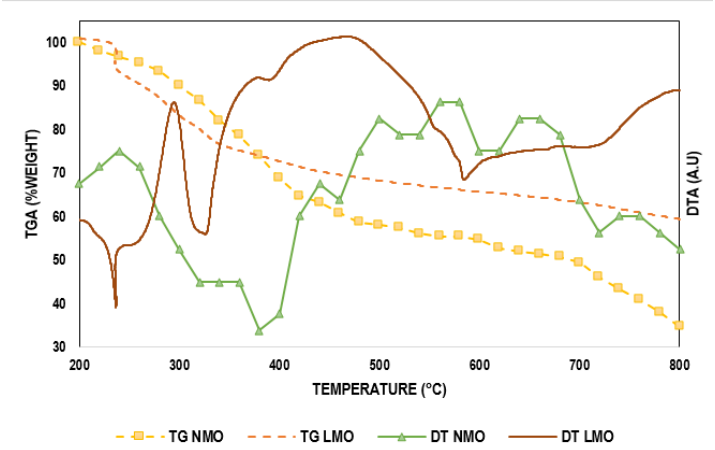

Figure 2. Thermogravimetric profile of NMO samples from simplified measurement and LMO samples referred to previous study.

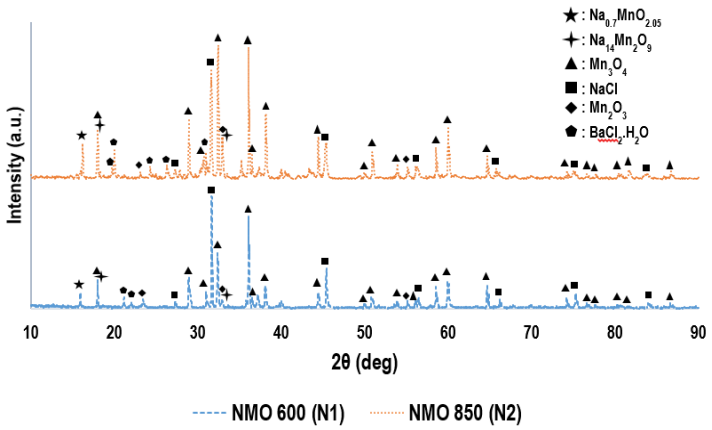

Figure 3. Diffraction Pattern of Samples N1 and N2

The TG/DTA profile of this NMO sample resembles the thermogravimetric profile of the LMO sample. However, there is a shift in the temperature range of the exothermic reaction zone, about 50°C and 135°C, respectively, for the start and end of the exothermic region. This is consistent with the facts found based on the visual inspection mentioned above.

3.2. Structure analysis

XRD tests were carried out to check the phase composition of the NMO sample powder obtained after calcination at the predicted formation zone, the diffraction pattern is shown in Figure 3. NMO samples were calcined at 600°C (N1) and 850°C (N2) for 2 hours.

Based on phase identification of N1 sample, at least six different phases were found, namely Mn_3O_4 (JCPDS 18-0803), NaCl (JCPDS 05-0628), Mn_2O_3 (JCPDS 02-0896), $BaCl_2.H_2O$ (JCPDS 39-1305), $Na_{14}Mn_2O_9$ (JCPDS 70-0725), and $Na_{0.7}MnO_{2.05}$ (JCPDS 27-0751). The desired phase is $Na_{0.7}MnO_{2.05}$ (JCPDS 27-0751) with hexagonal layered structure and main diffraction pattern around 2θ = 15.9° (Hou et al., 2015), or at 2θ = 15.8°, 36.0°, 39.7°, 49.0°, 64.8° were respectively, assigned to crystallographic plane (002), (100), (102), (104) and (110) (Gu et al., 2020).

As a note there is an alternative phase of sodium manganese oxide, $Na_2Mn_3O_7$ (JCPDS 78-0193), which has similar diffraction pattern with the desired phase. $Na_{0.7}MnO_{2.05}$ (JCPDS 27-0751) was preferred in the phase identification of N1 because it generated higher weight percentage than the alternative phase. With the Scherrer method, it is known that the crystallite size of $Na_{0.7}MnO_{2.05}$ (JCPDS 27-0751) of sample N1 is 148 nm (Miller index 002) as shown in Table 2.

Table 2. Identification of the diffraction pattern of N1

JCPDS Number	2θ (deg)	Miller index	Phase	Crystal system, Space group	Crystallite size (nm)
27-0751	15.944	002	$Na_{0.7}MnO_{2.05}$	Hexagonal axis	148
39-1305	**21.165**	**102**	$BaCl_2.H_2O$	Orthorhombic, Pnma	135
18-0803	28.924	112	Mn_3O_4	Tetragonal, I41/amd	56
05-0628	**31.671**	**200**	NaCl	Cubic, Fm3m	287
18-0803	32.364	004	Mn_3O_4	Tetragonal, I41/amd	94
02-0896	**32.897**	**222**	Mn_2O_3	Cubic, Ia3	87
70-0725	32.999	112	$Na_{14}Mn_2O_9$	Hexagonal axis, P-3	96
18-0803	**36.095**	**211**	Mn_3O_4	Tetragonal, I41/amd	129
05-0628	45.409	220	NaCl	Cubic, Fm3m	359

Table 3 . Identification of the diffraction pattern of N2

JCPDS Number	2θ (deg)	Miller index	Phase	Crystal system, Space group	Crystallite size (nm)
27-0751	16.227	002	$Na_{0.7}MnO_{2.05}$	Hexagonal axis	176
70-0725	18.024	011	$Na_{14}Mn_2O_9$	Hexagonal axis, P-3	89
39-1305	20.04	102	$BaCl_2.H_2O$	Orthorhombic, Pnma	154
18-0803	28.94	112	Mn_3O_4	Tetragonal, I41/amd	241
05-0628	31.647	200	NaCl	Cubic, Fm3m	63
18-0803	32.425	004	Mn_3O_4	Tetragonal, I41/amd	192
70-0725	32.506	112	$Na_{14}Mn_2O_9$	Hexagonal axis, P-3	113
02-0896	32.918	222	Mn_2O_3	Cubic, Ia3	88
18-0803	36.111	211	Mn_3O_4	Tetragonal, I41/amd	513
05-0628	45.410	220	NaCl	Cubic, Fm3m	46

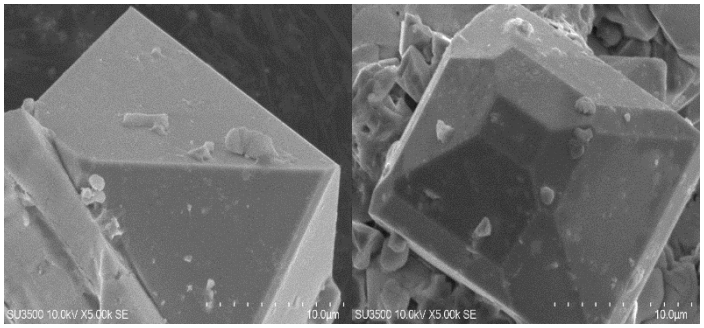

Figure 4. Morphology of N1 samples at 600°C

At first, it is inferred that the peak of $Na_{0.7}MnO_{2.05}$ (JCPDS 27-0751) which has not yet dominated the diffraction pattern of the sample because of the calcination temperature given is still too low to provide sufficient energy for the crystallization of $Na_{0.7}MnO_{2.05}$ (JCPDS 27-0751). It is expected that increasing the calcination temperature may increase the crystallinity and weight percentage of the sodium manganese oxide as the previous study of the lithium manganese oxide (Balai Besar Bahan dan Barang Teknik, 2020). Thus, the calcination of sample N2 was carried out at higher temperature, 850°C. With the Scherrer method, it is known that the crystallite size of $Na_{0.7}MnO_{2.05}$ (JCPDS 27-0751) of sample N2 is 176 nm (Miller index 002) as shown in Table 3.

Based on the analysis of the diffraction pattern of the samples at higher calcination temperature, it could be inferred that the crystalinity of sodium manganese oxide was increased, besides the growing of the crystallite occured, yet higher weight percentage of $Na_{0.7}MnO_{2.05}$ (JCPDS 27-0751) was not gained. Instead, weight percentage of Mn_3O_4 (JCPDS 18-0803) and Mn_2O_3 (JCPDS 02-0896) getting higher. Based on this observation, it could be inferred that previous step, sol gel method, should be investigated further to obtain the desired phase with high purity, one of which is adjusment of molar ratio of the precursors.

3.3. Morphology analysis

SEM test was carried out to determine the morphology of the calcined NMO sample at 600°C, as shown in Figure 4. Truncated tetragonal solids were observed. Based on the XRD pattern of the N1 sample in Figure 4, it is known that the form of this truncated tetragonal is a Mn_3O_4 (JCPDS 18-0803) crystal which still dominates the N1 sample at 600°C. This truncated shape may occured as the preferred orientation of the manganese oxide phase. This sample morphological in accordance with diffraction pattern identification mentioned above, while the regular hexagonal-platelet morphology of $Na_{0.7}MnO_{2.05}$ (Hou et al., 2015) was not observed as well.

4. CONCLUSION

Sodium manganese oxide has been synthesized from table salt using sol gel and calcination methods based on simple thermogravimetry measurements, while the purity of the desired phase was too low regarding several phases of other compounds still dominate the diffraction pattern. Based on the

structural and morphological analysis, it was found that two temperature ranges that were formerly thought to be NMO formation zones were not significant to obtain pure $Na_{0.7}MnO_{2.05}$ without modification of sol-gel method. In other words, further investigation should be carried out on sol gel method instead of thermal treatment. We suggested to adjust the molar ratio of the precursor and also use other precursors to obtain the desired phase.

ACKNOWLEDGMENT

The authors would like to express their deepest gratitude to the Head of B4T for the direction, financial support, facilities, opportunities, and all other support given, especially regarding to collaborative research and downstreaming of sodium ion batteries with Prof. Bambang Sunendar, Lab. Advanced Material Processing, Engineering Physics ITB.

REFERENCE

Adamczyk, E., & Pralong, V. (2017). $Na_2Mn_3O_7$: A Suitable Electrode Material for Na-Ion Batteries? *American Chemical Society*, *29*, 4645–4648. https://doi.org/10.1021/acs.chemmater.7b01390

Armstrong, A. R., & Bruce, P. G. (1996). Synthesis of layered $LiMnO_2$ as an electrode for rechargeable lithium batteries.pdf. Nature. https://doi.org/doi.org/10.1038/381499a0

Balai Besar Bahan dan Barang Teknik. (2020). *Laporan Kegiatan Riset Baterai - LK-A-08 - Produksi Litium Mangan Oksida Skala Lab yang Diperbesar sebagai Material Aktif Baterai Ion Litium melalui Metode Sol-Gel*. Bandung.

Danks, A. E., Hall, S. R., & Schnepp, Z. (2016). The Evolution of Sol-Gel Chemistry as A Technique for Materials Synthesis. *Materials Horizons*, *3*, 91–112. https://doi.org/10.1039/C5MH00260E

Ernowo, Sunuhadi, D. N., & Awaludin, M. (2020). Ketersediaan Nikel dan Kobalt untuk Bahan Industri Baterei Listrik di Indonesia. Retrieved from http://psdg.geologi.esdm.go.id/index.php?option=com_content&view=article&id=1214&Itemid=610

Gu, F., Yao, X., Sun, T., Fang, M., Shui, M., Shu, J., & Ren, Y. (2020). Studies on micron‐sized $Na_{0.7}MnO_{2.05}$ with excellent cycling performance as a cathode material for aqueous rechargeable sodium‐ion batteries. *Applied Physics A*, 1–8. https://doi.org/10.1007/s00339-020-03799-6

Guo, S., Yu, H., Jian, Z., Liu, P., Zhu, Y., & Guo, X. (2014). A High-Capacity , Low-Cost Layered Sodium Manganese Oxide Material as Cathode for Sodium-Ion Batteries. *Chemsuschem*, *210093*, 2115–2119. https://doi.org/10.1002/cssc.201402138

Hou, Y., Tang, H., Li, B., Chang, K., Chang, Z., Yuan, X., & Wang, H. (2015). Hexagonal-layered $Na_{0.7}MnO_{2.05}$ via solvothermal synthesis as an electrode material for aqueous Na-ion supercapacitors. *Materials Chemistry and Physics*, 1–8. https://doi.org/10.1016/j.matchemphys.2015.12.009

Hwang, J., Myung, S., & Sun, Y. (2017). Sodium-ion batteries : present and future. *Chemical Society Reviews*. https://doi.org/10.1039/c6cs00776g

Lee, M., Lee, S., Oh, P., Kim, Y., & Cho, J. (2014). High Performance $LiMn_2O_4$ Cathode Materials Grown with Epitaxial Layered Nanostructure for Li-Ion Batteries. *American Chemical Society*, *14*, 993–999.

Liu, C., Neale, Z. G., & Cao, G. (2016). Understanding electrochemical potentials of cathode materials in rechargeable batteries. *Materials Today*, *19*(2), 109–123. https://doi.org/10.1016/j.mattod.2015.10.009

Liu, W., Farrington, G. C., Chaput, F., & Dunn, B. (1996). Synthesis and Electrochemical Studies of Spinel Phase $LiMn_2O_4$ Cathode Materials Prepared by the Pechini Process Synthesis and Electrochemical Studies of Spinel Phase $LiMn_2O_4$ Cathode Materials Prepared by the Pechini Process. *Journal of The Electrochemical Society*, *143*(3), 879–884. https://doi.org/10.1149/1.1836552

Lu, D., Yao, Z. J., Li, Y. Q., Zhong, Y., Wang, X. L., Xie, D.,Tu, J. P. (2020). Sodium-rich manganese oxide porous microcubes with polypyrrole coating as a superior cathode for sodium ion full batteries. *Colloid and Interface Science*, *565*, 218–226. https://doi.org/10.1016/j.jcis.2020.01.023

Nishi, Y. (2001). Lithium ion secondary batteries; Past 10 years and the future. *Journal of Power Sources*, *100*(1–2), 101–106. https://doi.org/10.1016/S0378-7753(01)00887-4

Nitta, N., Wu, F., Lee, J. T., & Yushin, G. (2015). Li-ion battery materials: Present and future. *Materials Today*, *18*(5), 252–264. https://doi.org/10.1016/j.mattod.2014.10.040

Parker, J. F., Chervin, C. N., Pala, I. R., Machler, M., Burz, M. F., Long, J. W., & Rolison, D. R. (2017). *Rechargeable nickel–3D zinc batteries: An energy-dense, safer alternative to lithium-ion* (Vol. 418).

Pegeng, Z., Huiqing, F. A. N., Yunfei, F. U., Zhuo, L. I., & Yongli, D. (2006). Synthesis and electrochemical properties of sol-gel derived LiMn,O, cathode for lithium-ion batteries, *25*, 0–4.

Rahardi, S. S. (2016). *Sintesis litium mangan oksida melalui metode sol gel dengan bio template selulosa bakteri sebagai bahan katoda baterai ion litium (Thesis Master)*. Institut Teknologi Bandung.

Salim, Z., & Munadi, E. (2016). *Info Komoditi Garam*. Jakarta: Badan Pengkajian dan Pengembangan Perdagangan, Kementerian Perdagangan Republik Indonesia. Retrieved from http:// bppp.kemendag.go.id/media_content/2017/08/Isi_BRIK_Garam.pdf

Song, B., Tang, M., Hu, E., Borkiewicz, O. J., Wiaderek, K. M., Hu, Y., Liu, J. (2019). Understanding the Low-Voltage Hysteresis of Anionic Redox in $Na_2Mn_3O_7$. *American Chemical Society*, *31*, 3756–3765. https://doi.org/10.1021/acs.chemmater.9b00772

Sun, Y. (1997). Synthesis of Spinel $LiMn_2O_4$ by the Sol - Gel Method for a Cathode-Active Material in Lithium Secondary Batteries. *American Chemical Society*, 4839–4846. https://doi.org/10.1021/ie970227b

Supriadi, A., Sunarti, Kencono, A. W., Kurniasih, T. N., Prasetyo, B. E., Kurniawan, F., Anggraeni, D. (2017). *Kajian Dampak Hilirisasi Mineral Mangan Terhadap Perekonomian Regional*. Jakarta: Pusat Data dan Teknologi Informasi Energi dan Sumber Daya Mineral.

Thackeray, M. M., & Rossouw, M. H. (1994). Synthesis of Lithium-Manganese-Oxide Spinels : A Study by Thermal Analysis. *Journal of Solid State Chemistry*, 441–443. https://doi.org/10.1006/jssc.1994.1393

Xiao, N., Mcculloch, W. D., & Wu, Y. (2017). Reversible Dendrite-Free Potassium Plating and Stripping Electrochemistry for Potassium Secondary Batteries. *American Chemical Society*, 0–3. https://doi.org/ 10.1021/jacs.7b04945

Zheng, P., Su, J., Wang, Y., Zhou, W., Song, J., Su, Q., Guo, S. (2020). A high-performance primary nanosheet heterojunction cathode composed of $Na_{0.44}MnO_2$ tunnels and layered $Na_2Mn_3O_7$ for Na-ion batteries. *Chemsuschem*.https://doi.org/10.1002/cssc.201903543

Vol. 11 No. 2 (2020) 35-42

Jurnal Riset
Teknologi Pencegahan Pencemaran Industri

Journal homepage : http://www.jrtppi.id

Kementerian Perindustrian
REPUBLIK INDONESIA

Zinc Removal from ZnO Industrial Wastewater by Hydroxide Precipitation and Coagulation Methods: The Role of pH and Coagulant Dose

Ratnawati[1], Marcelinus Christwardana[1], Sudirman[2], Enjarlis[1*]
[1]Chemical Engineering Department, Institut Teknologi Indonesia
[2]Badan Tenaga Atom Nasional, Kawasan Puspiptek, Serpong

ARTICLE INFO

Article history:
Received 01 September 2020
Received in revised form 05 October 2020
Accepted 05 October 2020
Available online 19 November 2020

Keywords :
Zn
pH
Coagulant
Turbidity
COD

ABSTRACT

Liquid waste from the ZnO industry must be treated to meet the quality standards of wastewater into water bodies, according to the Minister of Environment Regulations No.5, 2014. It still contains 79 mg/L of Zn metal, cloudy with turbidity above 500 NTU, and COD value around 222 mg/L. This study aims to determine the effect of pH on reducing Zn metal and the coagulant dose to minimize turbidity and COD in liquid waste produced by the ZnO factory in Depok, West Java. The waste treatment has been carried out by adding alkaline to neutralize the acid conditions in the equalization basin. However, the results have not met the requirements. It is necessary to vary the pH (8.5; 9.0; 9.5; 10.0 and 10.5) to precipitate of Zn optimally, modify the dose of coagulants (50; 100 and 150 mg/L) and reaction times (10; 15 and 20 minutes) to reduce its turbidity and COD concentration. The best results were obtained at a pH of 9.5 with a coagulant dose of 50 mg/L and a reaction time of 10 minutes. This condition can reduce Zn concentration (79 to 3.71 mg/L), turbidity (557 to 1.42 NTU), COD (222 to 68 mg/L) with a removal efficiency of 95.3%; 99.7%; and 69.4% respectively. These values have met the standard requirements according to government regulations.

1. INTRODUCTION

The Industrial wastewater that contains various organic and inorganic pollutants is one source of water pollutions, which at high concentrations can endanger the environment. Inorganic industrial waste such as lead (Pb), zinc (Zn), cadmium (Cd), copper (Cu), chromium (Cr), arsenic (As), nickel (Ni) can be toxic that harmful to human and other lives (Renu et al., 2017a). These metals can damage the liver and nerves. Based on the toxicological point of view, these heavy metals can be divided into two types. The first type is an essential heavy metal in which living organisms need their presence in a certain amount, but in excessive amounts it can cause oxic effects. Examples of these heavy metals are Zn, Cu, Fe, Co, Mn, and others. At the same time, the second type is non-essential or toxic heavy metals in which its presence in the body is still unknown or can even be toxic such as Hg, Cd, Pb, Cr, and others (Azimi et al., 2017).

Zinc (Zn^{2+}) is a reactive and toxic heavy metal that affects considerably human's body due to its accumulation in the food chain. However, in less quantity, it is essential for human health (Jamshaid et al., 2018). It frequently found in industrials effluent such as battery, mining, metallurgy, electroplating, pigment, paint, smelting, fossil fuel combustion, polymer stabilizers, fertilizer, pesticide, and municipal wastewater treatment plants (Jamshaid et al., 2018; Zhang et al., 2017) According to Environmental Protection Agency (EPA), Zn^{2+} is a dangerous pollutant that causes poisoning cases with symptoms such as dehydration,

*Correspondence author.
E-mail : en_jarlis@yahoo.com (Enjarlis)

doi : https://10.21771/jrtppi.2020.v11.no.2.p35-42

Accreditation number : (LIPI) 756/Akred/P2MI-LIPI/08/2016

stomachache, electrolyte imbalance, skin irritation, vomiting (Renu et al., 2017a), and nausea (Baloch et al., 2019). The reducing of Zn of concentration is very severe or crucial to fulfill the World Health Organization recommendation or Indonesian Minister of Environment Regulation No 5, 2014 that acceptable Zn level is 5.0 mg/L (Zhang et al., 2017). Numerous treatment technologies have been applied to eliminate Zn ions from wastewater include physicochemical methods such as adsorption using activated carbon from agricultural waste (Zhang et al., 2017), biosorption using chemically treated rice husk (Baloch et al., 2019), ion flotation (Hosseinian et al., 2018) membrane filtration, ion exchange, reverse osmosis, chemical coagulation/flocculation (Eggermont et al., 2020), chemical or electrochemical precipitation (John et al., 2016; Zainuddin et al., 2019) and solvent extraction (Jamshaid et al., 2018). The other method is biological methods using various kinds of several microorganisms and microalgae (Jamshaid et al., 2018). Many attempts are also performed to utilize waste materials as adsorbents to reduce the cost of processing heavy metal pollutants. The comparison among wastewater treatment technologies has also been reported by previous researchers (Renu et al., 2017b).

One of the industries that produce zinc oxide (ZnO) treats its zinc-loaded wastewater by making a Waste Water Treatment Plant (WWTP). This waste comes from product analysis in its laboratory that has acid characteristics. Therefore, the waste in the equalization tank is acidic and has only been added alkaline to get the neutral pH. However, the processing results do not meet the quality standards of industrial effluent to the environment because it still has high Zn concentration, turbid with high Chemical Oxygen Demand (COD) as can be seen in the following Table 1. Therefore, it needs improvement in treating the waste.

The commonly used method to treat the zinc removal from wastewater is the precipitation of this heavy metal as hydroxides with the addition of lime, $Ca(OH)_2$ or NaOH (Azimi et al., 2017) in pH variation to get optimum process which is characterized by the most optimum amount of zinc settling (Eggermont et al., 2020; Zainuddin et al., 2019). This process is an inexpensive and simple method (Azimi et al., 2017; John et al., 2016). A study on zinc removal from the plating industry by chemical precipitation with NaOH was performed by (John et al., 2016), and NaOH and Na_2S were done by Zainuddin et al. (Zainuddin et al., 2019). On the other hand, polyaluminium chloride (PAC) was employed for heavy metal and phosphate removal (Ghorpade et al., 2018;Chen et al., 2019).

Table 1. The characteristic of ZnO industrial wastewater before and after neutralization

	pH	Zn concentration, Ppm	COD, ppm	Turbidity, NTU
Before neutralization	4	79.0	222	557
After neutralization	7	33.2	222	557

In this study, heavy metals removal was performed by the addition of NaOH with pH variation (8.5 - 10.5) to form hydroxide precipitation. Subsequently, the variation of coagulant dose (50 - 150 ppm) was added to the supernatant to reduce the turbidity and COD. The PL-50 coagulant (blends of inorganic and organic coagulants with the composition of Al_2O_3 and cationic polymer) was used. The choice of coagulant dose refers to the previous jar test, and this chemical is relatively cheap. Therefore, the purpose of this study is to determine the effect of pH on Zn removal and Al_2O_3 based coagulant dosage on turbidity and COD reduction from ZnO plant wastewater.

2. METHODS

The ZnO waste sample was taken from the equalization tank of the Waste Water Treatment Plant (WWTP) of the ZnO factory in West Java, Indonesia. The chemicals needed in this study are: $K_2Cr_2O_7$, H_2SO_4, $HgSO_4$ for the making of High Concentrate Digestion Solution, Ag_2SO_4 for reagent solution (Merck), Sulfamic Acid (NH_2SO_3H) (Seidler Chemical), Potassium Hydrogen

Ptalate Solution 425 ppm ($C_8H_5KO_4$) (Merck), Distilled water (electrical transmission <2μS/cm), Coagulant Katfloc PL-50/Al_2O_3-Cationic Polymer (PT Puji Lestari Purnama), Technical NaOH (Asahimas Chemical), Phosphate Buffer Solution (KH_2PO_4, K_2HPO_4, $Na_2HPO_4.7H_2O$, NH_4Cl) (Merck), $CaCl_2$ Solution (PT Mufasa Specialties Indonesia), BOD Seed Solution (Hach InterLab LTD), Standard BOD Solution, Hydrazine Sulfate Solution ($(NH_2)_2H_2SO_4$) (Merck), Hexa Methylene Tetramine Solution ($(CH_2)_6N_4$) ($(NH_2)_2H_2SO_4$) (Merck), 4000 NTU Turbidity Parent Suspension, 40 NTU Turbidity Suspension, Purified Water, Standart Solution of Fe, Pb, Mn, Cu, Co, Cd, Ni, Zn 2000 mg/L, $MgSO_4$ for Magnesium Sulfate Solution (Pudak Scientific), and $FeCl_3$ (Merck).

The equipments used are UV-Vis Spectrophotometer Genesys 10S UV-Vis (Thermo Fisher Scientific USA) with λ from 400 - 700 nm, Digestion Vessel SC150 Environmental Express (Thomas Scientific) with specifications Poly Ethylene 10 - 100 ml, Heating Block SC150 (Environmental Express) with 25 samples, 150 °C, Magnetic Stirrer C-MAG HS-7 (IKA) for 50 - 1500 rpm, Analytical Balance AUY 220 (Shimadzu) for 0.1 mg, Nephelometer/Turbidity Meter ECTN 100 IR (Thermo Scientific) for 0 - 2000 NTU, Atomic Absorption Spectrophotometer A 7099 (GBC Scientific) for λ 185 - 900 nm, pH meter HI 991001 (Hanna) with accuracy ± 0.02, BOD Refrigerated Incubator + RDO/DO Benchtop Meter BOD Kit with Orion Star A213 Model (Thermo Fisher Scientific USA) for Stores over 300 BOD Bottles (300 mL) + AutoStir.

The measurement of heavy metal content is performed by the duplicated method and the measurement results are the average. The removal of zinc metal (Zn) is carried out by precipitation of the sample as hydroxide with the NaOH addition by following a predetermined pH variation, stirring with 80 rpm for 5 minutes and allowed 60 minutes for precipitation to occur. The supernatant of the precipitate results was tested for metals concentration (Zn, Fe, Pb, Mn, Cu, Cd, Co, and Ni) by the AAS.

The supernatant samples were also evaluated for turbidity, COD, and BOD through the addition of coagulant Al_2O_3-based at various loading and reaction times. COD levels were determined using a spectrophotometric closed reflux method according to SNI 6989.2 year 2009 (BSN, 2009). These measurements were carried out by mixing the samples which consist of digestion solution and sulfuric acid, then it heated 150°C and refluxed for 2 hours. After that, the mixed solution was cooled until room temperature and followed by COD measurement. While turbidity was measured with a Nephelometer in accrdance with the SNI 06-6989.25 year 2005 (BSN, 2005).

BOD measurement was carried out by giving seed to a sample that had been diluted, incubated at 20 °C for 5 days. Dissolved Oxygen (DO) was measured before and after the incubation period. BOD was calculated from the difference in the initial DO values (0 days) and after 5 days in accordance with the SNI 6989.72 year 2009 (BSN, 2009). Measurement of the initial conditions is also carried out to determine the process efficiency. All measurements are carried out in duplicate, and the final result is the average.

3. RESULT AND DISCUSSION

The average results of the initial heavy metal concentration of the waste that measured duplicated for 3 days can be depicted in Table 2. From Table 2, it can be stated that the initial Zn concentration is still far above the permitted standard quality. However, for other heavy metals, their concentrations meet the recommended specifications. Figure 1 shows the effect of pH on Zn concentration after the process. All metals, especially Zn, precipitate as hydroxide by the addition of NaOH. The chemical rection mechanism to the formation of the percipitate can be explained as follows:

$$Zn^{2+} + 2\ NaOH \rightarrow Zn(OH)_2 + 2\ Na^+ \quad (1)$$

The curve with a minimum point indicates the highest % Zn removal or minimum solubility was achieved, and it occurs at pH 9.5 with the NaOH addition of 5.3 mg for 1 L of wastewater.

Tabel 2. Heavy metal concentration (mg/L) according to standard quality, initial condition and after process at pH variation.

Metal	Zn	Fe	Pb	Mn	Cu	Cd	Co	Ni
St. quality	5	5	0.1	2	2	0.05	0.4	0.2
Initial concentration	79	0.034	0.013	0.140	0.014	0.017	0.033	0.041
pH 8.5	5.701	0.022	0.000	0.031	0.003	0.002	0.002	0
pH 9.0	4.905	0.007	0.000	0.032	0.003	0.002	0.000	0
pH 9.5	3.710	0.009	0.000	0.028	0.003	0.002	0.000	0
pH 10.0	4.530	0.011	0.000	0.031	0.003	0.002	0.000	0
pH 10.5	4.620	0.016	0.000	0.033	0.000	0.002	0.000	0

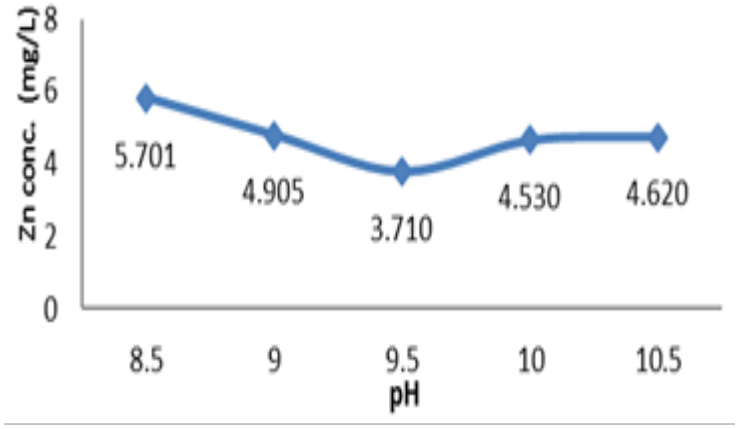

Figure 1. The effect of pH on effluent Zn concentration

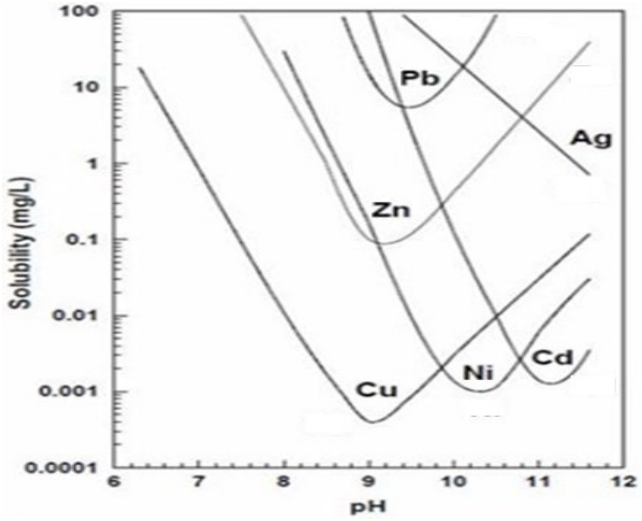

Figure 2. The solubility of metals hydroxide at different pH (Zhang et al., 2018)

Figure 1 shows that the best pH for Zn precipitation occurs at pH 9.5 because it generates the lowest effluent Zn concentration of 3.71 mg/L with 95.3% removal. However, the optimum pH is 9.0, with 93.8% removal. At that condition, the effluent of Zn concentration already below 5.0 mg/L (fulfill the acceptable discharge concentration in accordance with the Minister of Environment regulation). Therefore, it utilizes NaOH slightly below compare to at pH 9.5. The results obtained are in accordance with the previous study (Lewis, 2017). Besides, the effluent waste also contains other metals such as Fe, Pb, Mn, Cu, Cd, Co, and Ni. For all metals, the initial conditions of the waste have met the quality standard except Zn. However, after the process at pH ≥ 9.0, all heavy metals comply with the acceptable discharge concentration. When the wastewater containing metal (Zn^{2+}) is added by Na(OH) and followed by mixing, the precipitation of $Zn(OH)_2$ is formed according to reaction presented in the equation (1).

The solubility of metals hydroxide at deferent pH can be seen in Figure 2 in which each type of metal hydroxide is favorable to precipitate at a specific pH range (Zhang et al., 2018). Actually, the temperature differences also affects the solubility of metal hydroxide. According to that figure, the best pH for Zn metal to precipitate take place on the range 9.0 to 9.5. This phenomenon is similar with this study. If the pH condition is not in a suitable range, the metal hydroxide precipitate prefers to resolubilize (Chen et al., 2018).

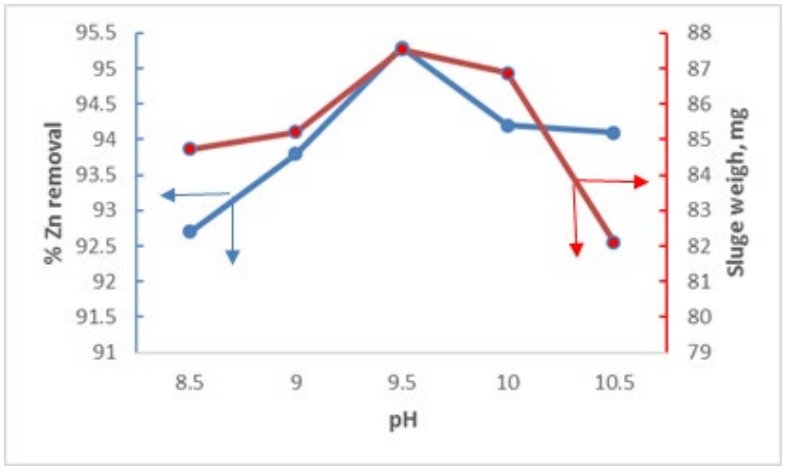

Figure 3. Percentage Zn removal and dry sludge weight at various pH for 1 L wastewater

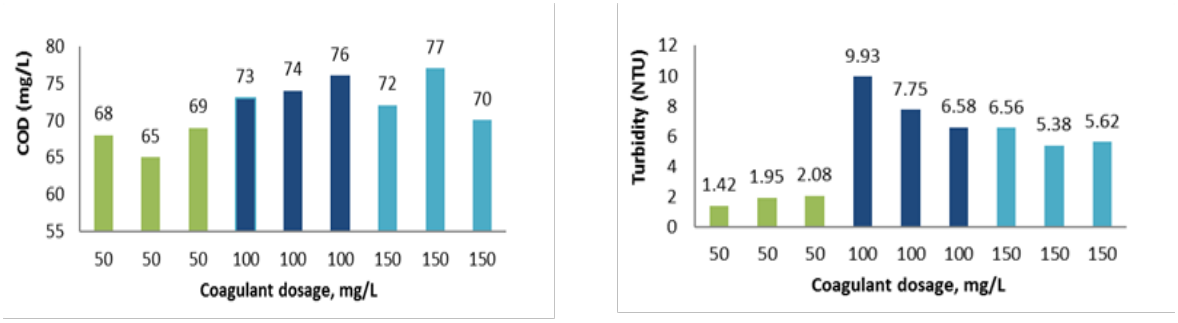

a) b)

Figure 4. a) COD and b) Turbidity at various coagulant dose and mixing time with 80 rpm (green color for 10 minutes, dark blue for 15 minutes, and light blue for 20 minutes).

Figure 3 shows the % Zn removal and the dry sludge weight obtained at various pH. The maximum point indicates the highest percentage removal efficiency at pH of 9.5 due to the linear correlation between the lowest Zn final concentration, maximum % removal, and maximum dry sludge weight.

After the Zn deposition process at pH 9.5, the supernatant result is still turbid with turbidity 557 NTU and COD 222 mg/L. Therefore, this wastewater still does not meet the industrial waste quality standards. Consequently, this waste must be treated by adding Katfloc PL-50/Al_2O_3-Cationic Polymer coagulant (Al_2O_3-based coagulant) with the dosage of 50, 100, and 150 mg/L and stirring time of 10, 15 and 20 minutes. This variation value is based on the jar test results conducted previously. Figure 4 shows the effect of coagulant dosage and reaction time on COD and turbidity reduction. Based on figure 4, the increasing of the coagulant dose until the optimum value (50 mg/L), results in a higher COD value and turbidity. However, the increasing of mixing time relatively did not affect to the COD and turbidity.

Coagulation-flocculation is a physicochemical method to remove colloids with a negative charge, very fine solid suspension, and some soluble compound present in wastewater (Renu et al., 2017a). The concept is a destabilization of the solution. It is neutralized by mutual collision with opposite ions (coagulant) and followed by the formation of the flock or a process that transforms colloidal particles into flock (Ghafoorisadatieh et al., 2019). Eventually, the flock undergoes sedimentation. This process can also be used for absorbing dissolved organic matter on to the surface of the flock/particulate aggregates

(Bongiovani et al., 2016). Therefore, coagulants' addition will reduce COD since COD illustrates the amount of O_2 needed to oxidize organic substances in the waste. In this case, the decreasing COD occurred due to the formation of the flock and absorption of the organic matter by the flock (Ghafoorisadatieh et al., 2019). Increasing the amount of coagulant until 50 mg/L, the possibility of contact between coagulant and colloidal particles becomes frequent. It results in increasing flock formation until it reaches the maximum point. Hereafter, additional coagulant was not able to create precipitation flock (no flock formation). Therefore, extra coagulant remained in the water until reached saturation, and finally, COD increased doe to the availability coagulant on the aqueous solution. Some coagulants have been used for pollutants and turbidity removal (Ghafoorisadatieh et al., 2019) and pulp/paper wastewater treatment (Irfan et al., 2017).

From a turbidity point of view, it is indicating the amount of suspended solids that proportional to the amount of colloid and suspended solids in wastewater that cannot be precipitated in the usual method (Ghafoorisadatieh et al., 2019). It can scatter the light. Similar to the COD explanation, the excessive amount of coagulant to maximum point caused turbidity in the water and reduction in the turbidity removal percentage (Malik, 2018). In other words, over dozing of coagulant caused charge reversal, and particles start restabilizing.

Figure 4 shows the optimum COD and turbidity removal. It was achieved at coagulant dose of 50 mg/L with 10 minutes reaction time since both the COD and turbidity reduced to 68 mg/L (≤ 100 mg/L) and 1.42 NTU (≤ 2 NTU), respectively. It has met the quality standard with a removal efficiency of 69.4% and 99.7%, respectively. At the optimum condition, the BOD sample was reduced from 7.22 to 3.14. This condition is according to the acceptable discharge concentration. The study was also conducted to evaluate the concentrations of metals after the addition of coagulant on the supernatant. This addition does not reduce Zn concentration marginally (only reduced 1.5% from the initial condition). For other metals, the final concentration of Fe, Co and Cd can drop to zero. To summarize, the effluent has fulfilled the acceptable discharge concentration.

4. CONCLUSION

In this study, the effects of pH on Zn removal and doses of coagulant on the reduction efficiency of COD and turbidity were performed experimentally. The pH affected the decrease of Zn concentration. The best pH took place at 9.5 due to it increased the quantities of $Zn(OH)_2$ deposition with a reduction in the Zn concentration of 95.3%. Hydroxyte precipitation was directly related to Zn removal and pH. Meanwhile, the addition of coagulant of 50 ppm to the supernatant resulting from the $Zn(OH)_2$ deposition with reaction time of 10 minutes can reduce COD, BOD, and turbidity. However, it only has a slight effect on reducing other metals concentration.

5. ACKNOWLEDGMENT

The authors would like to thank Pusat Riset dan Pengabdian Masyarakat (PRPM) Institut Teknologi Indonesia and the ZnO industry in West Java for the opportunity given to perform this study. Thanks also to Fikri Rizka Akbar and Iqbal Fadly Abdillah for the data collection.

6. REFERENCE

Azimi, A., Azari, A., Rezakazemi, M., Ansarpour, M. "Removal of Heavy Metals from Industrial Wastewaters: A Review". ChemBioEng Reviews, vol 4(1), 37-59, 2017

Badan Standarisasi Nasional SNI 06.6989.2:2009 Air dan Air Limbah-Bagian 2: Cara Uji Kebutuhan Oksigen Kimiawi (Chemical Oxygen Demand/COD) dengan Refluks Tertutup secara Spektrofotometri, Badan Standarisasi Nasional, Jakarta.

Badan Standarisasi Nasional SNI 6989.25:2005 Air dan Air Limbah-Bagian 25: Cara Uji Kekeruhan dengan Nefelometer, Badan Standarisasi Nasional, Jakarta.

Badan Standarisasi Nasional SNI 6989.72:2009 Air dan Air

Limbah-Bagian 72: Cara Uji Kebutuhan Oksigen Biokimia (Biochemical Oxygen Demand/BOD), Badan Standarisasi Nasional, Jakarta.

Baloch, A., Qaisrani, Z.N., Zahid1, I., Hussain, S., Mengal, A.N., Sami, S.K., Amin, M., Siddique, M., Sultan, S.H. "Removal of Zinc (II) from municipal wastewater using chemically modified activated carbon developed from Rice husk and Kikar charcoal". Journal of Applied and Emerging Sciences, vol 9(1), 2019.

Bongiovani, M.C.,Camacho, F. P., Coldebella, P.F., Valverde, K.C., Nishi, L., Bergamasco, R. "Removal of natural organic matter and trihalomethane minimization by coagulation/flocculation/filtration using a natural tannin". Desalination and Water Treatment, vol 57(12), pp. 5406-5415, 2016.

Chen Q., Yao, Y., Li, X., Lu, J., Zhou, J., Huang, Z. "Comparison of heavy metal removals from aqueous solutions by chemical precipitation and characteristics of precipitates". Journal of Water Process Engineering, vol 26, pp. 289-300, 2018.

Chen, Y., Lin, H., Yan, W., Huang, J., Wang, G., Shen, N. "Alkaline fermentation promotes organics and phosphorus recovery from polyaluminum chloride-enhanced primary sedimentation sludge". Bioresource Technology, vol 294, 122160, 2019.

Eggermont, S. G. F., Prato, R., Dominguez-Benetton, X., Fransaer, J. "Metal Removal from Aqueous Solutions: Insights from Modeling Precipitation Titration Curves". Journal of Environmental Chemical Engineering, vol 8, pp 1-8, 2020

Ghafoorisadatieh, A., Almatin, E., Bam, M. S. N., Gholipour, A. "Estimating of Optimal Dose of PACL for Turbidity Removing from Water". Arxiv org, pp 1-8, 2019.

Ghorpade, A. Ahammed, M. M. "Water Treatment Sludge for Removal of Heavy Metals from Electroplating Wastewater". Environ. Eng. Res, vol 23(1), pp 92-98, 2018.

Hosseinian, F., S., Irannajad, M., Azadmehr, A. R. "Removal of Zn(II) from Wastewater by Ion Flotation: Determination of Optimum Conditions". Amirkabir Journal of Civil Engineering, vol 49(4), pp 679-686,2018.

Irfan, M., Butt, T., Imtiaz, N., Abbas, N., Khan, R. A., Shafique, A. "The Removal of COD, TSS, and Colour of Black Liquor by Coagulutation-Flocculation Process at Optimized pH, Settling, and Dosing Rate". Arabian Journal of Chemistry, vol 10, pp s2307-s2318, 2017.

Jamshaid, M., Khan, A.A., Ahmed, K., Saleem M. "Heavy metal in drinking water its effect on human health and its treatment techniques – a review". International Journal of Biosciences, vol 12(4), 223-240, 2018.

John, M., Heuss-Aßbichler, S., Ullrich, A. "Recovery of Zn from Wastewater of Zinc Plating Industry by Precipitation of Doped ZnO Nanoparticles". International Journal Environmental Science Technology, vol 13, pp 2127-2134, 2016.

Lewis, A. "Precipitation of Heavy Metals". Sustainable Heavy Metal Remediation, pp. 101-120, 2017

Malik, Q. H. "Perfomance of Alum and Assorted Coagulants in Turbidity Removal of Muddy Water". Applied Water Science, vol 8(40), pp 1-4, 2018.

Renu, Agarwal, M., Singh, K., "Heavy Metal Removal from Wastewater using Various Adsorbents: a review". Journal of Water Reuse and Desalination, vol 7(4), 387-419, 2017a.

Renu, Agarwal, M., Singh, K. "Methodologies for removal of heavy metal ions from wastewater: an overview". Interdiscipline Enviromental Review, vol 18(2), 124, 2017b.

Zainuddin, N. A., Mamat, T. A. R., Maarof, H. I., Puasa, S. W., Yatim., S. R. M. "Removal of Nickel, Zinc, and Copper from Plating Process Industrial Raw Effluent Via Hydroxide Precipitation Versus Sulphide Precipitation". IOP Conf. Series. Matereralls Science and Engineering, vol 551, pp 1-6, 2019.

Zhang, X., Hao, Y., Wang, X. Chen, Z. "Rapid Removal of Zinc (II) from Aqueous Solutions using a Mesoporous Activated Carbon Prepared from Agricultural Waste". Materials, vol 10(9), pp 1-18, 2017.

Zhang, Y., Zhang, H., Zhang, Z., Liu, C. Sun, W. Zhang, Marhaba, T. "pH Effect on Heavy Metal Release from a Polluted Sediment". Journal of Chemistry, pp. 1- 7, 2018.

Vol. 11 No. 2 (2020) 43-50

Jurnal Riset
Teknologi Pencegahan Pencemaran Industri

Journal homepage : http://www.jrtppi.id

Kementerian Perindustrian
REPUBLIK INDONESIA

Processing of Granite Quarry Solid Waste into Industrial High Silica Materials using Leaching Process with HCl Concentration Variation

Muhammad Amin[1], Slamet Sumardi[1], Roniyus Marjunus[2], Frista Clarasati[2], David Candra B[1], Muhammad Al Muttaqi[1], Kusno Isnugroho[1], Yusup Hendronursito[1]

[1]Research Unit for Mineral Technology, Indonesian Institute of Sciences (BPTM-LIPI)

[2]Department of Physics, Faculty of Mathematics and Natural Sciences, University of Lampung

ARTICLE INFO

Article history:
Received 17 September 2020
Received 27 October 2020
Accepted 27 October 2020
Available online 19 November 2020

Keywords :
Granite
Silica
Leaching
HCl

ABSTRACT

This study was aimed to increase granite's silica content using the leaching process with HCl concentration variation. The granite used in this study came from Lematang, South Lampung. This study aims to determine the effect of variations in HCl concentration, particle size, and rotational speed on the crystalline phase and chemical elements formed in the silica product produced from granite. The HCl concentration variations were 6.0 M, 7.2 M, 8.4 M, and 9.6 M, the variation in particle size used was 270 and 400 mesh. Variations in rotational speed during leaching were 500 and 750 rpm. Granite powder was calcined at 1000 ºC for 2 hours. Characterization was performed using X-Ray Fluorescence (XRF), X-Ray Diffraction (XRD), and Inductively Coupled Plasma-Optical Emission Spectroscopy (ICP- OES). The results showed that the silica content increased with increasing HCl concentration, the finer the particle size, and the higher the rotational speed. XRF analysis showed that the silica with the highest purity was leached with 9.6 HCl with a particle size of 400 mesh and a rotational speed of of 750 rpm, which was 73.49%. Based on the results above, by leaching using HCl, the Si content can increase from before. The XRD diffractogram showed that the granite powder formed the Quartz phase.

1. INTRODUCTION

Lampung Province, with an area of ± 3,528,835 ha, has a very diverse natural resource potential, especially mineral resources. The diversity of mineral resources in Lampung Province includes metal minerals, industrial minerals, energy minerals, and construction minerals. Lampung Province produces industrial excavation of 117,184 m^3 andesites, 234,375 m^3 feldspars, and 62,232,727 m^3 granite (ESDM, 2019). These data show that industrial granite excavation has the potential to be developed. One of the potential granite rocks in Lampung Province is in the Lematang Village area, Tanjung Bintang, South Lampung Regency.

Granite is a deep igneous rock (intrusive). The mineral is coarse-grained to medium light, has many colors, generally white, gray, pink, or red. This color is caused by the color variation of the mineral feldspar. Granite is formed from magma (Judson, Deffeyes & Hargraves, 1978). So far, in Lematang Village, granite is only used as a foundation stone. Silica is refined from granite to increase granite value, which can be used as an advanced material application. So far, small granite quarries measuring 50 mm and below have been discarded, so they are not used because they are used as foundation stones which are larger than 100 mm in size. Therefore mineral silica can be obtained from pumice stone

*Correspondence author.
E-mail : yusuph_ugm07@yahoo.com (Yusup Hendronursito)

doi : https://10.21771/jrtppi.2020.v11.no.2.p43-50

Accreditation number : (LIPI) 756/Akred/P2MI-LIPI/08/2016

(Mourhly, Khachani, Hamidi, Kacimi Halim & Arsalane, 2015), diatomite (Puntharo, Sankram, Chantaramee & Pokmanee, 2013), and quartz sand (Saleh, Ibrahim & Salman, 2015). Apart from quartz sand, granite is a mineral with a high silica content of up to 72.04% (Harvey & Tracy, 1997). Some researchers using several methods to synthesize silica, including combustion (Rozainee Ngo, Salema, Tan, Ariffin & Zainura, 2008), sol-gel (Le, Thuc & Thuc, 2013), leaching acid (Umeda & Kondoh, 2010), the precipitation (Yuvakkumar, Elango, Rajendran & Kannan, 2012). The method leaching and deposition have the advantage that the resulting silica is higher than the silica synthesized by other methods from some of the above methods. The leaching and deposition method is a simple and economical method for silica purification (Ha, Akhtar & Malik, 2014).

Leaching is the extraction of certain materials to remove material impurities by dissolving it (Matori, Haslinawati, Wahab, Sidek, Ban & Ghani, 2009). Inorganic impurities can be removed through a process leaching using an acid solution to obtain high purity silica before the combustion process. Researchers have carried out the process leaching before conducting the thermal process using HCl, H_2SO_4, HNO_3 (Matori, Haslinawati, Wahab, Sidek, Ban & Ghani, 2009), citric acid (Umeda & Kondoh, 2010), and oxalic acid (Kalapathy, Proctor & Shultz, 2002). The use of HCl because HCl is a strong acid and is more reactive than other acids.

Several studies have been conducted to obtain large amounts of silica using the method leaching. For example, Darwis et al. (2017) purified silica from quartz sand using the method leaching with HCl. From XRF results showed that 99.90% of silica obtained from 5 hours-milled sample [14]. Abdellaoui et al. (2013), synthesizing silica with diatomite by method leaching using HNO_3 (Abdellaoui, Islam, Sakurai, Hamzaoui & Akimoto, 2018). Lahsen et al. (2016) also synthesized silica from granite using the method leaching with the solvent HCl. From this experiment, Lahsen et al. (2016) showed the maximum leaching efficiency was 92.4% and about 93.8% the leached can be separated (Lahsen, Mohamed, Cheira, Zaki & Allam, 2016). Therefore this study was aimed to purification of silica from granite quarry solid waste with different HCl concentration into industrial high silica.

Table 1. Variations in HCl concentration, particle size and rotational speed.

Sample	HCl (M)	Size (mesh)	Rotation speed (rpm)
1	6	270	500
2	7.2	270	500
3	8.4	270	500
4	9.6	270	500
5	6	270	750
6	7.2	270	750
7	8.4	270	750
8	9.6	270	750
9	6	400	500
10	7.2	400	500
11	8.4	400	500
12	9.6	400	500
13	6	400	750
14	7.2	400	750
15	8.4	400	750
16	9.6	400	750

Table 2. Result of Granit Stone before leaching

Compounds	Percentage (wt%)
SiO_2	62.806
Al_2O_3	18.365
P_2O_5	0.764
K_2O	10.112
TiO_2	0.623
Fe_2O_3	6.951

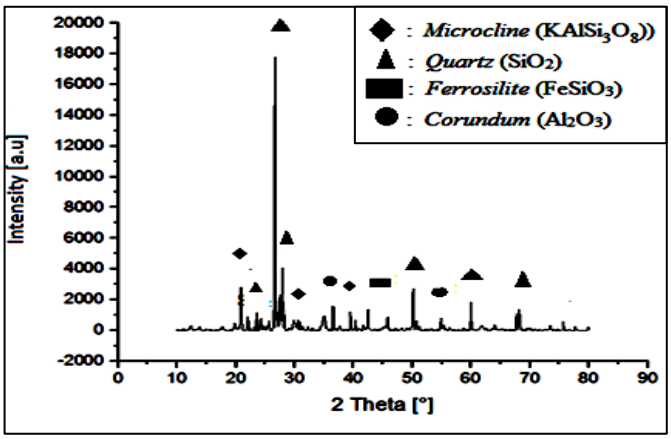

Figure 1. XRD analysis for granite

Table 3. The results of XRF Analysis *Leaching* Granite Stone with Particle Size 270 Mesh and Rotation Speed 750 rpm.

Compounds	% Leaching			
	6.0 M	7.2 M	8.4 M	9.6M
SiO_2	69.31	71.55	72.229	72.29
Al_2O_3	16.38	15.30	15.068	14.95
Fe_2O_3	-	2.373	2.361	2.413
TiO_2	0.528	0.515	0.500	0,491
K_2O	8.166	9.180	8.95	-
P_2O_5	0.661	0.073	0.711	0.716

2. METHODS

2.1. Material

Material used in this study included granite from Lematang-Tanjung South Lampung, 12.06 M HCl, and aquades.

2.2. Method

The powder preparation process refers to the research conducted by Lahsen et al. (2016), which started with washing granite stones using aquades until they were cleaned, then drying them for 2 hours at 120°C using an oven. Furthermore, the granites was refined using ball milling for 5 hours to produce granite powder, which was still in a rough state. Then the granite powder was dried using an oven for 2 hour at temperature of calcination. After drying, the granite powder is sieved with a 270 mesh and 400 mesh sieves to obtain a fine granite powder. Furthermore, granite's fine powder is weighed as much as 5 grams as a sample to be tested using XRD and XRF.

This refining process is a process carried out to obtain pure silica from granite with various treatments, as shown in Table 1.

This granite process leaching referred to research that has been conducted by Lahsen et al. (2016). First, the preparation of 100 mL of HCl, with concentration variations of 6.0 M, 7.2 M, 8.4 M, 9, 6 M. After the solution has been prepared, 10 grams of granite powder was dissolved into each of the HCl solutions that have been prepared. Each solution was then stirred for 7 hours while stirring at a rotational speed as in Table 1 and heated to purify the silica contained in granite powder. The next stage was the result stirrer used filtered with filter paper Whatman No. 41. The filtered residue was then oven-dried for 2 hours at a temperature of calcination. Then it was calcined with furnace at for 2 hours, then characterized by XRD and XRF.

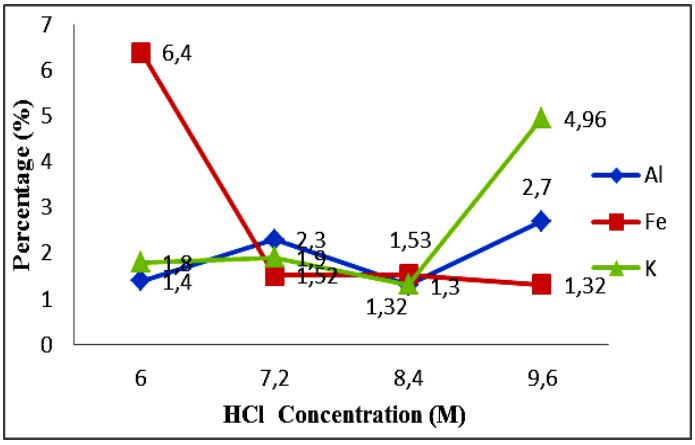

Figure 2. The graph of the relationship between HCl concentration and the solubility of Al, Fe, and K, the graph of a particle size of 270 mesh and a rotating speed of 750 rpm.

3. RESULT AND DISCUSSION

Granite structures were analyzed using XRF Analysis. Leaching process were conducted using HCl 6.0 M; 7.2 M; 8.4 M and 9.6 M for 7 hours at 110 °C. After that it was filtered with Whatmann filter paper no. 2, then calcined for 2 hours at a temperature of 1000 °C. Last tested with XRD and XRF. The results of the XRF analysis of granite are as in Table 2.

The results of XRD analysis for granite as shown in Figure 1. The phases formed are Quartz (SiO_2), Microcline ($KAlSiO_2$), Corundum (Al_2O_3), and Ferrosilite ($FeSiO_3$). The highest peak is at 2θ = 26.6251° Quartz (SiO_2).

The analysis results of XRF leaching granite with 270 mesh particle size and 750 rpm rotation speed are as in Table 3.

Based on Table 3, XRF analysis results showed that the percentage of SiO_2 compound after leaching was higher than before leaching. The SiO_2 highest produced was found in samples leached with a concentration of 9.6 M. In this study, the silica obtained continued to increase the concentration of HCl was used. The concentration of HCl affects the hydrolysis's speed and condensation reactions of the material, which affects the silica gain and the crystallinity of the material (Hilmy, 2007).

Leaching using HCl can dissolve other metals, including Fe, Al, and K, so that after leaching, the levels of other metals such as Fe, Al, and K decreased, and the silica content in the sample increased, as the concentration of HCl is used (Hasbi, Sigit, Indah, Septian & Efendi Bintang, 2016). Analysis the solution sample was leaching analyzed using ICP-

OES to detect chemical elements dissolved during the process leaching. Graph of analysis results from ICP-OES leaching granite with a particle size of 270 mesh, and a rotating speed of 750 rpm is presented as in Figure 2. Dissolving with HCl on elements Al, Fe, and K does not have trend the same due to HCl's ability, which is not completely dissociated so that it cannot dissolve the metal completely (Fitri, 2013).

The XRD analysis results for leaching granite stone with a particle size of 270 mesh and a rotating speed of 750 rpm are as shown in Figure 3.

Table 4. The results of XRF Analysis for Leaching Granite with Particle Size 400 Mesh and Spin Speed 750 rpm.

Compounds	% Leaching			
	6.0 M	7.2 M	8.4 M	9.6M
SiO_2	71.25	71.49	72.81	73.49
Al_2O_3	15.1	14.38	14.29	13.1
Fe_2O_3	2.89	2.64	2.53	267
TiO_2	0.50	0.44	0.42	0.48
K_2O	9.29	9.08	8.90	9.22
P_2O_5	0.73	0.73	0.74	0.78

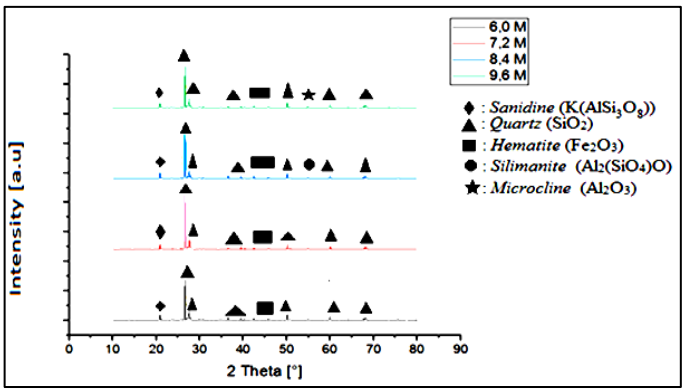

Figure 3. The XRD analysis results for granite with a particle size of 270 mesh and a rotational speed when leaching 750 rpm.

Based on Figure 3, it can be seen that the results of XRD characterization on variations samples leaching of granite with variations in HCl concentrations of 6.0 M, 7.2 M, 8.4 M, and 9.6 M indicate that the phase that dominates the diffraction peaks is Quartz (SiO_2), Sanidine ($K(AlSi_3O_8)$), Hematite (Fe_2O_3), Sillimanite ($Al_2(SiO_4)O$) and Microcline (Al_2O_3) consecutively. Phase Quartz (SiO_2) is the phase that dominates the diffraction peaks because SiO_2 is calcined at temperatures of 800 and 1000 °C (Wibawa, Eko & Anggoro, 2015). The XRF analysis results for leaching granite with a particle size of 400 mesh and a rotation speed of 750 rpm are as in Table 4.

Based on Table 3. and Table 4. it can be seen that the resulting silica content in leaching granite with a particle size of 400 mesh is higher than the silica produced in leaching granite with particle size 270 mesh. This result agreed with the theory of particle size, namely the smaller the particle size, the larger its surface area. Hence, reaction will be faster, and the resulting product will be more and more (Bentz, Garboezi, Haecker & Jensen, 1999).

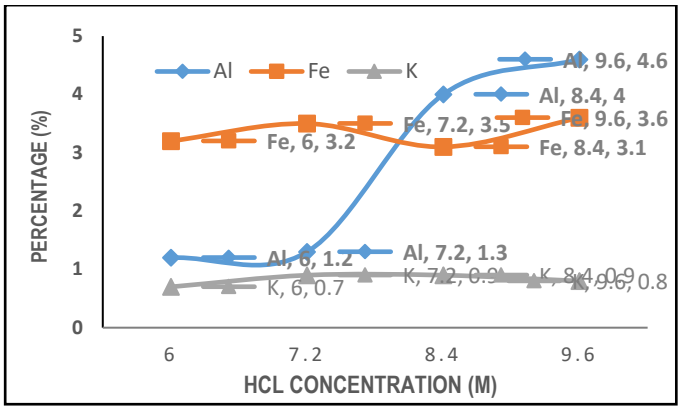

Figure 4. The relationship between HCl concentration and the solubility of Al, Fe, and K, at a particle size of 400 mesh and a rotational speed of 750 rpm.

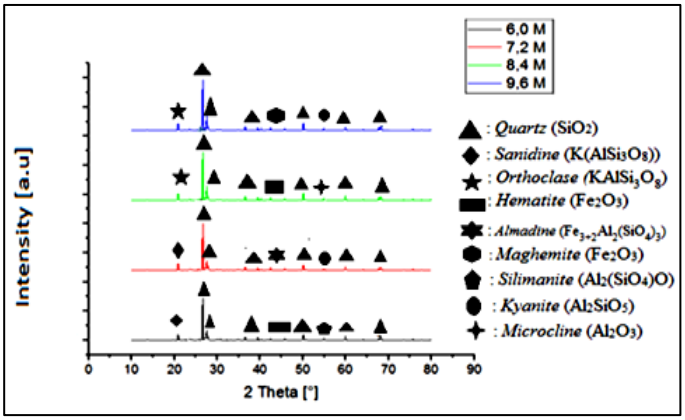

Figure 5. The XRD analysis of granite with a particle size of 400 mesh and rotational speed *leaching* of 750 rpm.

The analysis sample of the solution was leaching analyzed using ICP-OES to detect chemical elements dissolved during the process leaching. Graph of analysis results

from ICP-OES leaching granite with a particle size of 400 mesh and a rotating speed of 750 rpm is presented as in Figure 4.

The XRD analysis results leaching stone granite with a particle size of 400 mesh and rotation speed 750 rpm are shown in Figure 5.

Based on Figure 5, it can be seen that the phase that dominates the diffraction peaks is Quartz (SiO_2), Sanidine ($K(AlSi_3O_8)$), Orthoclase ($KAlSi_3O_8$), Hematite and Maghemite (Fe_2O_3), Almandine ($Fe_{3+2}Al_2(SiO_4)_3$), Kyanite (Al_2SiO_5), Mullite ($Al_{2.35}Si_{.64}O_{4.82}$), Sillimanite ($Al_2(SiO_4)O$) and Microcline ($Al_2O_3$). Phase Quartz ($SiO_2$) is the phase that dominates the diffraction peaks.

The resuls of XRF of leaching granite with 270 mesh particle pize and 500 rpm rotation speed are as in Table 5.

Table 5. The results of XRF Analysis for Leaching Granite with 270 Mesh Particle Size and 500 rpm Rotation Speed.

Compounds	% Leaching			
	6.0 M	7.2 M	8.4 M	9.6M
SiO_2	68.33	69.05	69.05	69.14
Al_2O_3	16.76	16.57	16.59	16.36
Fe_2O_3	3.08	2.66	2.77	2.73
TiO_2	0.71	0.70	0.70	0.72
K_2O	10.06	9.96	9.84	9.99
P_2O_5	0.79	0.8	0.78	0.8

Table 6. Results of XRF analysis for Leaching Granite with Particle Size 400 Mesh and Rotation Speed 500 rpm.

Compounds	% Leaching			
	6.0 M	7.2 M	8.4 M	9.6M
SiO_2	68.57	68.92	70.17	70.24
Al_2O_3	17.55	17.73	16.6	16.20
Fe_2O_3	2.44	2.23	2.22	2.35
TiO_2	0.65	0.62	0.65	0.66
K_2O	9.87	9.60	9.44	9.37
P_2O_5	0.71	0.7	0.71	0.77

Based on Table 2 and Table 5, it can be seen that the silica produced in leaching granite with a particle size of 270 mesh with a rotating speed of 750 and 500 rpm, the greater the silica made at speed turn 750 rpm. This is following the stirring speed's effect, the faster the stirring of a particle. When the faster stirred, the contact between the granite powder and the HCl will occur, and the more product is produced at the highest stirring speed (Fitri, 2013).The solution's analysis sample was leaching analyzed using ICP-OES to detect chemical elements dissolved during leaching. Graph of analysis results ICP-OES leaching granite with a particle size of 270 mesh, and a rotating speed of 500 rpm is presented as in Figure 5.

The results of XRD analysis leaching stone granite with a particle size of 400 mesh and rotation speed 750 rpm are shown in Figure 6.

Based on Figure 6, it found that the phase dominates the diffraction peaks such as Quartz (SiO_2), Sanidine ($K(AlSi_3O_8)$), Hematite (Fe_2O_3), Ferrosilite and Clinoferrosilite (Fe_2SiO_3), Kyanite (Al_2SiO_5), Mullite ($Al_{4.75}Si_{1.25}O_{9.63}$), Corundum ($Al_2O_3$) and microcline ($Al_2O_3.K_2O.6SiO_2$). Phase Quartz ($SiO_2$) is the phase that dominates the diffraction peaks.

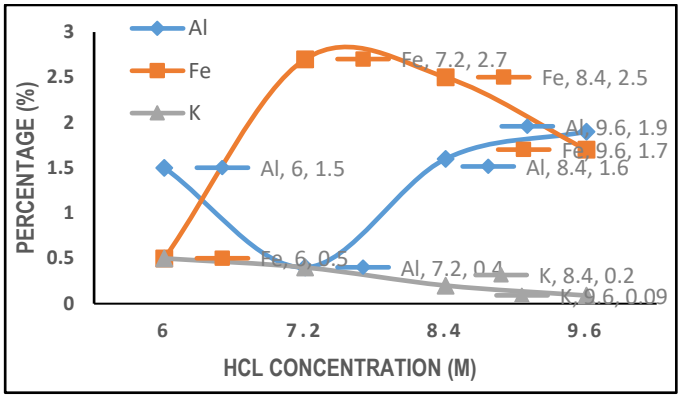

Figure 5. The graph of the relationship between HCl concentration and the solubility of Al, Fe and K, a particle size of 400 mesh and a rotational speed of 750 rpm.

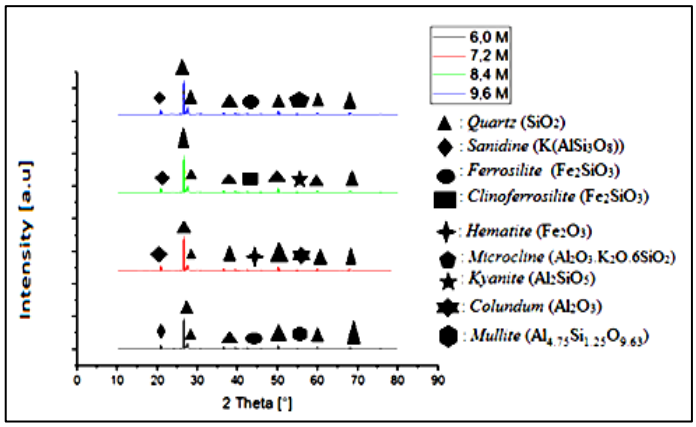

Figure 6. The results of XRD analysis of granite with a particle size of 400 mesh and rotational speed leaching of 750 rpm.

The XRF analysis results of Leaching Granitewith a Particle Size of 400 Mesh and Rotation Speed of 500 rpm are as in Table 6.

Based on Table 5 and Table 6, it can be seen that the silica produced in leaching granite with a particle size of 270 mesh with particle size of 400 is greater than the resulting silica when the particle size is 400 mesh. The silica produced when the particle size is 270 mesh with a rotating speed of 750 rpm as in Table 3 bigger than the silica when particle size is 270 mesh with a rotating speed of 500 rpm as shown in Table 6. So that, the highest silica results at the particle size 400 mesh and leaching at 750 rpm rotational speed.The solution sample was leaching analyzed using ICP-OES to detect chemical elements dissolved during the process leaching. Graph of analysis results ICP-OES leaching granite with a particle size of 400 mesh, and a rotating speed of 500 rpm is presented as in Figure 7.

The results of XRD analysis leaching stone granite with a particle size of 400 mesh and rotation speed 750 rpm are shown in Figure 8.

Based on Figures 9, it can be seen that the silica produced in leaching linear granite rises upward along with the large concentration of HCl used and the fine particle size. Silica with a particle size of 400 mesh is larger than the silica produced in leaching granite with a particle size of 270 mesh. Based on rotation speed, it can be seen that the silica produced in leaching linear granite rises upward along with the amount of HCl concentration used and the rotational speed used. The silica produced in leaching at a rotational speed of 750 rpm is greater than the silica produced in leaching granite at a rotational speed of 500 rpm.

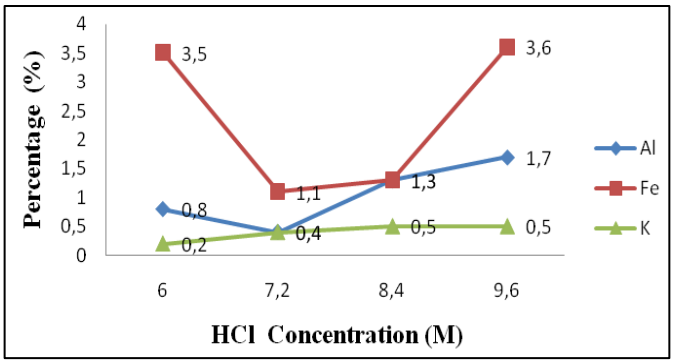

Figure 7. The Graph of the relationship between HCl concentration and the solubility of Al, Fe and K, at a particle size of 400 mesh and a rotational speed of 500 rpm.

Table 7. Phases and types of minerals formed.

Type of mineral	Phase	Percentage (%)
Quartz	SiO_2	67
Sanidine	$K(AlSi_3O_8)$	8
Orthoclase	$KAlSi_3O_8$	1.13
Hematite	Fe_2O_3	8
Maghemite	Fe_2O_3	1.13
Almadine	$Fe_{3+2}Al_2(SiO_4)_3$	1.13
Ferrosilite	Fe_2SiO_3	3.4
Clinoferrosilite	Fe_2SiO_3	1.13
Silimanite	$Al_2(SiO_4)O$	1.7
Microdine	Al_2O_3	1.13
Kyanite	Al_2SiO_5	1.7
Mullite	$Al_{2.35}Si_{.64}O_{4.82}$	0.56
Colundum	Al_2O_3	0.56
Mullite	$Al_{4.75}Si_{1.25}O_{9.63}$	0.56
Microdine	$Al_2O_3.K_2O.6SiO_2$	0.56
Andalusite	$Al_2(SiO_4)O$	0.56

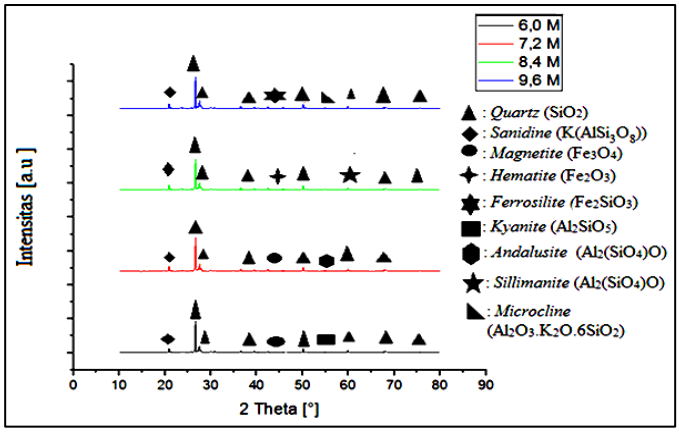

Figure 8. The results of XRD analysis of granite leaching with a particle size of 400 mesh and rotational speed of 500 rpm.

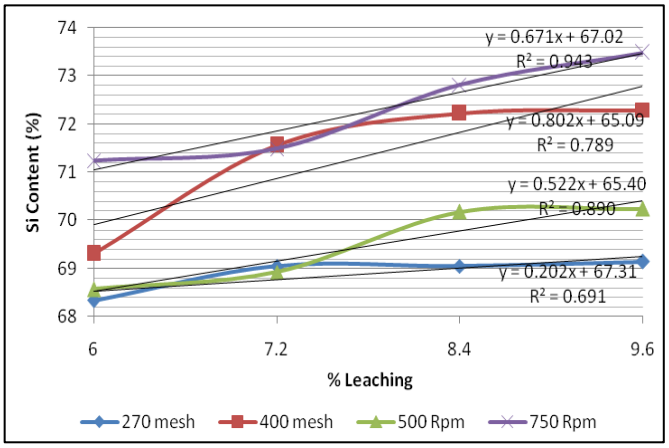

Figure 9. The relationship between silica concentration and various parameters

Several phases and minerals formed in the diffractogram pattern in the XRD analysis are presented in Table 7.

4. CONCLUSION

The highest silica obtained at a concentration of 9.6 M. Thus, the higher the concentration of HCl is used, then the higher the SiO_2 obtained. So that the concentration of the HCl solution affects the solubility of impurity oxides other than SiO_2. The silica obtained at a particle size of 400 mesh is higher than that of 270 mesh. This shows that the finer the particle size, the higher the silica is obtained. This is due to the wider the surface area of the particles, the faster the HCl solution will reduce impurity oxides other than SiO_2. Silica obtained during leaching at a rotational speed of 750 rpm is higher than at 500 rpm. This shows that the higher the rotational speed when leaching, the higher the silica will be obtained. This is because the rotational speed affects the friction that occurs, so the higher the rotational speed or, the faster the stirring, the faster the HCl solution will dissolve other impurity particles besides SiO_2.

ACKNOWLEDGMENT

Thanks are conveyed to BPTM-LIPI and PPII, who has provided the facilities and infrastructure for this research, and the Physics of the Faculty of Mathematics and Natural Sciences, the University of Lampung, who has guided until this research is complete. Contributors statement: In this paper, all authors are main contributors.

REFERENCE

ESDM. Ketersediaan Batu Granit di Lampung; 2019 [cited 15 march 2020]. Available from: *http://psdg.bgl.esdm.go.id/index.php?option=com_content&view=article&id=1301&Itemid=742.*

Judson S, Deffeyes K S, Hargraves R B. *Physical Geology*. New Delhi. Prentice-Hall of India Privat Limited.1978.

Mourhly A, Khachani M, Hamidi A E, Kacimi M, Halim M, Arsalane S. The Synthesis and Characterization of Low-Cost Mesoporous Silica SiO_2 from Local Pumice Rock. *Nanomaterials and Nanotechnology.* 2015;5:1-7.

Puntharod R, Sankram C, Chantaramee N, Pookmanee P. Synthesis and Characterization of Wollastonite from Egg Shell and Diatomite by Hydrothermal Method. *Journal Ceramics Process Research.* 2013;14:198-201.

Saleh NJ, Ibrahim RI, SalmanAD.Characterization of Nano-Silica Prepared From Local Silica Sand and Its Application in Cement Mortar Using Optimization Technique. *Advanced Powder Technology.* 2015;26:1123-1133.

Harvey B, Tracy RJ.*PetrologiEdisiKedua.* New York: Freeman;1997:66. ISBN0-7167-2438-3.

Rozainee M, NgoSP, Salema AA, Tan KG, AriffinM, Zainura ZN. Effect of Fluidising Velocity on the Combustion of Rice Husk in a Bench-scale Fluidised Bed Combustor for the Production of Amorphous Rice Husk Ash. *Bioresource Technology.* 2008;99:703-713.

Le VH, ThucCNH,Thuc HH. Synthesis of Silica Nanoparticles from Vietnamese Rice Husk by Sol-gel Method. *Nanoscale Research Letters.* 2013;8:1-10.

UmedaJ,KondohK. High-Purification of Amorphous Silica Originated from Rice Husk by Combination of Polysaccharide Hydrolysis and Metallic Impurities Removal. *Industrial Crops and Products.* 2010;32:539-544.

YuvakkumarR, ElangoV, Rajendran V, Kannan N. High-purity Nano Silica Powder from Rice Husk Using a Simple Chemical Method. *Journal of Experimental Nanoscience.* 2012;9:272-281.

Haq IU, Akhtar A, Malik A. Effect of Experimental Variables on the Extraction of Silica from the Rice Husk Ash. *Journal of Chemical Society of Pakistan* 2014; 36:382-387.

MatoriKA, Haslinawati MM, Wahab ZA, SidekHAA, Ban TK, Ghani WAWAK. Producing Amorphous White Silica from Rice Husk. *MASAUM Journal of Basic and Applied Sciences.* 2009.;1:512-515.

Kalapathy U, Proctor A, Shultz J. An Improved Method for Production of Silica from Rice Hull Ash. *Bioresource Technology.* 2002; 85:285-289.

Darwis D, Khaeroni R, Iqbal. Purification and Characterization of Silica Using Purification (Leaching) Method with Variations of Milling Time from Quartz Sand on Pasir Putih Village South Pamona Sub-district of Poso District. Natural

Science: Journal of Science and Technology. 2017;6(2):187-193

Abdellaoui I, Islam MM, Sakurai T, Hamzaoui S, Akimoto K. Impurities removal process for high-purity silica production from diatomite. Hydrometallurgy. 2018;179:207-214.

Lahsen TA, Mohamed SA, Cheira MF, Zaki DI, Allam EM. Leaching and Recovery of Rare Earth Elements from Altered Alkaline Granite Rock from Nusab El-Balgum Area, South Western Desert, Egypt. Research Article. 2016; 4:787-801.

Hilmy MA. *Pengaruh Konsentrasi HCl dan Temperatur Perlakuan Hidrotermal Terhadap Kristalinitas Material Mesopori Silika SBA-15.* Jakarta: Universitas Indonesia; 2007.

Hasbi MY, Sigit DY, Indah NC, Septian AC, Efendi Bintang A. Penggunaan Aqua Regia dan HCl Sebagai Larutan Pelindian pada Proses Pemurnian Silikon Tingkat Metalurgi dengan Variasi pH.*Seminar Nasional Sains dan Teknologi.* 2016:1-7.

Fitri NTD. *Ekstraksi dan Penentuan Kadar Ion Aluminium Hasil Ekstraksi dari Fly Ash Batubara.* Skripsi. Jurusan Kimia Universitas Negeri Jember; 2013.

Wibawa A, Eko TS, Anggoro TM. Pengaruh Variasi Temperatur pada Proses Kalsinasi Silika Amorf dari PLTP Dieng. *Pemaparan Hasil Penelitian Geoteknologi.* 2015:2-6.

Bentz DP, Garboezi EJ, Haecker CJ, Jensen OM. Effects of Cement Particle Size Distribution on Performance Properties of Portland Cement-Based Materials. *Cement and Concrete Research.* 1999;29:1663-1671.